MICROCOPY RESOLUTION TEST CHART
NATIONAL BUREAU OF STANDARDS-1963-A

155900-21-T

AD-A159 440

Topic Report

SAR DATA COLLECTION AND PROCESSING SUMMARY-1984 SARSEX EXPERIMENT

E.S. KASISCHKE
R.A. SHUCHMAN
R.W. LARSON
D.R. LYZENGA
J.C. CLINTHORNE
P.L. JACKSON

Radar Division

MARCH 1985

∑ ENVIRONMENTAL
RESEARCH INSTITUTE OF MICHIGAN

BOX 8618 ● ANN ARBOR ● MICHIGAN 48107

DTIC
ELECTE
SEP 1 9 1985
S D

85 8 26 003

REPORT DOCUMENTATION PAGE

1a. REPORT SECURITY CLASSIFICATION	1b. RESTRICTIVE MARKINGS
Unclassified	

2a. SECURITY CLASSIFICATION AUTHORITY	3. DISTRIBUTION/AVAILABILITY OF REPORT
	Distribution Unlimited
2b. DECLASSIFICATION/DOWNGRADING SCHEDULE	

4. PERFORMING ORGANIZATION REPORT NUMBER(S)	5. MONITORING ORGANIZATION REPORT NUMBER(S)
155900-21-T	

6a. NAME OF PERFORMING ORGANIZATION	6b. OFFICE SYMBOL (If applicable)	7a. NAME OF MONITORING ORGANIZATION
Environmental Research Institute of Michigan		Office of Naval Research

6c. ADDRESS (City, State and ZIP Code)	7b. ADDRESS (City, State and ZIP Code)
P.O. Box 8618 Ann Arbor, MI 48107	800 N. Quincy Street Arlington, VA 22217

8a. NAME OF FUNDING/SPONSORING ORGANIZATION	8b. OFFICE SYMBOL (If applicable)	9. PROCUREMENT INSTRUMENT IDENTIFICATION NUMBER
Office of Naval Research		Contract No. N00014-81-C-0692

8c. ADDRESS (City, State and ZIP Code)	10. SOURCE OF FUNDING NOS.			
	PROGRAM ELEMENT NO	PROJECT NO.	TASK NO.	WORK UNIT NO
800 N. Quincy Street Arlington, VA 22217				

11. TITLE (Include Security Classification) SAR Data Collection & Processing Summary-1984 SARSEX Experiment

12. PERSONAL AUTHOR(S)
E. Kasischke, R. Shuchman, R. Larson, D. Lyzenga, J. Clinthorne, P. Jackson

13a. TYPE OF REPORT	13b. TIME COVERED	14. DATE OF REPORT (Yr., Mo., Day)	15. PAGE COUNT
Topic	FROM 5-84 TO 2-85	85 March	146

16. SUPPLEMENTARY NOTATION

17. COSATI CODES			18. SUBJECT TERMS (Continue on reverse if necessary and identify by block number)
FIELD	GROUP	SUB. GR.	Synthetic Aperture Radar, Data Processing Analysis Plans, Oceanography, Internal Waves, Data Collection, CV-580 SAR

19. ABSTRACT (Continue on reverse if necessary and identify by block number)

This report describes the SAR data collection and processing activities performed to date for the SAR Internal Wave Signature Experiment (SARSEX). During SARSEX, a total of 88 passes of X- and L-band SAR data were collected over two test areas by the ERIM/CCRS CV-580 SAR System. These data were collected over an instrumented ocean site located 100 km south of Long Island, NY and a calibrated reflector array site. A description of the CV-580 SAR System is presented. The location of each SAR pass, along with a listing of the SAR and aircraft parameters, are given. All SAR data have been precision optically processed and reviewed. A selected subset of data have been digitally processed and a preliminary engineering assessment of the quality of the SAR imagery performed. The results of this assessment are presented, as are representative examples of optically- and digitally-processed SAR imagery collected during SARSEX. Finally, the analysis plans for the SAR data are discussed, including a presentation of the procedure to calibrate the SAR imagery.

20. DISTRIBUTION/AVAILABILITY OF ABSTRACT	21. ABSTRACT SECURITY CLASSIFICATION
UNCLASSIFIED/UNLIMITED ☒ SAME AS RPT ☐ DTIC USERS ☐	Unclassified

22a. NAME OF RESPONSIBLE INDIVIDUAL	22b. TELEPHONE NUMBER (Include Area Code)	22c. OFFICE SYMBOL
Eric Kasischke	(313) 994-1200	

PREFACE

The work described in this report was conducted between May of 1984 and February of 1985 by personnel in the Radar Division of the Environmental Research Institute of Michigan (ERIM). The work was supported by the Office of Naval Research under Contract No. N00014-81-C-0692. The technical monitor for this work was Mr. Robert Winokur.

The co-principal investigators for this project were Dr. Robert A. Shuchman and Mr. Eric S. Kasischke. Mr. Richard W. Larson directed the SAR calibration efforts. Dr. Philip L. Jackson and Mr. James C. Clinthorne performed the preliminary engineering analysis of the SAR data. Dr. David R. Lyzenga assisted in the development of the SAR data analysis plan, and prepared the section on SAR image modeling.

iii

ACKNOWLEDGMENTS

The success of the SAR data collection and processing activities associated with the 1984 SARSEX experiment is due in large part to the assistance of numerous individuals and organizations who we would like to acknowledge at this time.

Mr. B. Bayer of the Canadian Centre for Remote Sensing (CCRS) assisted in the preliminary planning of the SAR flight lines, while Dr. C. Livingstone of CCRS provided radar engineering support during the SAR data collection missions.

Special thanks go to the crew and operators of the ERIM/CCRS CV-580 SAR (Messrs. A. MacDonald, A. Gignac, B. Bayer, S. Bertrand and R. Whitter), whose extra efforts insured the success of this experiment.

The efforts of Mr. M. Winokur of the Federal Aviation Adminsitration in the coordination of logistical activities at Long Island's MacArthur Field are greatly appreciated.

Mr. R. Winokur of ONR, personnel of the Navy's Fleet Aircraft Control Facility of NAS Oceana, VA, and personnel at the New York Air Route Traffic Control Center, especially Mr. Eugene Barrow, are thanked for their assistance in arranging flight clearances for the aircraft participating in SARSEX.

Mr. W. Rusmussmen of Grumman Aerospace Corporation is acknowledged for coordinating the use of the Peconic River Airport as a site for the calibrated reflector array.

Numerous individuals at ERIM assisted in the field program, data processing and preliminary analysis of the SAR data sets and the publication of this report. These individuals are: S. Barsch, B. Beatty, C. Caruthers, D. Clarke, W. Kerce, L. Kime, T. Kladzyk, E. Lettvin, J. Losee, J. Marks, R. Rau, F. Smith, and L. Sutherland.

TABLE OF CONTENTS

TABLE OF CONTENTS
(Continued)

LIST OF FIGURES

LIST OF FIGURES
(Continued)

LIST OF FIGURES
(Continued)

LIST OF FIGURES
(Continued)

LIST OF TABLES

LIST OF TABLES
(Concluded)

SAR DATA COLLECTION AND PROCESSING SUMMARY
1984 SARSEX EXPERIMENT

1
INTRODUCTION

This report presents a summary and preliminary engineering assessment of the aircraft synthetic aperture radar (SAR) imagery collected during the 1984 SAR Internal Wave Signature Experiment (SARSEX). This experiment was conducted between 27 August and 7 September 1984 at a test site located approximately 100 km south of Long Island, New York (see Figure 1). The overall objective of this experiment was to generate a data base which can be used to further investigate SAR imaging of ocean surface patterns, in this case, patterns associated with internal waves which are generated at the edge of the Continental Shelf.

During SARSEX, the ERIM/CCRS CV-580 X- and L-band SAR System was flown over the test area while a variety of ship- and buoy-based oceanographic measurements were being collected by the R/V Cape and USNS Bartlett. For a more detailed description of the SARSEX experiment plan, the reader is referred to Gasparovic, et al. (1984).

During the 12-day SARSEX experiment, ten data collection missions were flown by the CV-580 SAR System. A total of 88 passes of SAR data were collected, 65 of internal wave surface patterns and 23 over the calibrated corner reflector array.

This data description report contains six chapters, including this introduction. Chapter 2 presents an executive summary which outlines the contents of this report. Chapter 3 describes the CV-580 SAR System. Chapter 4 presents a description of the SAR data set collected during SARSEX, and presents representative examples of the SAR imagery. Chapter 5 presents a preliminary engineering assessment of the SAR imagery. Finally, Chapter 6 presents recommendations for further processing and analysis of the SAR data set collected during SARSEX.
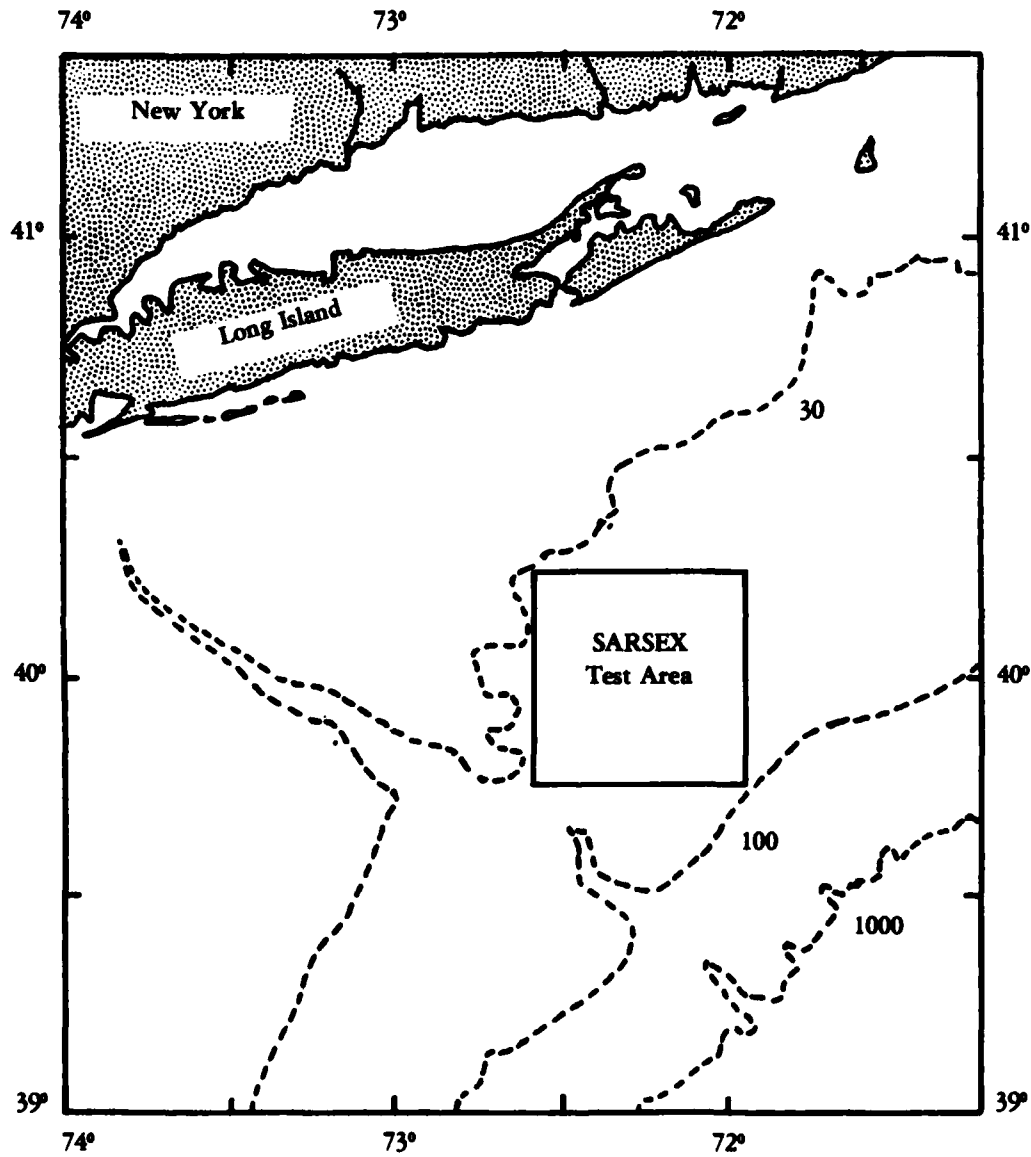
Figure 1. Location of SARSEX Test Area (After Gasparovic, et al., 1984)

2
EXECUTIVE SUMMARY

The SAR Internal Wave Signature Experiment (SARSEX) is an ocean-ographic experiment sponsored by the Office of Naval Research (ONR) to investigate synthetic aperture radar (SAR) imaging of internal wave surface patterns. The objectives of this experiment are to:

1. Investigate the basic hydrodynamic and electromagnetic mech-anisms responsible for imaging of internal wave surface pat-terns by SAR,

2. Test theories and models for quantitative predictions of internal wave signatures from oceanic and radar parameters, and

3. Quantify the range of internal wave-induced current modula-tions that are observable in SAR images.

A preliminary analysis of the SARSEX data set indicates that these objectives are achievable (Apel, et al., 1985).

This report summarizes the data collection and processing activ-ities conducted to date by scientists and engineers at the Environmental Research Institute of Michigan (ERIM). These activ-ities include:

1. *Planning for and coordination of ten SAR data collection missions during the August/September 1984 SARSEX study,*

2. *Deployment of a calibrated corner reflector array at Grumman's Peconic River Airport,*

3. *Optical processing of all optically-recorded SAR data,*

4. *Digital processing of selected scenes of digitally-recorded SAR data,*

3

5. Performing an engineering evaluation of the optically and digitally processed SAR imagery and SAR calibration signals, and

6. Performing a preliminary analysis on the SAR imagery collected during SARSEX.

It also discusses in detail the data processing, and analysis activities which will be conducted at ERIM on the SARSEX data set.

The ERIM/CCRS CV-580 SAR System was used for the SARSEX experiment. A total of 88 passes of X- and L-band SAR imagery were collected during ten missions, 65 over the SARSEX test site and 23 over the calibrated corner reflector array. Table 1 summarizes these SAR data collection flights. The SAR was configured to transmit and receive the same polarization (VV or HH), to optically record two channels of data with a swath width of 10.8 km (slant range) and digitally record two channels of data with a swath width of 6.1 km (slant range).

The SAR system and aircraft flight parameters for each mission are summarized in this report. Figures with the ground locations of all SAR passes are presented. The types and sizes of the calibrated corner reflectors which were deployed at the Grumman Peconic River Airport are presented, as are their locations.

All optically-recorded data have been processed into image films. Copies of this imagery are archived at ERIM, the Applied Physics Laboratory (APL) and the Defence Research Establishment-Pacific (DREP). A selected subset of data digitally recorded on high density digital tape (HDDT) have been transcribed to computer compatible tape (CCT). Both ERIM and APL are presently processing these data into imagery. Representative examples of this imagery are presented in this report.

TABLE 1
SUMMARY OF SAR DATA COLLECTED DURING SARSEX

Mission	Date	Time (EDT)	Internal Wave Passes	Calibration Passes
SARSEX-1	8-28-84	10:35-12:23	6	0
SARSEX-2	8-28-84	16:45-17:25	0	3
SARSEX-3	8-30-84	14:05-17:11	7	2
SARSEX-4	8-31-84	16:29-19:54	9	2
SARSEX-5	9-03-84	13:27-17:07	9	3
SARSEX-6	9-04-84	14:54-18:33	7	4
SARSEX-7	9-05-84	13:19-17:32	9	3
SARSEX-8	9-06-84	8:47-12:12	8	2
SARSEX-9	9-06-84	14:35-16:42	6	0
SARSEX-10	9-07-84	10:26-12:53	4	4
		Total	65	23

A preliminary engineering assessment of the SAR data set has been completed. This assessment indicates that the SAR data collected are of high quality, with few SAR system malfunctions occuring during the ten missions. Image quality measurements (system impulse response resolution and sidelobe level, background noise, signal-to-noise ratio, clutter-to-noise ratio, and image contrast) were equal to or better than similar measurements made on SAR data collected during previous oceanographic experiments. The analysis of the intensities of the SAR signal histories from surface internal wave patterns imaged during SARSEX-4 indicate that the intensities from both X- and L-band were within the linear response region of the SAR system.

Some initial analyses have been performed on the SAR data collected on 31 August 1984 during SARSEX-4, Passes 5 and 8. The L-band data from Passes 5 and 8 have been calibrated, while the X-band data from Pass 5 has been calibrated. Comparisons of the scans along both the Bartlett's and Cape's tracks resulted in the following observations:

1. The L-band internal wave signature has a definite increase and decrease relative to the background, while the X-band signature is characterized by an increase only,

2. The magnitude of the L-band signature is greater than the X-band signature,

3. The peaks of the X- and L-band signatures do not always occur in the same position, and

4. The L-band signature is greater for the range-traveling internal wave (Pass 5) than it is for the azimuth-traveling case (Pass 8).

Hydrodynamic inputs were obtained from the Applied Physics Laboratory and inputted into a hydrodynamic/electromagnetic

interaction model. The modeled results compared quite favorably to the observed L-band imagery, but did not compare well with the X-band imagery.

Recommendations for future SAR data processing and analysis activities are presented. SAR image processing priorities are identified to meet the SARSEX analysis goals. SAR calibration is discussed, and examples of calibrated backscatter scans of internal wave signatures are presented.

Proposed analysis activities will focus on ERIM's SAR ocean imaging model. These activities will include further theoretical development and validation of the model and comparison of model outputs to SAR imagery collected during SARSEX.

The further theoretical development of this model will focus on non-Bragg or quasi-specular scattering from the ocean surface. This phenomena was observed on imagery collected during SARSEX-8. Efforts will also be made to further validate the "background noise" component of the theoretical model, through analysis of the wind and surface gravity wave data collected during SARSEX. SAR data will also be compared to surface CW radar data, video camera data and airborne laser scatterometer data in an effort to further understand microwave backscattering from the ocean surface.

The overall model will then be exercised and the results compared to calibrated SAR image intensity scans. These empirical comparisons will be used to study the relationship between:

1. SAR surface internal wave signatures and surface strain rate,

2. SAR surface internal wave signatures and wind speed and direction,

3. SAR surface internal wave signatures and surface gravity waves,

4. SAR surface internal wave signatures and SAR incidence angles,

5.   SAR surface internal wave signatures and SAR azimuth angles, and

6.   SAR surface internal wave signatures and radar frequency.

In the above six analyses, hydrodynamic inputs for ERIM's SAR imaging model will be provided by other team investigators.

It is anticipated that the activities outlined above will occur over a two-year period. Through the analysis of the SARSEX data, it is expected that a greater understanding of the SAR imaging mechanisms responsible for detection of ocean surface patterns will evolve.

3
CV-580 SAR SYSTEM DESCRIPTION

From 1978 through 1984, ERIM operated a multifrequency and multipolarization SAR in conjunction with CCRS. This SAR system was maintained through a leasing agreement between ERIM and CCRS and is called the CV-580 SAR System. This facility was used extensively over the past six years in a variety of oceanographic and terrestrial research programs. The leasing agreement between ERIM expired at the end of CY84. At this time, the CV-580 SAR System is not available for U.S. Government sponsored research programs. Efforts are underway to transfer this system into a U.S.-owned aircraft (Shuchman, et al., 1984).

The CV-580 SAR System was essentially an X-band radar to which an L-band and a C-band capability was added. Because of this configuration, the X-band channels were always available, and, in addition, one could operate either the L-band or the C-band channels simultaneously with the X-band channel. For each frequency band, two orthogonal polarizations were available. The radar could transmit either horizontal or vertical polarization and receive both the parallel- and perpendicular-polarized returns. The radar antenna could be pointed so as to image on either side of the aircraft. Table 2 summarizes the relevant radar parameters for this system.

Figure 2 presents a functional diagram of the CV-580 SAR System. The major components of the SAR are its antennas, the transmitters and receivers, the calibration signal generator, the optical film recorders, the digital tape recorder and the X-band real-time processor.

Figure 3 presents a more detailed diagram of the reference oscillators, transmitters and receivers of the SAR system. This diagram shows how the L-band and C-band wavelengths are returned to X-band.

TABLE 2
CV-580 SAR SYSTEM PARAMETERS

Parameter	X-Band	C-Band	L-Band
Center Frequency	9.35 GHz	5.3 GHz	1.245 GHz
Wavelength	3.2 cm	5.7 cm	24.0 cm
Nominal Altitude	7 km	7 km	7 km
Nominal Platform Velocity	250 knots	250 knots	250 knots
Swath Width/Channel (slant range)	5.2 km	5.2 km	5.2 km
Incidence Angle	0° - 90°	0° - 90°	0° - 90°
FM Rate	33.3 MHz/μsec	33.3 MHz/μsec	33.3 MHz/μsec
Pulse Length	2.7 μsec	2.7 μsec	1.8 μsec
Bandwidth	89 MHz	89 MHz	60 MHz
Azimuth Beamwidth	1.15°	2.5°	7°
Nominal Slant Range Resolution	3 m	3 m	3 m
Nominal Azimuth Resolution	3 m	3 m	3 m
Azimuth Scale Factor (Approx.)	15,000	15,000	41,500
Range Scale Factor (Approx.)	196,000	196,000	196,000
Data Recording	Real Time Image	Real Time Image	Optical Signal Film
	Opt. Sig. Film	Opt. Sig. Film	Digital Tape
	Dig.Tape (HDDT)	Digital Tape	
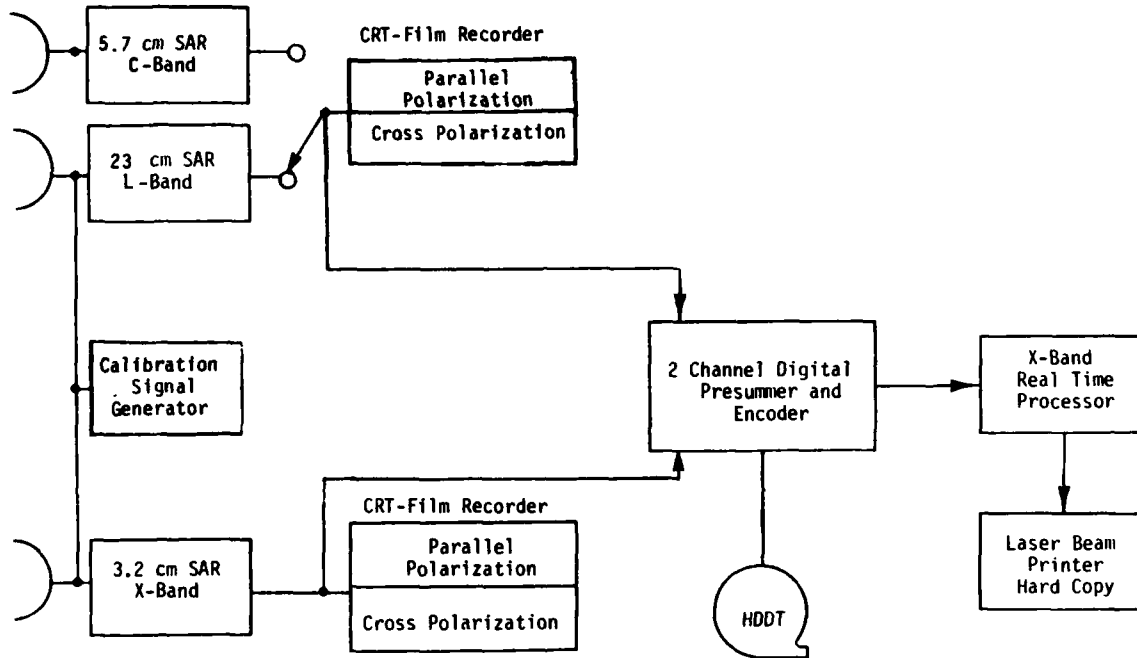
Figure 2. Schematic Diagram of CV-580 X/C/L SAR System

11
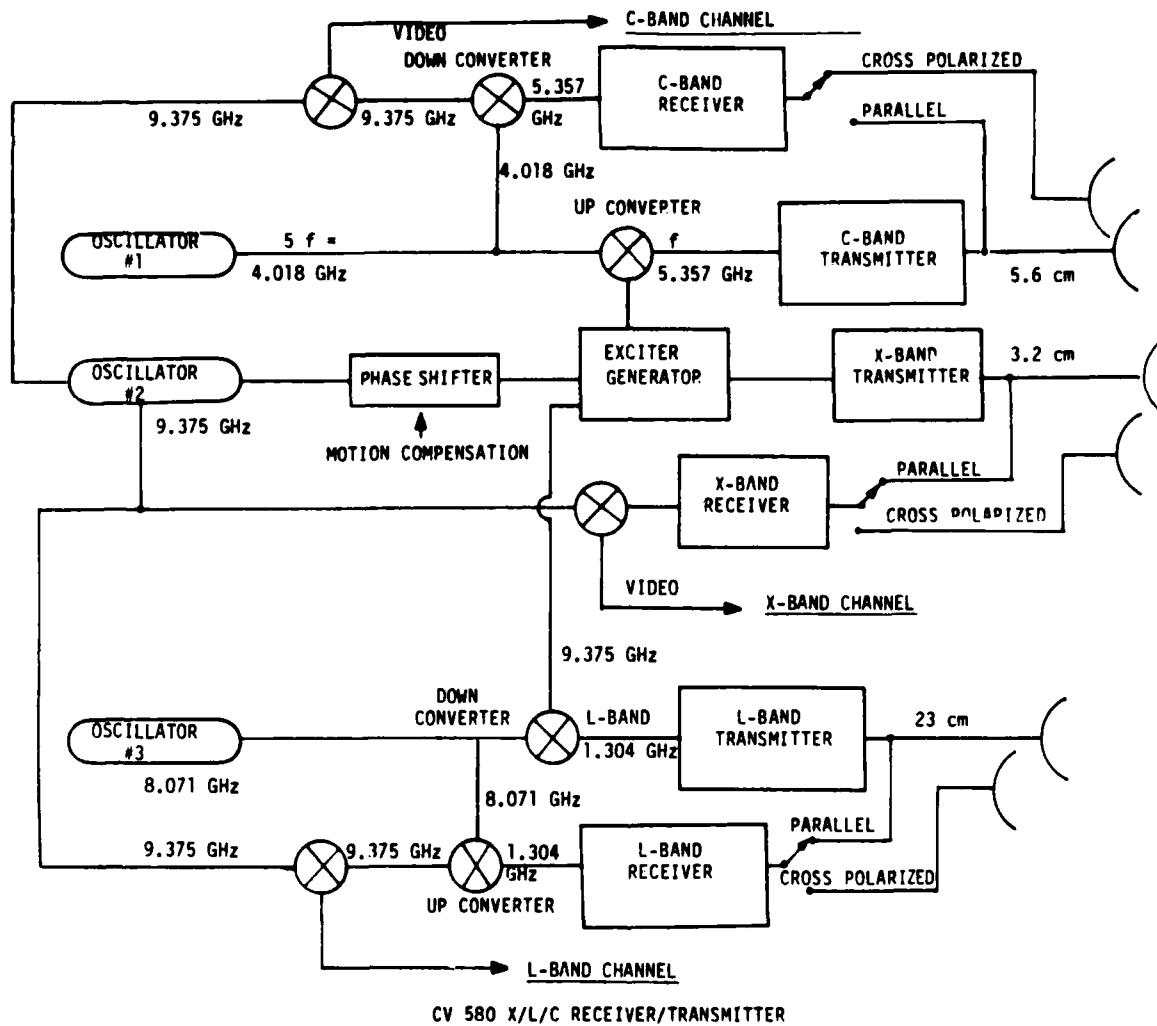
Figure 3. Schematic Diagram of CV-580 SAR Receiver/Transmitter

Figure 4 presents a diagram of the calibration signal generator (CSG) system, which is used as a monitoring and reference source for the periodic verification of the SAR's system transfer function. The calibration signal generator produces synthetic target signals which are added into the radar receiver (Walker and Larson, 1981; Larson, et al., 1981; 1982; 1985). The form of the synthetic target corresponds to a given range, and the intensity is controlled by an accurately calibrated R.F. attenuator. At specific times during the imaging flight, the calibration signals are inserted into the receiver at the antenna connection, so that the radar receiver detects them as a radar return. Using a sequence of such signals with different intensities, along with the processed signals from the corner reflectors, a calibration curve can be produced of output signal power versus radar cross section (σ_0). When combined with measurements of precision corner reflectors, CSG measurements can be used to achieve absolute calibration of the SAR (see Walker and Larson, 1981; or Larson, et al., 1985). The synthetic targets from the CSG can be recorded both optically and digitally, but only at X- and L-band.

Figure 5 presents an optically processed L-band image of the calibration signals. Table 3 summarizes the signal power and equivalent radar cross sections for these calibration signals.

The three SARs which comprised the CV-580 SAR System are similar in that they all use the synthetic aperture technique to produce imagery with fine cross-range resolution. These SARs used pulse compression to achieve fine resolution in the range dimension. Each recording channel was adjusted to produce imagery of a selected swath parallel to the flight direction. The width of the imaged swath was determined by the range increment of signals displayed on the recording system. The displacement of the recorded swath from the flight line was adjustable by the radar operator. The CV-580 SAR System is extensively described by Rawson, et al. (1975) and CCRS (1983).

13
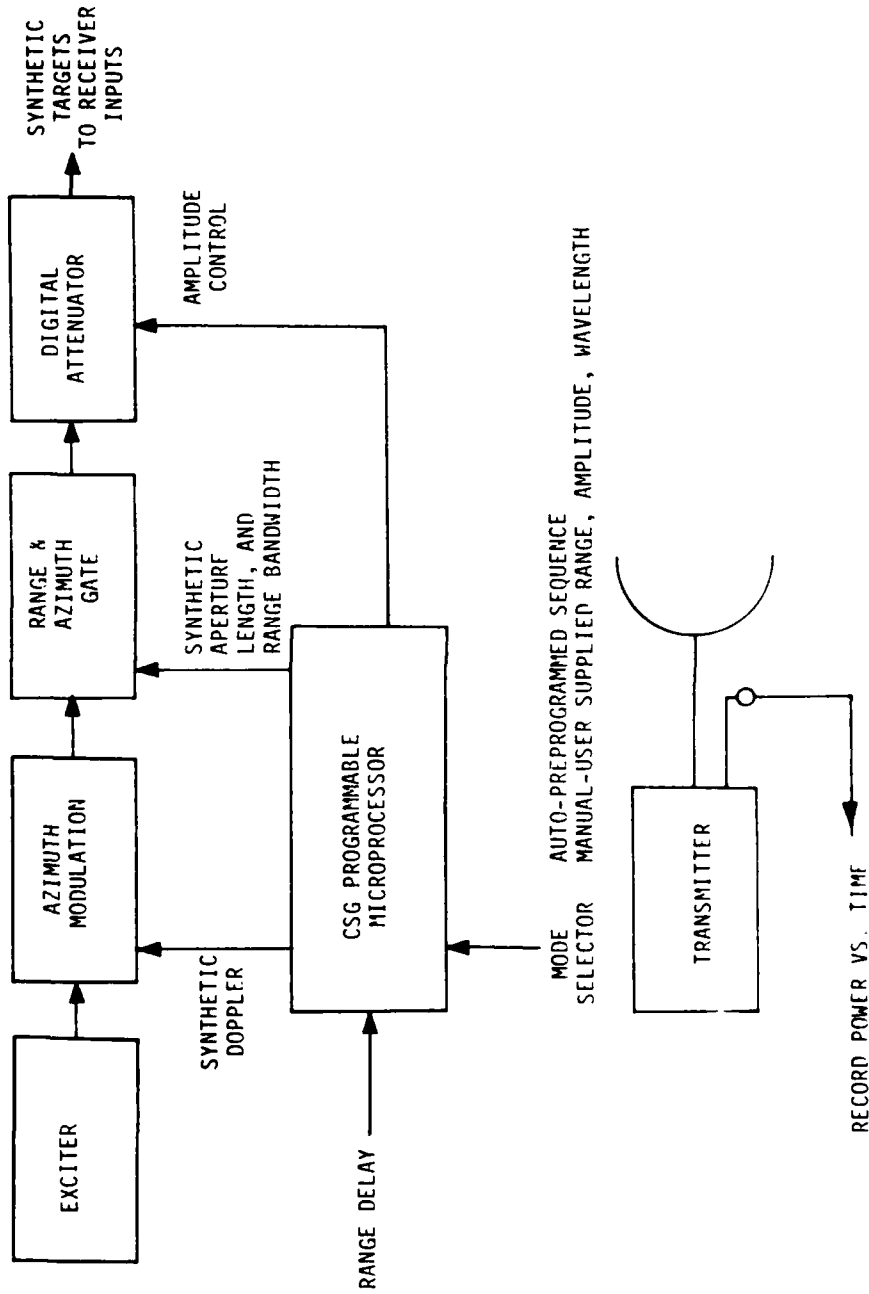
Figure 4. Schematic Diagram of CV-580 SAR X/L Calibration Signal Generator

14
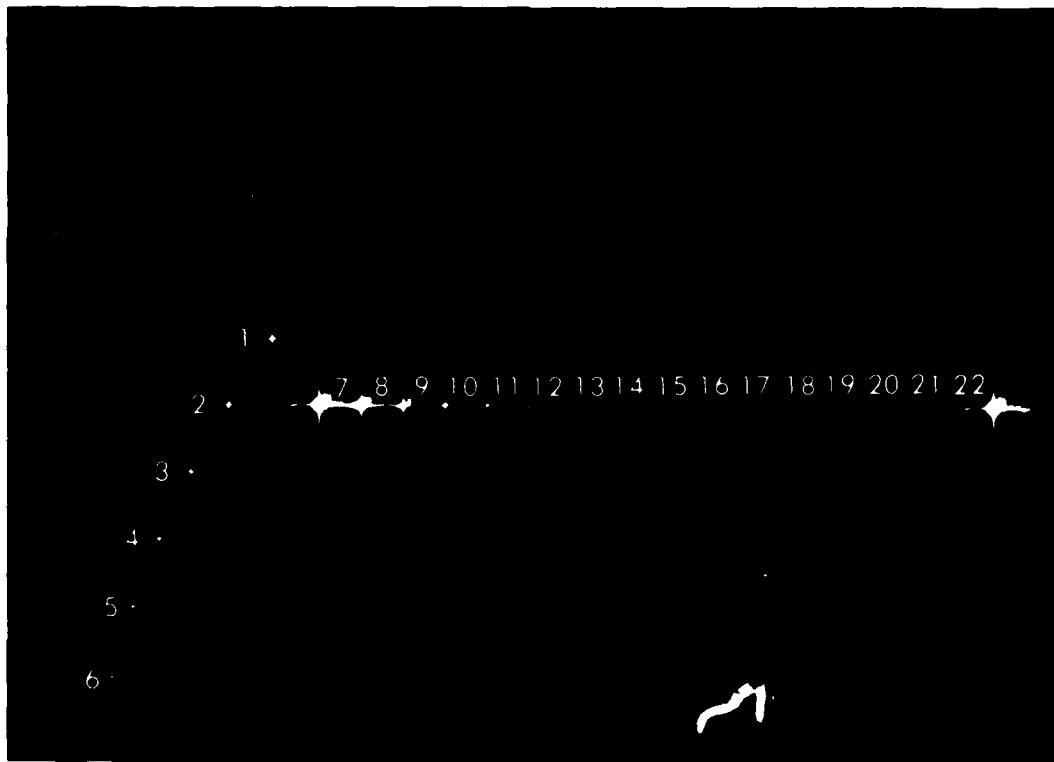
Figure 5.   Image of L-band Calibration Signals

TABLE 3
INTERNAL CALIBRATION SIGNAL POWER AND EQUIVALENT RADAR
CROSS SECTIONS AT A RANGE OF 10 KM

Cal. Signal Number	Cal. Signal Power in dB Relative to 1 mW	Equivalent Cross Section 10 km in dB Relative to 1 m^2
1-6*	-95	15
7	-65	45
8	-70	40
9	-75	35
10	-80	30
11	-85	25
12	-90	20
13	-95	15
14	-100	10
15	-105	5
16	-110	0
17	-115	-5
18	-120	-10
19	-125	-15
20	-130	-20
21	-135	-25
22	-95	15

*Cal signals 1-6 have the same power and are injected at a variable range. Signals 7-22 are at the same range.

The SAR phase histories were recorded onboard the aircraft both optically on 70 mm film and digitally on high density digital tape (HDDT). The optical recording system recorded four data channels, while the digital system was restricted to recording only two of the four data channels during data collection. In addition to the optical and digital recorders, a real-time digital SAR processor on-board the CV-580 generated X-band imagery. The real-time imagery was not intended to be of high quality, but provided "quick-look" data necessary for system performance evaluation and planning pur-poses during data collection missions. It was also used to select digital data of interest for subsequent processing and analysis. Table 4 presents the various data recording options available on the system. Figure 6 schematically illustrates the various SAR data re-cording and processing options.

TABLE 4
PRESENT X-, C- AND L-BAND SAR DATA RECORDING CAPABILITY

SAR Mode	Optical Recording (2 Recorders)		Digital Recording (A+B)			Real-Time Processor		Comments
	Channels	Swath	Channels	Swath	Resolution	Channels	Swath	
X-band wide swath	1 (2 films)	20 km	A and B	12 km 20 km	3 m 6 m	Near range 12 km	6 km	Data buffer required
4 channel X, C or X, L	4	5.2 km	A any channel B X, C, L, like, cross	6 km	3 m	X- or C-band Channel A only	6 km	Scene illumination depends on altitude and incidence angle range
3 channel X, C or X, L	3	10 km 5.2 km	A and B, wide swath channel or A, B independent assignment	12 km 6 km	3 m 6 m	X- or C-band Channel A only	6 km	Wide swath channel illumination strongly affected by antenna pattern and imaging geometry
2 channel X, C or X, L	2	10 km	A and B (either channel)	12 km	3 m	Channel A if not L-band	6 km	As above

Note: 1. The extended swath recording modes enhance the system signal to noise for weak returns on the optical recordings only.

2. An X-band signal film will contain approximately 215 nautical miles of data, a high density digital tape will contain approximately 130 nautical miles of data.

18
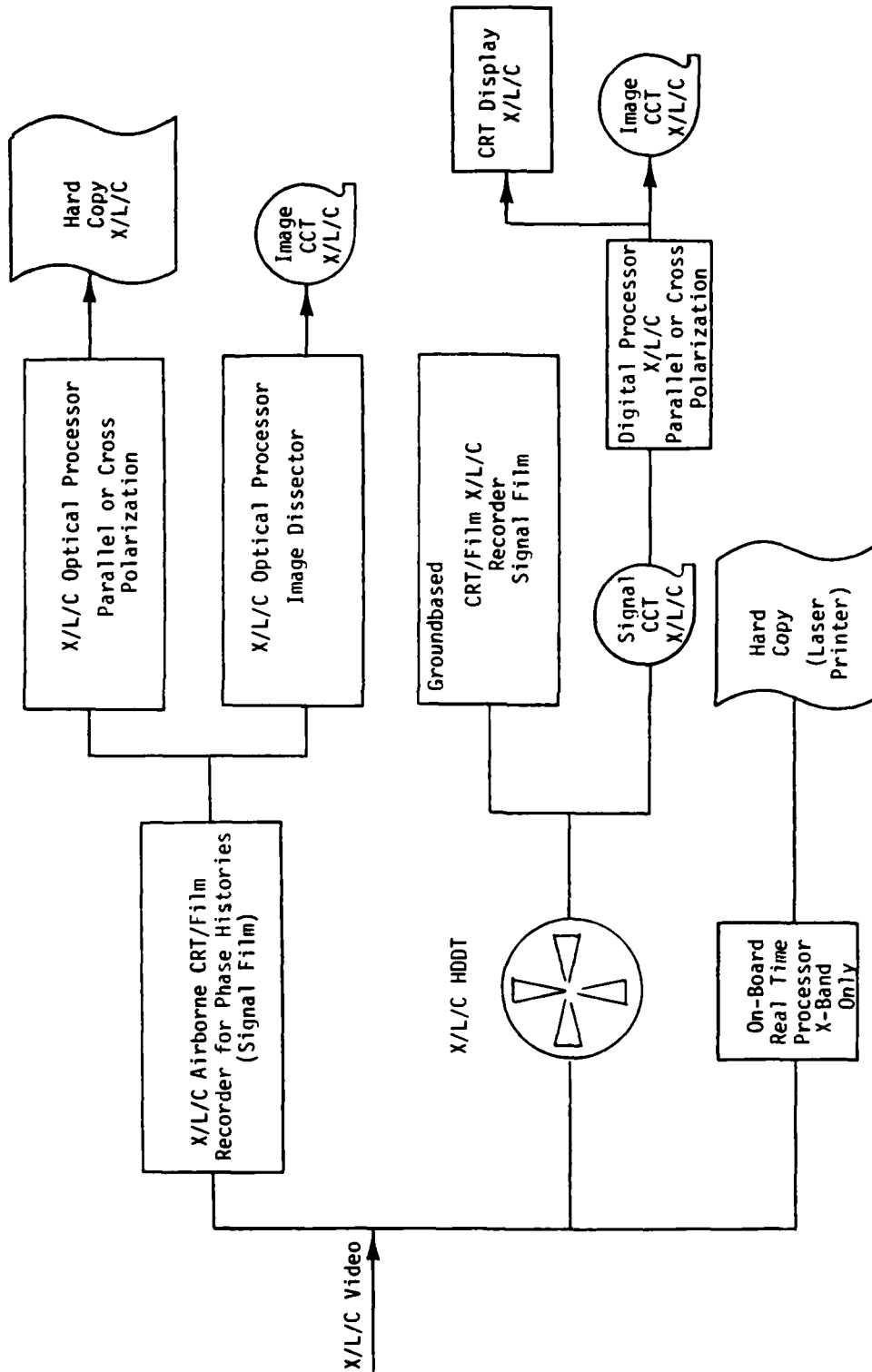
Figure 6.   CV-580 SAR Signal Recording and Processing Options

4
DATA DESCRIPTION

This chapter presents a summary of all SAR data collection missions conducted during SARSEX, a description of all processing of the SAR data performed to date, and a discussion of the calibrated reflectors deployed during SARSEX. The following sections present descriptions of the various SAR missions, as well as diagrams of the locations of the SAR passes and representative SAR imagery.

4.1 SAR DATA

Twelve data collection missions were flown during which SAR imagery were collected. These missions are summarized in Table 1. During SARSEX, the CV-580 SAR system collected X- and L-band data. It was configured in its two-frequency, narrow-swath mode when it collected imagery over the calibrated corner reflector array and was configured in its two-frequency, wide-swath mode when it collected data over the internal wave test site. The wide-swath mode was used in order to have a better chance of imaging the USNS _Bartlett_ and R/V _Cape_ during the experiment.

In its two-frequency, narrow swath mode, the SAR collects four channels of imagery, each with a slant range swath width of 5.4 km to 6.1 km, depending on how the data are recorded. The polarization of the transmitted microwave radiation was primarily horizontal (H), with some vertical (V) being transmitted during SARSEX-10. Both horizontal and vertical polarizations were received, resulting in four channels of SAR data (X_{HH}, X_{HV}, L_{HH}, L_{HV} or X_{VV}, X_{VH}, L_{VV}, L_{VH}). Two of these channels (X_{HH}, L_{HH} or X_{VV}, L_{VV}) were recorded digitally. After every pass, calibration signals were recorded optically and digitally.

In its two-frequency, two-channel mode, the SAR collects two channels of imagery, each with a swath width of 10.8 km in slant

21

range. During SARSEX, horizontally-polarized microwave energy was both transmitted and received with the SAR in this mode (X_{HH}, L_{HH}). Only the first 6.1 km (slant range) of the 10.8 km are recorded digitally.

All SAR data optically recorded during SARSEX have been survey-optically-processed at ERIM. Original output negatives of all imagery are archived at ERIM, the Applied Physics Laboratory (APL) and the Defense Research Establishment-Pacific (DREP). A select set of SAR data digitally recorded on high density digital tape have been transcribed to computer compatible tape and digitally processed into imagery. Representative optically- and digitally-processed imagery will be presented in this report.

Table 5 contains a summary of the preliminary engineering assessment of the SAR data collected during SARSEX. An in-depth discussion of this assessment is presented in Chapter 5. Shown in Table 5 are the mission, pass number, location of the pass, the image quality of the optically processed imagery, and the quality of the calibration data for that pass. The image and calibration data quality ratings are intended to provide a general guide as to the suitability of the data for further analysis. A three-star (***) rating implies the data are of the highest quality, and suitable for further analysis. A two-star (**) rating implies there are some potential problems with the data, but that they still may be suitable for further analysis. A one star (*) or no star rating implies the data are of low quality, and probably not suitable for further analysis. Note that the ratings listed in Table 5 were based primarily upon the analysis of optically-processed imagery. Comparisons between a limited set of optically- and digitally-processed imagery indicates that the digitally recorded data may be of higher quality than the optically processed data. Therefore, the ratings in Table 5 should be used as a general guide only. Chapter 5 contains an in-depth discusssion on how these ratings were obtained.

TABLE 5
SUMMARY OF SARSEX-SAR DATA QUALITY*

Mission	Pass	Area	Optical Image Quality		Calibration Data Quality	
			X-Band	L-Band	X-Band	L-Band
SARSEX-1	1	IW	***	***	**	**
	2	IW	***	***	**	**
	3	IW	***	***		
	4	IW	***	***	**	**
	5	IW	*	**	*	*
	6	IW	*	**	*	*
SARSEX-2	1	CA	***			
	2	CA	***	***	***	***
	3	CA	*	***		
SARSEX-3	1	CA	***	***	***	***
	2	CA	***	***	**	***
	3	IW	***	***	***	***
	4	IW	***	***	***	***
	5	IW	***	***	***	***
	6	IW	***	***	***	***
	7	IW	***	***	***	***
	8	IW	***	***	***	***
	9	IW	***	***	***	***
SARSEX-4	1	IW	**	***	***	***
	2	IW	***	***	***	***
	3	IW	**	***	***	***
	4	IW	**	***	***	***
	5	IW	**	***	***	***
	6	IW	***	***	***	***
	7	IW	**	***	***	***
	8	IW	***	***	***	***
	9	IW	***	***	***	***
	10	Aborted				
	11	CA	***	***	***	***
	12	CA	***	***	***	***

+ Quality Key
*** High Quality, no problem with data
 ** Medium Quality, some potential problems with data
  * Low Quality, definite problems with data.

TABLE 5
SUMMARY OF SARSEX-SAR DATA QUALITY (Continued)

Mission	Pass	Area	Optical Image Quality		Calibration Data Quality	
			X-Band	L-Band	X-Band	L-Band
SARSEX-5	1	CA	***	***	**	**
	2	CA	***	***	**	**
	3	CA	**	***	**	**
	4	IW	***	***	**	**
	5	IW	***	***	**	**
	6	IW	***	***	**	**
	7	IW	***	***	**	**
	8	IW	**	***	**	**
	9	IW	**	***	**	**
	10	IW	***	***	**	**
	11	IW	***	***	**	**
	12	IW	***	***	**	**
SARSEX-6	1	CA	***	***	***	***
	2	CA	***	***	***	***
	3	CA	***	***	**	**
	4	CA	***	***	***	***
	5	IW	***	***	***	***
	6	IW	***	***	***	***
	7	IW	***	***	***	***
	8	IW	***	***	***	***
	9	IW	***	***	***	***
	10	IW	***	***	***	***
	11	IW	***	***	***	***
SARSEX-7	1	CA	***	***	***	***
	2	CA	***	***	**	**
	3	CA	***	***	***	***
	4	IW	***	***	***	**
	5	IW	**	***	***	***
	6	IW	***	***	**	***
	7	IW	***	***	**	***
	8	IW	***	***	**	***
	9	IW	***			***
	10	IW	***	***	**	***
	11	IW	***	***	***	***
	12	IW	***	***	***	***

+   Quality Key
*** High Quality, no problem with data
** Medium Quality, some potential problems with data
*   Low Quality, definite problems with data.

24

TABLE 5
SUMMARY OF SARSEX-SAR DATA QUALITY (Concluded)

Mission	Pass	Area	Optical Image Quality		Calibration Data Quality	
			X-Band	L-Band	X-Band	L-Band
SARSEX-8	1	CA	★★★	★★★	★★	★★★
	2	CA	★★★	★★★	★★	★★★
	3	IW	★★★	★★★	★★	★★★
	4	IW	★★★	★★★	★★	★★★
	5	IW	★★★	★★★	★★	★★★
	6	IW	★★★	★★★	★★	★★★
	7	IW	★★★	★★★	★★	★★★
	8	IW	★★★	★★★	★★	★★★
	9	IW	★★★	★★★	★★	★★★
	10	IW	★★★	★★★	★★	★★★
SARSEX-9	1	IW	★★★	★★★	★★	★★★
	2	IW	★★★	★★★	★★	★★★
	3	IW	★★★	★★★	★★	★★★
	4	IW	★★★	★★★	★★	★★★
	5	IW	★★★	★★★	★★	★★
	6	IW	★★★	★★★	★★	★★★
SARSEX-10	1	CA	★★★	★★★	★★	★★★
	2	CA	★★★	★★★	★★	★★★
	3	CA	★★★	★★★	★★	★★★
	4	CA	★★★	★★★	★★	★★★
	5	IW	★★★	★★★	★★	★★★
	6	IW	★★★	★★★	★★	★★★
	7	IW	★★★	★★★	★★	★★★
	8	IW	★★★	★★★	★★	★★★

+ Quality Key
★★★ High Quality, no problem with data
★★ Medium Quality, some potential problems with data
★ Low Quality, definite problems with data.

In the remainder of this section, we will discuss the SAR data collected during SARSEX. For each SAR mission, a table summarizing the aircraft and SAR parameters, and diagrams of the locations of the SAR passes are presented. Also presented are representative examples of the SAR images of the internal wave surface patterns.

4.1.1 SARSEX-1 (28 August 1984 - 10:25 to 12:25 EDT)

The purpose of this mission was to perform a test of the communication and flight procedures for the SAR data collection portion of the SARSEX experiment. The CV-580 was flown along the same flight line over the SARSEX area for six passes. The antenna look direction was switched between passes so that the SAR was viewing the same general area during each pass.

The aircraft and SAR system parameters for SARSEX-1 are summarized in Table 6. The flight lines are presented in Figure 7. Also presented in Figure 7 are the positions of the four moored buoys deployed by NORDA which contained an array of acoustic current meters. The SAR passes were configured to image over the internal wave packet which was being measured by the RV-Cape and USNS Bartlett at that time, which was not necessarily the packet nearest the moored buoys.

During the earlier passes of SARSEX-1, the quality of the optically-processed X- and L-band imagery was excellent. Imagery from the last two passes was of fair to poor quality due to an apparent radar malfunction. No calibration signals were recorded after Passes 3 or 6 and the calibration signals after Pass 5 were incomplete.

TABLE 6. SUMMARY OF SAR AND AIRCRAFT PARAMETERS DURING SARSEX-1 (28 AUGUST 1984).

CV-580 AIRCRAFT PARAMETERS

PASS	HEADING (TRUE)	VELOCITY (KNOTS)	ALTITUDE (FEET)	START TIME (EDT)	STOP TIME (EDT)	START LATITUDE	START LONGITUDE	STOP LATITUDE	STOP LONGITUDE
1	250	274	22000	10:35:27	10:39:53	40:05.1	72:12.1	39:58.1	72:37.1
2	70	270	22000	10:53:10	10:57:39	39:58.6	72:36.7	40:05.3	72:12.1
3	250	269	22000	11:13:06	11:21:04	40:05.0	72:12.5	33:58.3	72:36.8
4	70	259	22000	11:33:16	11:37:54	39:59.1	72:37.0	10:06.0	72:12.6
5	250	276	22000	11:58:10	12:02:35	40:05.5	72:12.3	39:58.4	72:37.1
6	70	279	22000	12:18:48	12:23:09	39:58.8	72:37.1	40:05.5	72:12.5

SAR PARAMETERS

PASS	WAVELENGTHS	SAR MODE	LOOK	ANTENNA DEPRESSION ANGLE	POLARIZATION TRANS	POLARIZATION REC	DIGITAL CHANNEL	RANGE DELAY (USEC)	GAIN SETTINGS (dB ATTENUATION) X-B OPT.	L-B OPT.	X-D DIG.	L-B DIG.	TRANS POWER (WATTS) X-B	L-B
1	X,L	WIDE-SWATH	R	35	H	H	XHH,LHH	44	20	39	6	34	1682	5105
2	X,L	WIDE-SWATH	L	30	H	H	XHH,LHH	44	17	43	5	38	1707	5537
3	X,L	WIDE-SWATH	R	30	H	H	XHH,LHH	45	18	43	4	27	1677	5749
4	X,L	WIDE-SWATH	L	30	H	H	XHH,LHH	45	18	44	4	27	1736	5952
5	X,L	WIDE-SWATH	R	30	H	H	XHH,LHH	45	17	44	4	27	1663	5780
6	X,L	WIDE-SWATH	L	30	H	H	XHH,LHH	45	17	44	4	27	1757	5927
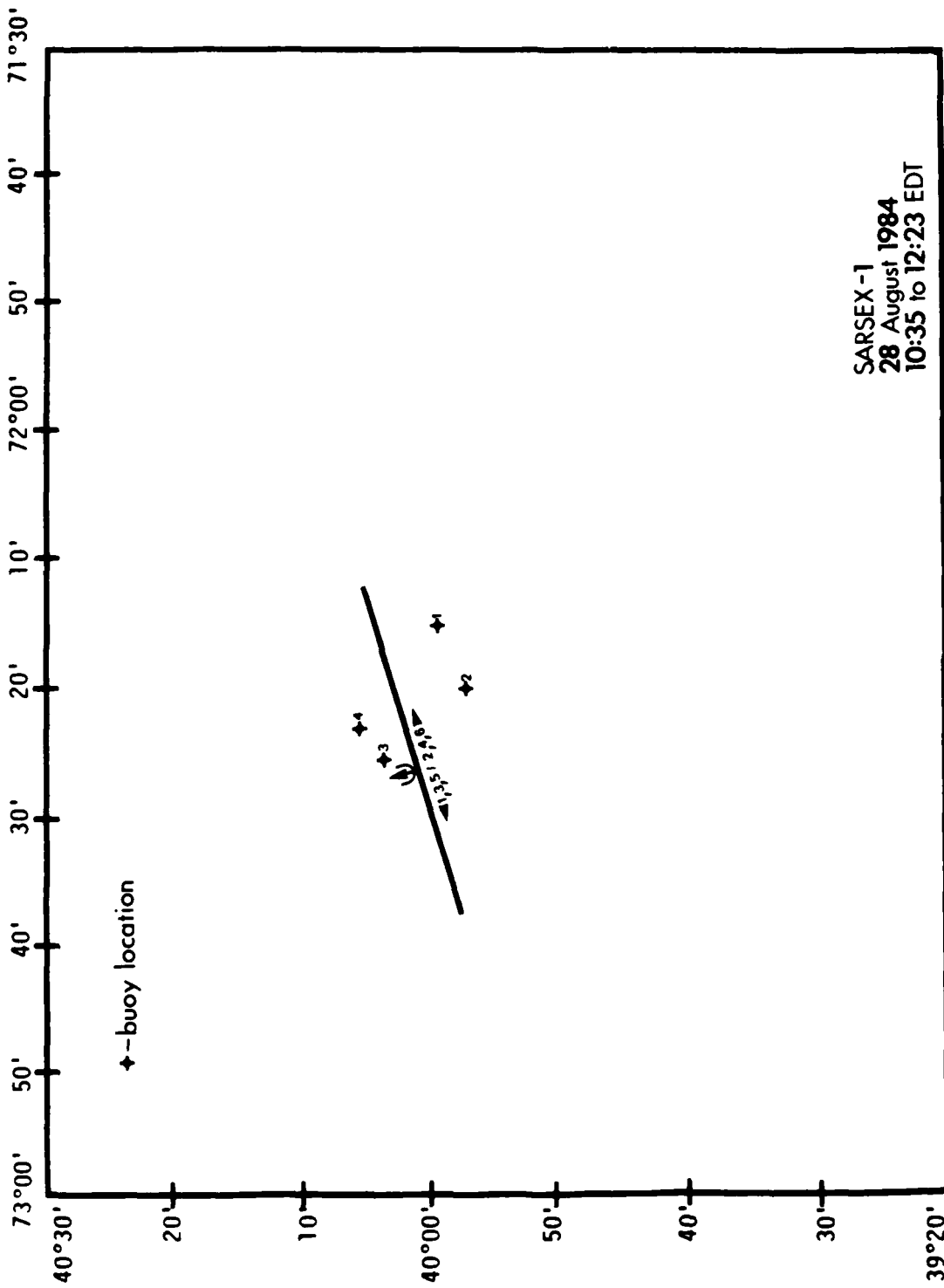
Figure 7. Locations of Aircraft Ground Tracks During SARSEX-1, Passes 1-6

4.1.2 SARSEX-2 (28 August 1984 - 16:45 to 17:25 EDT)

The purpose of this mission was to collect multiple-incidence angle SAR imagery over the SARSEX test site. Due to conflicts with other vessels within the operational area, the SAR data collection had to be cancelled. Instead, three passes were made over the calibration array.

The aircraft and SAR system parameters for SARSEX-2 are summarized in Table 7. The flight lines are presented in Figure 8. Overall, the optically-processed imagery from SARSEX-2 was of excellent quality. Several radar malfunctions occurred. No L-band data were recorded during Pass 1 and the X-band data from Pass 3 exhibited severe defocusing due to uncompensated motion of the aircraft. Calibration signals were recorded optically only after Pass 2.

30

TABLE 7. SUMMARY OF SAR AND AIRCRAFT PARAMETERS DURING SARSEX-2 (28 AUGUST 1984).

CV-580 AIRCRAFT PARAMETERS

PASS	HEADING (TRUE)	VELOCITY (KNOTS)	ALTITUDE (FEET)	START TIME (EDT)	STOP TIME (EDT)	START LATITUDE	START LONGITUDE	STOP LATITUDE	STOP LONGITUDE
1	311	255	22000	16:44:40	16:49:22	40:45.9	72:40.1	40:58.9	73:00.1
2	131	278	22000	17:01:11	17:05:29	40:58.4	73:00.6	40:45.4	72:40.4
3	311	256	22000	17:21:46	17:25:28	40:45.9	72:39.8	40:59.0	72:59.9

SAR PARAMETERS

PASS	WAVELENGTHS	SAR MODE	LOOK	ANTENNA DEPRESSION ANGLE	POLARIZATION TRANS	REC	DIGITAL CHANNEL	RANGE DELAY (USEC)	GAIN SETTINGS (dB ATTENUATION) X-B OPT.	L-B OPT.	X-B DIG.	L-B DIG.	TRANS POWER (WATTS) X-B	L-B
1	X,L	4-CHANNEL	R	33	H	HV	XHH,LHH	45	18	33	36	52	1630	6056
2	X,L	4-CHANNEL	L	33	H	HV	XHH,LHH	45	21	37	24	52	1580	5713
3	X,L	4-CHANNEL	R	33	H	HV	XHH,LHH	45	21	37	24	52	1643	6528
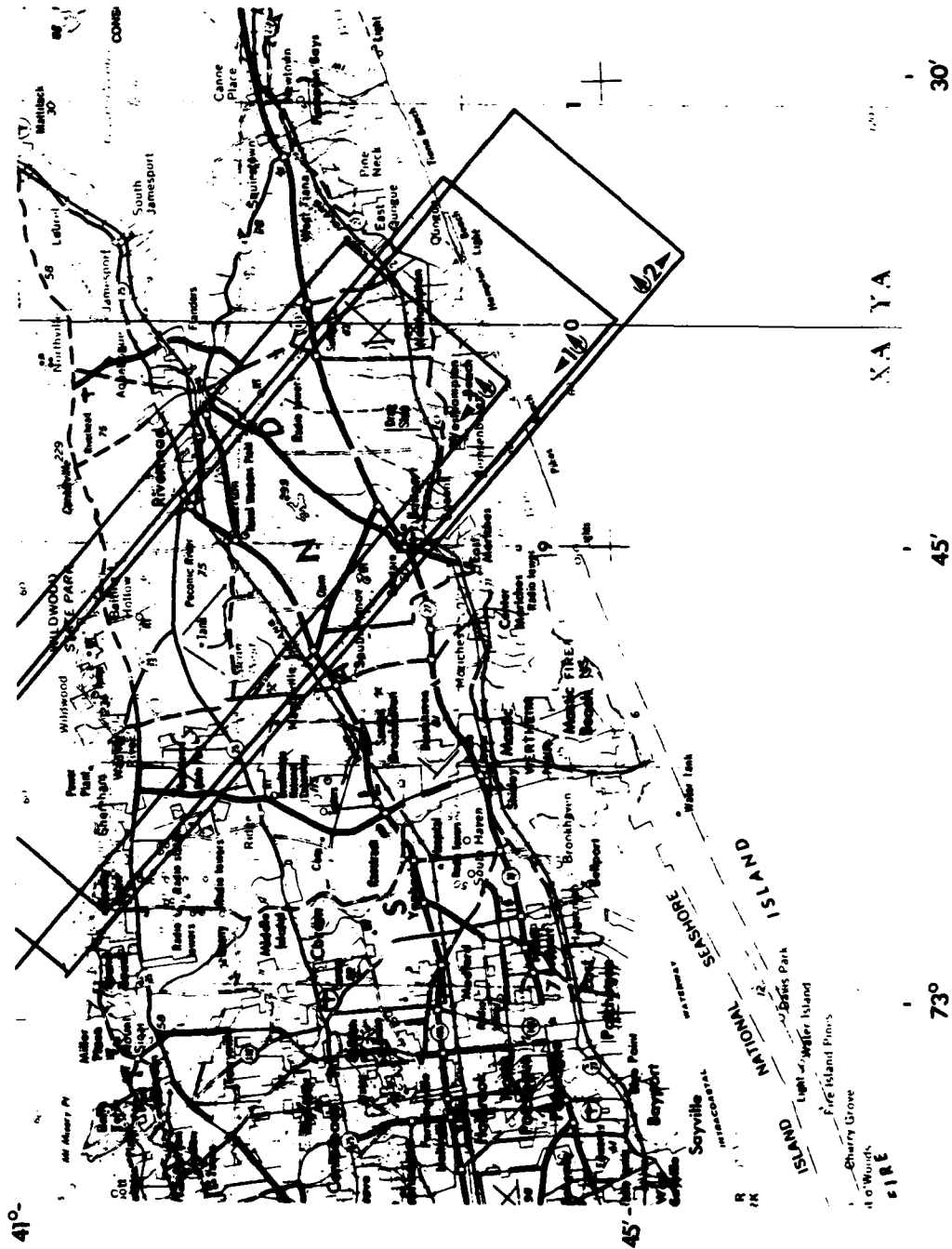
Figure 8. Locations of SAR Ground Coverage During SARSEX-2, Passes 1-3

4.1.3 SARSEX-3 (30 August 1984 - 14:05 to 17:11 EDT)

The purpose of this mission was to collect multiple-incidence angle SAR imagery over the SARSEX test site. Two passes of imagery were collected over the calibration array and seven passes over the SARSEX test site.

The aircraft and SAR system parameters for SARSEX-3 are summarized in Table 8. The flight lines are presented in Figures 9 and 10.

The quality of the optically-processed imagery is good to excellent for both X- and L-bands, and the quality of the calibration data also appears to be high and of acceptable quality.

TABLE 8. SUMMARY OF SAR AND AIRCRAFT PARAMETERS DURING SARSEX-3 (30 AUGUST 1984).

CV-580 AIRCRAFT PARAMETERS

PASS	HEADING (TRUE)	VELOCITY (KNOTS)	ALTITUDE (FEET)	START TIME (EDT)	STOP TIME (EDT)	START LATITUDE	START LONGITUDE	STOP LATITUDE	STOP LONGITUDE
1	311	249	22000	14:05:06	14:09:48	40:46.1	72:40.4	40:58.9	73:00.1
2	131	264	22000	14:23:27	14:27:59	40:58.7	73:00.2	40:45.8	72:40.3
3	178	255	22000	14:48:49	14:53:01	40:00.3	72:17.6	39:42.3	72:16.9
4	250	248	22000	15:08:39	15:13:31	39:52.2	72:07.0	39:45.2	72:31.6
5	250	251	22000	15:36:57	15:41:35	39:51.5	72:07.9	39:44.9	72:31.6
6	250	253	22000	15:58:54	16:03:40	39:51.8	72:06.8	39:44.9	72:31.4
7	250	253	22000	16:22:55	16:27:35	39:51.4	72:07.2	39:44.6	72:31.2
8	160	254	22000	16:43:05	16:47:38	40:03.2	72:21.4	39:44.6	72:12.5
9	340	275	22000	17:06:28	17:10:50	39:44.1	72:12.1	40:02.9	72:21.1

SAR PARAMETERS

PASS	WAVELENGTHS	SAR MODE	LOOK	ANTENNA DEPRESSION ANGLE	POLARIZATION TRANS	POLARIZATION REC	DIGITAL CHANNEL	RANGE DELAY (USEC)	GAIN X-B OPT	GAIN L-B OPT	GAIN X-B DIG	GAIN L-B DIG	TRANS POWER X-B	TRANS POWER L-B
1	X,L	4-CHANNEL	R	33	H	HV	XHH,LHH	45	20	38	24	52	1676	5073
2	X,L	4-CHANNEL	L	30	H	HV	XHH,LHH	46	20	35	24	52	1679	5743
3	X,L	WIDE-SWATH	R	30	H	H	XHH,LHH	46	18	39	13	46	1675	5636
4	X,L	WIDE-SWATH	R	30	H	H	XHH,LHH	46	18	39	13	36	1683	5730
5	X,L	WIDE-SWATH	R	30	H	H	XHH,LHH	46	19	42	13	32	1674	5984
6	X,L	WIDE-SWATH	R	30	H	H	XHH,LHH	46	19	42	13	36	1694	6123
7	X,L	WIDE-SWATH	R	30	H	H	XHH,LHH	46	19	42	13	36	1683	6006
8	X,L	WIDE-SWATH	R	30	H	H	XHH,LHH	46	19	43	13	39	1701	6134
9	X,L	WIDE-SWATH	L	30	H	H	XHH,LHH	46	19	43	10	39	1686	5584

Figure 9. Locations of SAR Ground Coverage During SARSEX-3, Passes 1-2
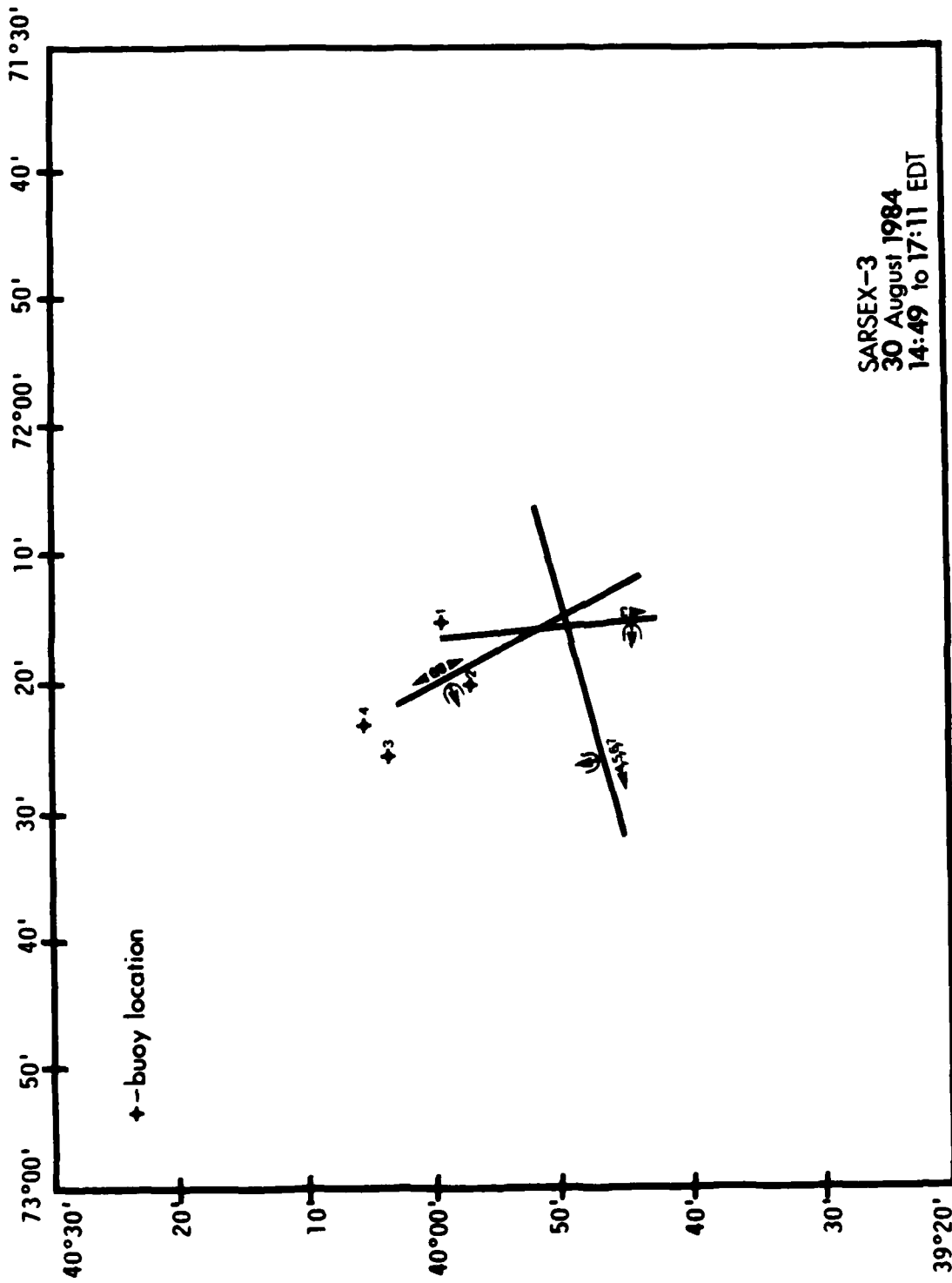
Figure 10. Locations of Aircraft Ground Tracks During SARSEX-3, Passes 3-9

SARSEX-3
30 August 1984
14:49 to 17:11 EDT

+ -buoy location

4.1.4 SARSEX-4 (31 August 1984 - 16:29 to 19:54 EDT)

The purpose of this mission was to collect multiple-incidence angle and multiple-azimuth angle SAR data over the SARSEX test area. Two passes of imagery were collected over the calibration array and nine passes were collected over the SARSEX test site. One pass was aborted because of an equipment malfunction.

The aircraft and SAR system parameters are summarized in Table 9. The flight lines are presented in Figures 11 and 12.

The quality of the optically-processed imagery is excellent for L-band and good for X-band. The quality of the calibration data appears to be high. Figure 13 presents X- and L-band imagery generated from digitally processed data collected during Pass 5, which illustrate the strong internal wave surface patterns which were imaged on this data. The ship in this image is the USNS Bartlett. This imagery will be further discussed in Chapter 6.

Figure 14 presents digitally-processed X- and L-band imagery collected during Pass 8. During this pass, the aircraft direction was nearly perpendicular to its direction during Pass 5. This resulted in imaging the internal-wave packet when the waves were headed in the same direction as the SAR, i.e., azimuth travelling waves. The internal wave surface patterns are much less distinct on the Pass 8 imagery than they are on the Pass 5 imagery, illustrating the dependence on radar look direction (also referred to as the azimuth angle).

TABLE 9. SUMMARY OF SAR AND AIRCRAFT PARAMETERS DURING SARSEX-4 (31 AUGUST 1984).

CV-580 AIRCRAFT PARAMETERS

PASS	HEADING (TRUE)	VELOCITY (KNOTS)	ALTITUDE (FEET)	START TIME (EDT)	STOP TIME (EDT)	START LATITUDE	START LONGITUDE	STOP LATITUDE	STOP LONGITUDE
1	35	285	22000	16:28:41	16:31:59	39:51.2	72:18.2	40:14.1	71:56.0
2	215	246	22000	16:48:49	16:54:58	40:03.7	72:05.3	39:43.0	72:24.2
3	35	280	22000	17:07:47	17:12:05	39:46.7	72:20.4	40:03.2	72:05.5
4	215	253	22000	17:23:20	17:28:11	40:03.7	72:05.5	39:46.9	72:20.7
5	35	274	22000	17:42:13	17:46:37	39:46.9	72:20.4	40:03.2	72:05.5
6	215	255	22000	17:58:14	18:02:55	40:03.6	72:05.7	39:47.4	72:20.4
7	305	241	22000	18:14:32	18:19:34	39:54.5	72:03.2	40:06.0	72:25.0
8	125	286	22000	18:30:45	18:35:00	40:06.7	72:26.4	39:55.0	72:05.0
9	215	263	22000	18:51:14	18:55:51	40:08.5	72:14.8	39:52.2	72:29.9
11	130	302	17500	19:30:39	19:34:40	40:58.9	73:00.6	40:45.8	72:40.1
12	310	238	17500	19:43:18	19:54:23	40:45.4	72:40.8	40:58.4	73:01.1

SAR PARAMETERS

PASS	WAVELENGTHS	SAR MODE	LOOK	ANTENNA DEPRESSION ANGLE	POLARIZATION TRANS	POLARIZATION REC	DIGITAL CHANNEL	RANGE DELAY (USEC)	GAIN SETTINGS (dB ATTENUATION) X-B OPT.	L-B OPT.	X-B DIG.	L-B DIG.	TRANS POWER (WATTS) X-B	L-B
1	X,L	WIDE-SWATH	L	28	H	H	XHH,LHH	45	15	36	11	36	1660	4879
2	X,L	WIDE-SWATH	R	28	H	H	XHH,LHH	45	15	36	9	38	1693	5830
3	X,L	WIDE-SWATH	L	28	H	H	XHH,LHH	45	15	36	9	38	1695	5337
4	X,L	WIDE-SWATH	R	28	H	H	XHH,LHH	45	17	36	9	36	1730	5262
5	X,L	WIDE-SWATH	L	28	H	H	XHH,LHH	45	17	36	9	36	1700	5452
6	X,L	WIDE-SWATH	R	28	H	H	XHH,LHH	45	17	36	9	36	1724	5453
7	X,L	WIDE-SWATH	L	28	H	H	XHH,LHH	45	20	36	9	36	1736	5830
8	X,L	WIDE-SWATH	R	28	H	H	XHH,LHH	45	20	40	9	33	1705	5234
9	X,L	WIDE-SWATH	L	28	H	H	XHH,LHH	45	25	40	9	39	1738	5295
11	X,L	4-CHANNEL	L	26	H	HV	XHH,LHH	35	25	45	27	55	1698	5298
12	X,L	4-CHANNEL	R	26	H	HV	XHH,LHH	35	27	42	27	55	1742	5650
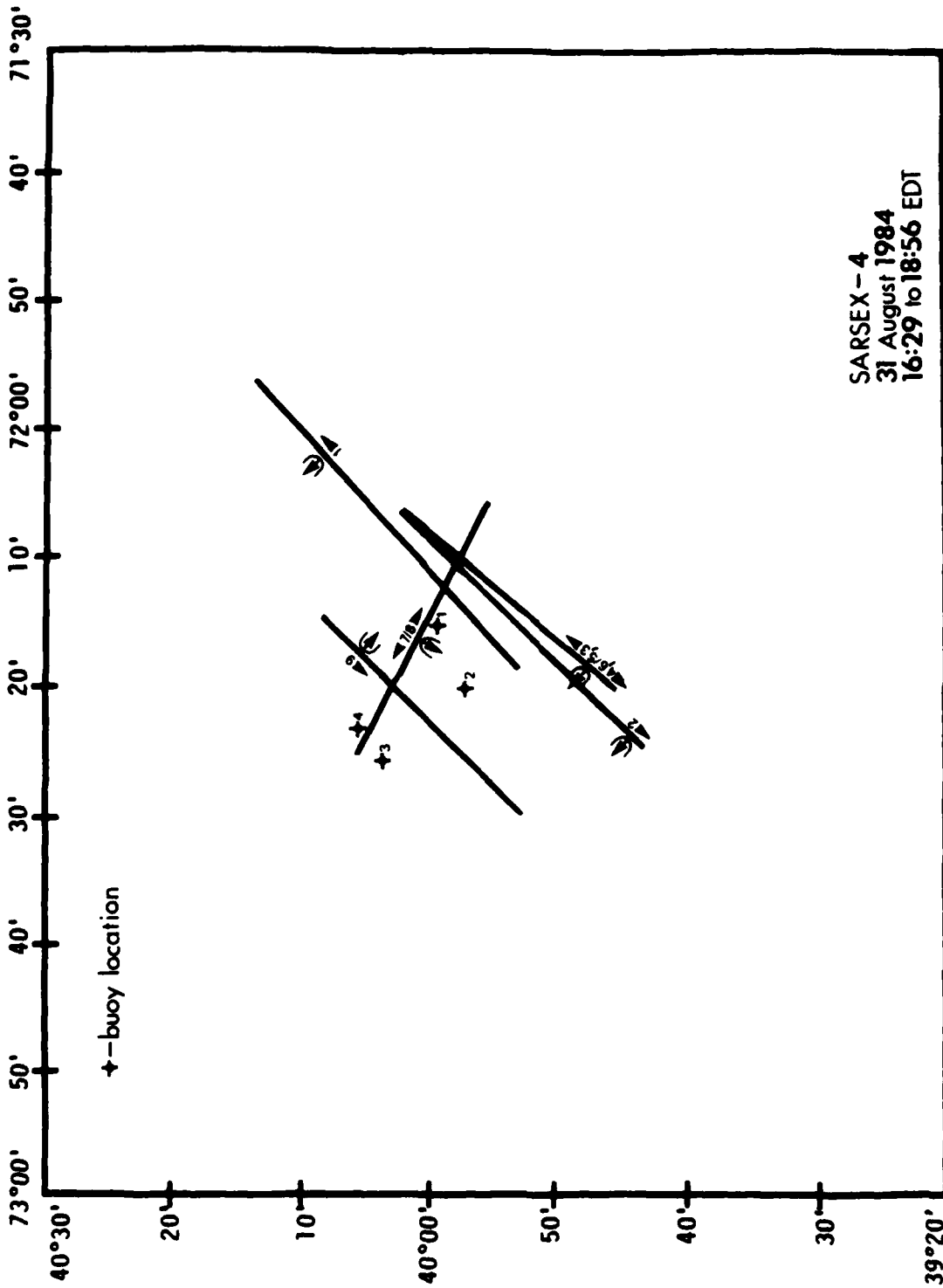
Figure 11. Locations of Aircraft Ground Tracks During SARSEX-4, Passes 1-9

Figure 12.   Locations of SAR Ground Coverage During SARSEX-4, Passes
            11-12

L-BAND

55°—
50°—
45°—
40°—
35°—
30°—
25°—
15°—

0   1000 m

X-BAND

USNS Bartlett
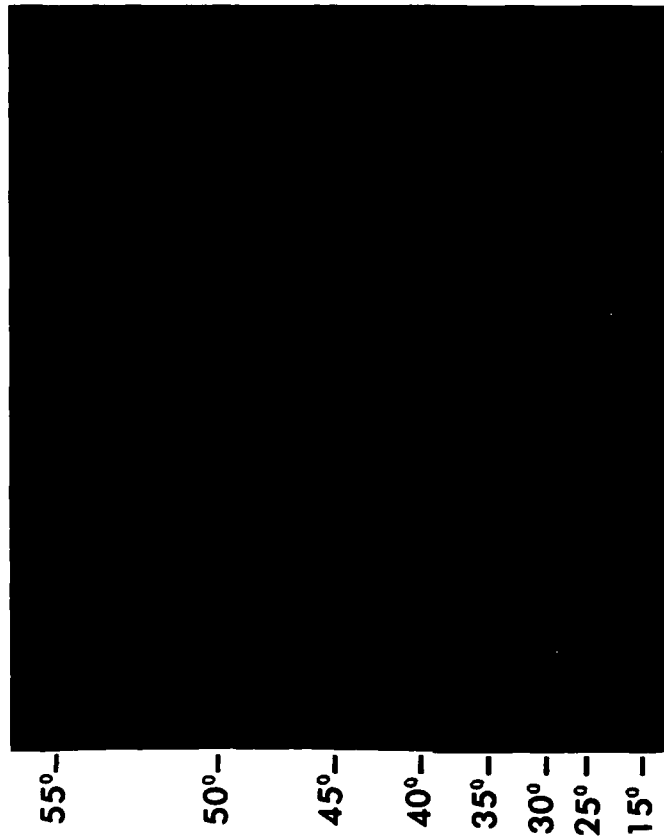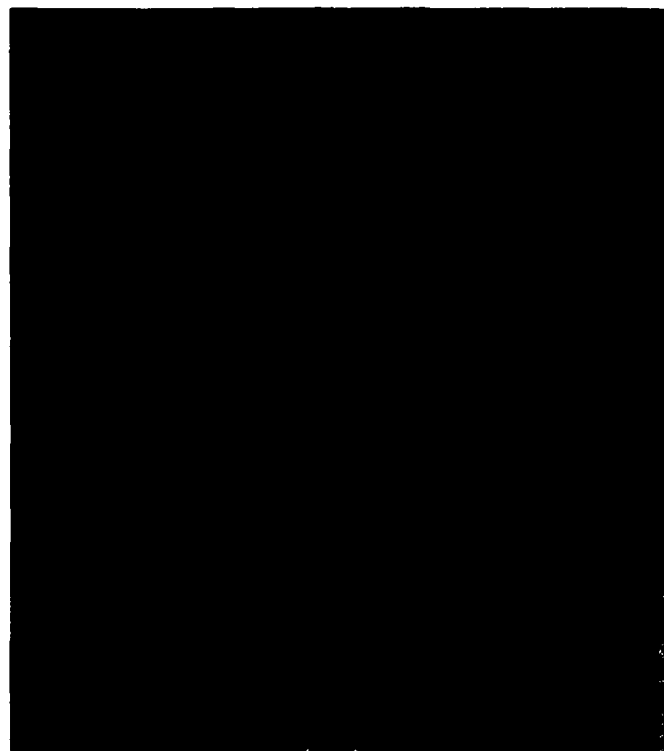
Figure 13.   Digitally-Processed X-and L-band SAR Imagery Collected
During SARSEX-4, Pass 5

L-BAND
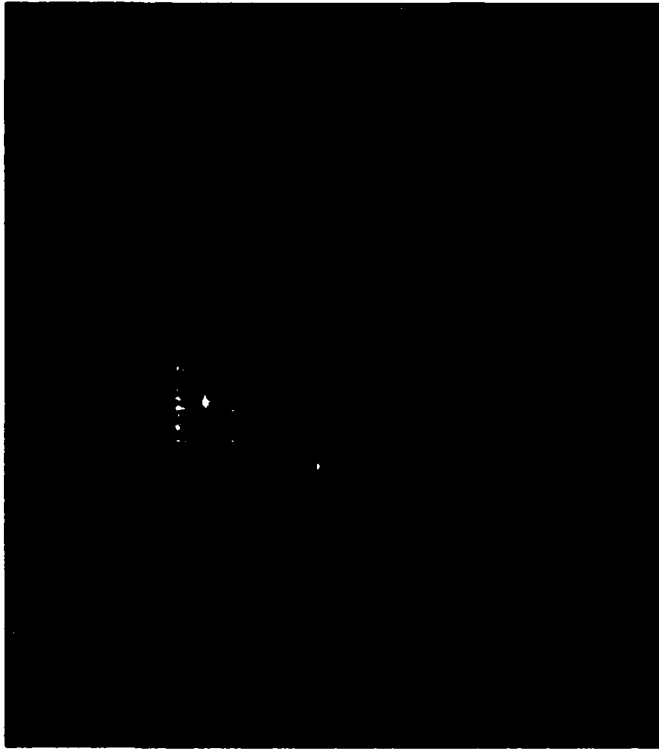
X-BAND

0 1000 m

Figure 14. Digitally-Processed X- and L-band SAR Imagery Collected During SARSEX-4, Pass 8

4.1.5 SARSEX-5 (3 September 1984 - 13:27 to 17:07 EDT)

The purpose of this mission was to collect multiple-incidence angle and multiple-azimuth angle SAR data of surface internal wave patterns present in the SARSEX test area. Three passes of imagery were collected over the calibration array and nine passes were collected over the SARSEX area.

The aircraft and SAR system parameters are summarized in Table 10. The flight lines are presented in Figures 15 and 16.

The quality of the optically processed SAR imagery was good to excellent. The optically-recorded calibration signals appear to be saturated and somewhat unfocused. An in-depth analysis of these signals is now being pursued to determine whether or not they are suitable for calibration purposes.

TABLE 10. SUMMARY OF SAR AND AIRCRAFT PARAMETERS DURING SARSEX-5 (3 SEPTEMBER 1984).

CV-580 AIRCRAFT PARAMETERS

PASS	HEADING (TRUE)	VELOCITY (KNOTS)	ALTITUDE (FEET)	START TIME (EDT)	STOP TIME (EDT)	START LATITUDE	START LONGITUDE	STOP LATITUDE	STOP LONGITUDE
1	310	230	22000	13:26:40	13:33:15	40:42.3	72:35.5	40:58.6	73:00.7
2	130	290	22000	13:44:58	13:50:05	40:58.3	73:00.2	40:42.3	72:35.5
3	310	230	22000	14:04:41	14:11:13	40:42.3	72:35.8	40:58.6	73:00.7
4	146	283	22000	14:32:54	14:37:06	40:09.5	72:17.6	39:53.0	72:03.2
5	230	239	22000	14:55:05	15:00:01	40:06.3	72:10.5	39:53.5	72:30.1
6	50	287	22000	15:12:23	15:16:35	39:53.5	72:30.5	40:06.3	72:10.5
7	275	229	22000	15:29:28	15:34:44	39:52.5	72:04.4	39:54.2	72:30.5
8	50	296	22000	15:48:47	15:52:52	39:53.5	72:30.4	40:06.3	72:10.5
9	230	241	22000	16:03:42	16:11:20	40:13.4	71:59.8	39:53.8	72:30.4
10	320	243	22000	16:25:14	16:30:13	39:46.9	72:12.3	40:02.1	72:29.2
11	140	284	22000	16:46:24	16:50:40	40:07.1	72:22.2	39:51.5	72:05.2
12	5	267	22000	17:01:50	17:07:07	39:43.6	72:23.7	40:07.0	72:21.1

SAR PARAMETERS

PASS	WAVELENGTHS	SAR MODE	LOOK	ANTENNA DEPRESSION ANGLE	POLARIZATION TRANS	POLARIZATION REC	DIGITAL CHANNEL	RANGE DELAY (USEC)	GAIN SETTINGS (dB ATTENUATION) X-B OPT.	L-B OPT.	X-B DIG.	L-B DIG.	TRANS POWER (WATTS) X-B	L-B
1	X,L	4-CHANNEL	R	28	H	HV	XHH,LHH	44	20	38	24	52	1685	5219
2	X,L	4-CHANNEL	L	28	H	HV	XHH,LHH	44	20	38	27	52	1692	4950
3	X,L	4-CHANNEL	R	28	H	HV	XHH,LHH	44	20	38	27	52	1679	5890
4	X,L	WIDE-SWATH	R	28	H	H	XHH,LHH	44	12	33	11	36	1696	4576
5	X,L	WIDE-SWATH	R	28	H	H	XHH,LHH	44	12	33	11	47	1735	5325
6	X,L	WIDE-SWATH	L	28	H	H	XHH,LHH	44	12	33	11	42	1719	5264
7	X,L	WIDE-SWATH	R	28	H	H	XHH,LHH	44	12	33	11	42	1711	5811
8	X,L	WIDE-SWATH	L	28	H	H	XHH,LHH	44	12	33	11	39	1701	6235
9	X,L	WIDE-SWATH	R	28	H	H	XHH,LHH	44	12	33	11	42	1730	6096
10	X,L	WIDE-SWATH	R	28	H	H	XHH,LHH	44	12	33	11	42	1747	6315
11	X,L	WIDE-SWATH	R	28	H	H	XHH,LHH	44	12	33	11	36	1723	6284
12	X,L	WIDE-SWATH	R	28	H	H	XHH,LHH	44	12	33	11	41	1733	5996
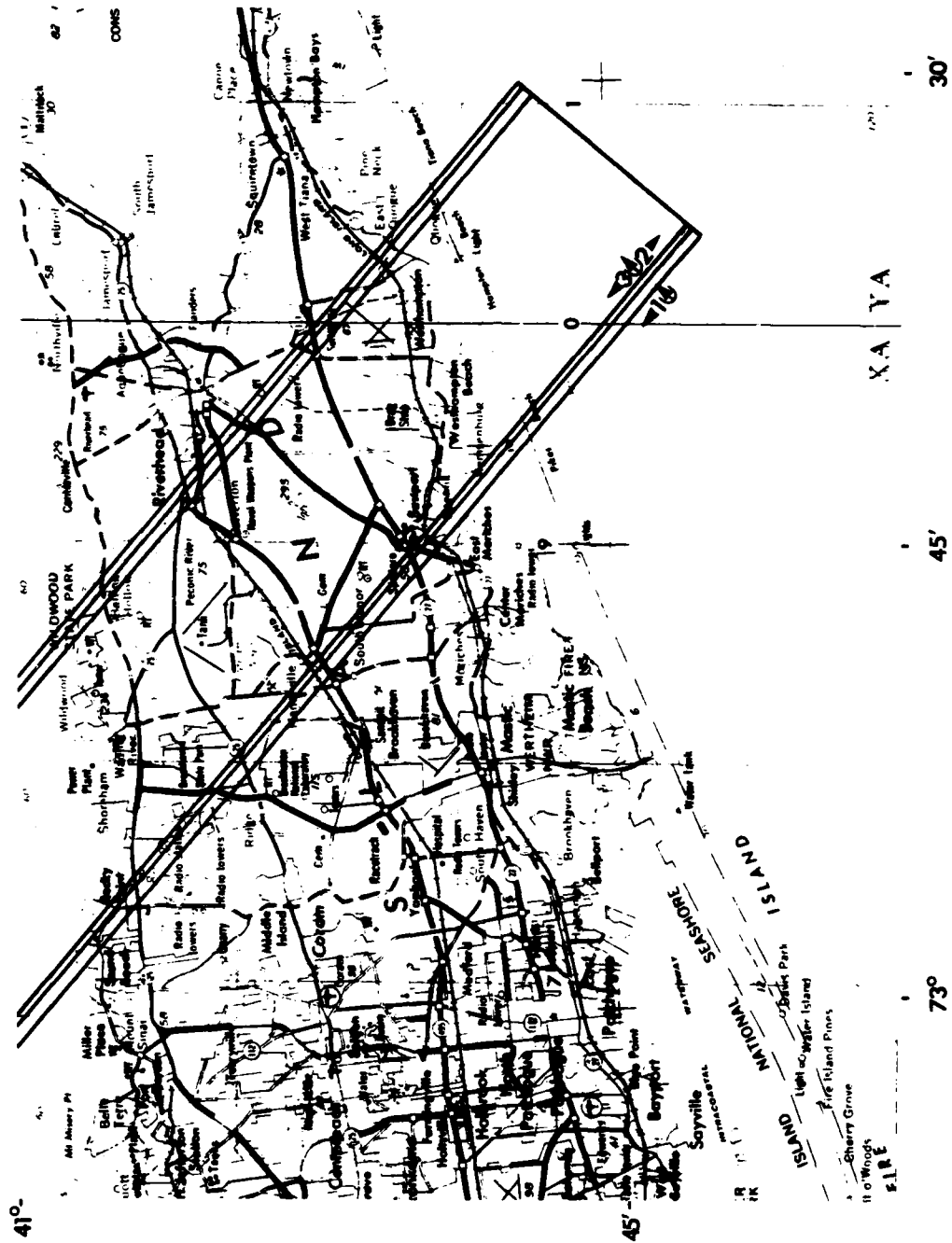
Figure 15.   Locations of SAR Ground Coverage During SARSEX-5, Passes 1-3

SARSEX-5
3 September 1984
14:33 to 17:02 EDT
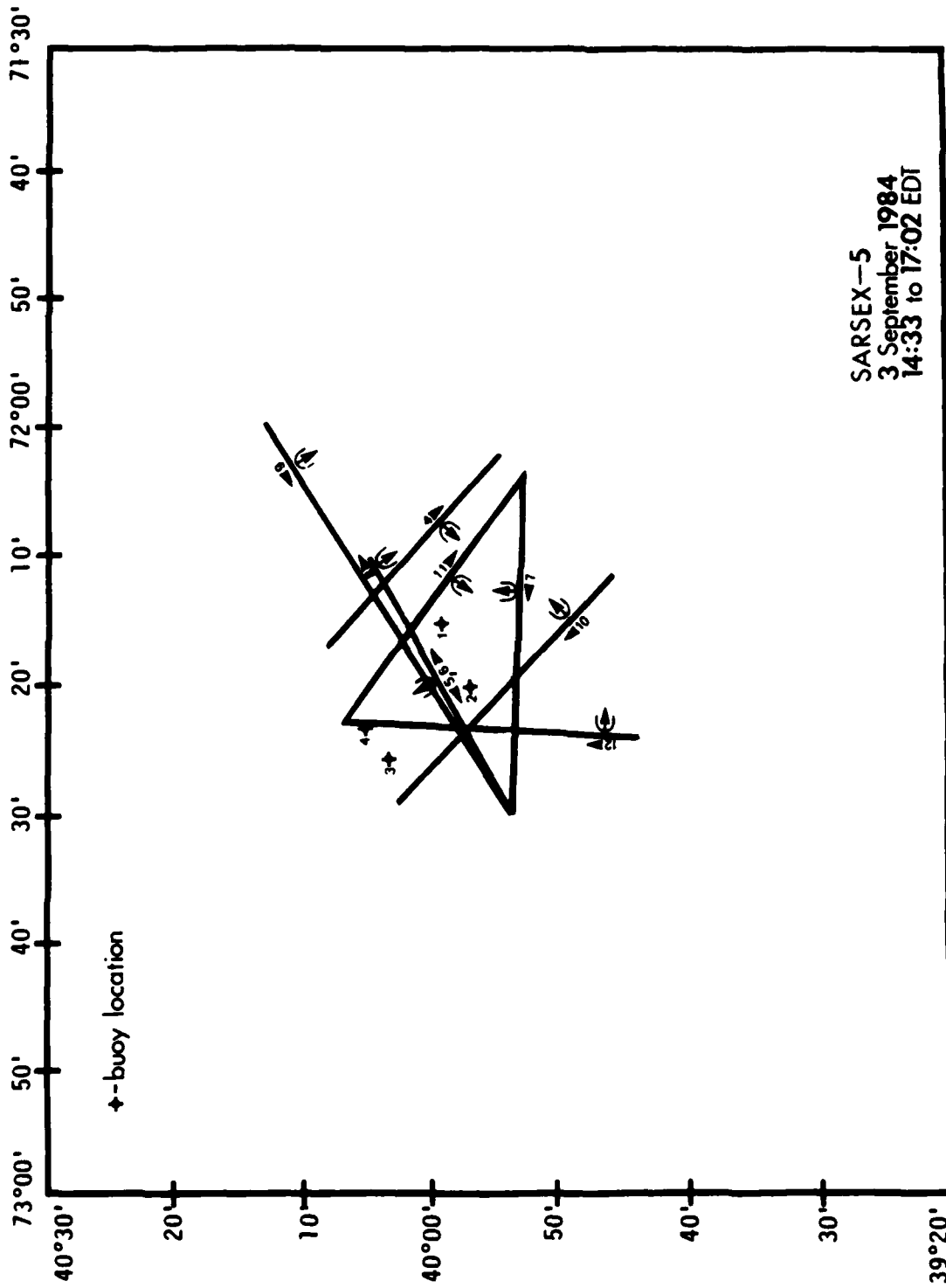
Figure 16. Locations of Aircraft Ground Tracks During SARSEX-5, Passes 4-12

+ - buoy location

4.1.6 SARSEX-6 (4 September 1984 – 14:54 to 18:33 EDT)

The purpose of this mission was to collect multiple-incidence angle SAR data of surface internal wave patterns present in the SARSEX test area. Four passes of imagery were collected over the calibration array and seven passes over the SARSEX area.

The aircraft and SAR system parameters are summarized in Table 11. The flight lines are presented in Figures 17 and 18.

The quality of the L-band optically processed imagery was excellent and the quality of the X-band imagery good to excellent. The quality of the calibration signals appears to be adequate to calibrate the imagery.

TABLE 11. SUMMARY OF SAR AND AIRCRAFT PARAMETERS DURING SARSEX-6 (4 SEPTEMBER 1984).

CV-580 AIRCRAFT PARAMETERS

PASS	HEADING (TRUE)	VELOCITY (KNOTS)	ALTITUDE (FEET)	START TIME (EDT)	STOP TIME (EDT)	START LATITUDE	START LONGITUDE	STOP LATITUDE	STOP LONGITUDE
1	310	238	22000	14:53:54	14:58:59	40:45.1	72:39.5	40:58.3	72:59.8
2	130	280	22000	15:08:50	15:13:05	40:57.4	72:59.6	40:44.6	72:39.8
3	310	240	22000	15:26:49	15:31:52	40:44.6	72:39.5	40:57.6	72:59.8
4	310	246	22000	16:04:18	16:09:07	40:45.4	72:40.6	40:58.3	73:00.4
5	150	220	22000	16:29:47	16:35:10	40:05.0	72:33.0	39:48.1	72:20.2
6	240	210	22000	16:50:37	16:56:23	40:00.3	72:08.5	39:50.2	72:31.2
7	60	296	22000	17:10:52	17:14:53	39:58.3	72:37.0	40:07.8	72:14.9
8	240	200	22000	17:29:49	17:35:42	40:08.2	72:14.5	39:58.1	72:37.1
9	90	289	22000	17:53:11	17:57:17	40:03.4	72:36.7	40:03.4	72:10.5
10	240	215	22000	18:12:35	18:18:07	40:01.4	72:09.5	39:51.5	72:32.2
11	0	260	22000	18:28:21	18:32:56	39:49.6	72:18.9	40:09.8	72:18.9

SAR PARAMETERS

PASS	WAVELENGTHS	SAR MODE	LOOK	ANTENNA DEPRESSION ANGLE	POLARIZATION TRANS	POLARIZATION REC	DIGITAL CHANNEL	RANGE DELAY (uSEC)	GAIN SETTINGS (dB ATTENUATION) X-B OPT.	L-B OPT.	X-B DIG.	L-B DIG.	TRANS POWER (WATTS) X-B	L-B
1	X,L	4-CHANNEL	R	28	H	HV	XHH,LHH	43	20	35	27	52	1701	5368
2	X,L	4-CHANNEL	L	28	H	HV	XHH,LHH	43	17	32	21	46	1697	4794
3	X,L	4-CHANNEL	R	28	H	HV	XHH,LHH	43	18	32	0	0	1720	5502
4	X,L	4-CHANNEL	L	28	H	HV	XHH,LHH	42	19	34	24	49	1708	5723
5	X,L	WIDE-SWATH	L	28	H	H	XHH,LHH	42	15	33	8	36	1718	6622
6	X,L	WIDE-SWATH	L	28	H	H	XHH,LHH	42	14	33	8	39	1733	6681
7	X,L	WIDE-SWATH	R	28	H	H	XHH,LHH	42	15	33	5	36	1726	5837
8	X,L	WIDE-SWATH	L	28	H	H	XHH,LHH	42	16	33	7	33	1806	6898
9	X,L	WIDE-SWATH	R	28	H	H	XHH,LHH	42	16	33	7	38	1711	5314
10	X,L	WIDE-SWATH	R	28	H	H	XHH,LHH	42	16	33	9	38	1736	5393
11	X,L	WIDE-SWATH	L	28	H	H	XHH,LHH	42	16	33	9	38	1741	5092
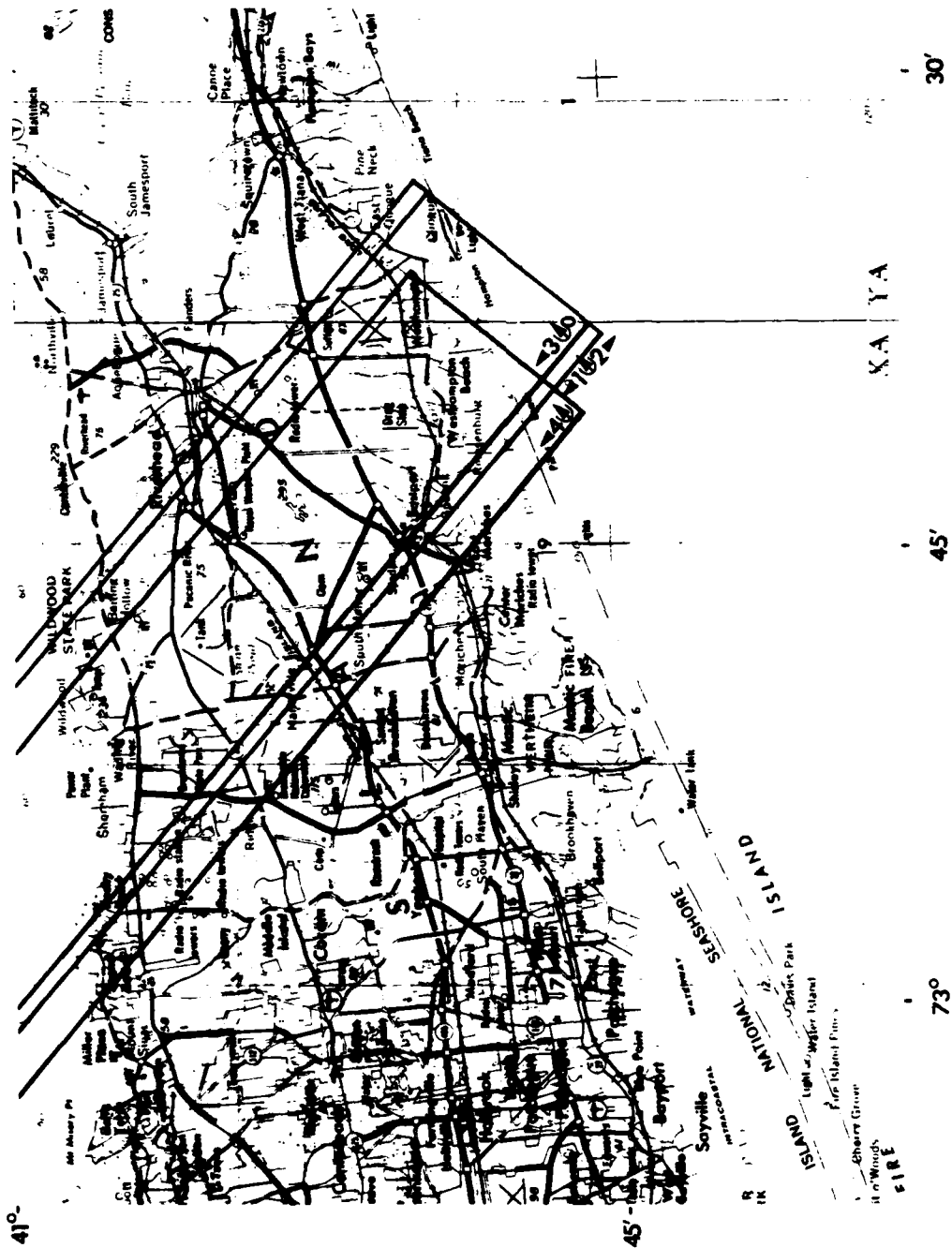
Figure 17. Locations of SAR Ground Coverage During SARSEX-6, Passes
            1-4

SARSEX-6
4 September 1984
16:30 to 18:33 EDT

+ -buoy location
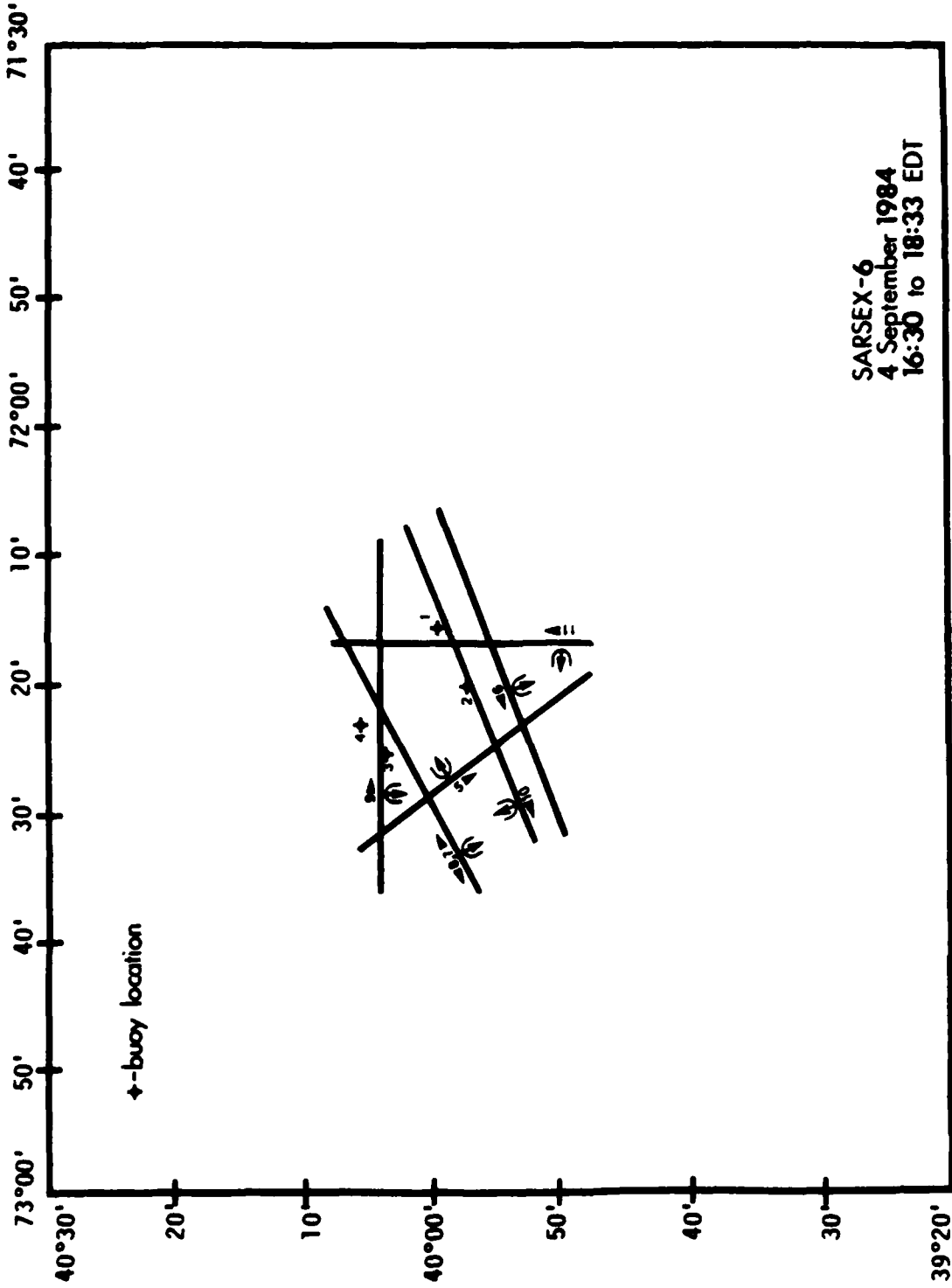
Figure 18. Locations of Aircraft Ground Tracks During SARSEX-6, Passes 5-11

4.1.7 SARSEX-7 (5 September 1984 - 13:19 to 17:32 EDT)

The purpose of this mission was to collect multiple-incidence angle and multiple-azimuth angle SAR data of internal wave surface patterns present in the SARSEX test area. Three passes of imagery were collected over the calibration array and nine passes over the SARSEX area.

The aircraft and SAR system parameters for SARSEX-7 are summarized in Table 12. The flight lines are presented in Figures 19 and 20.

The quality of optically-processed imagery was excellent for both X- and L-bands. The L-band optical recorder suffered an intermittent failure during Passes 8 and 9. The latter half of Pass 8 and none of Pass 9 were recorded optically. The optically-recorded X-band calibration signals were extremely saturated during this mission. Further analysis is required to determine if the digitally-recorded data are suitable for calibration purposes. The L-band calibration signals appear to be suitable for calibration purposes. An operator error resulted in no digital data being recorded for Passes 4 through 6.

Figure 21 presents optically-processed X- and L-band imagery from Pass 7. Note that the SAR imaged internal wave surface patterns are more subtle in this example than those observed during SARSEX-4.

TABLE 12. SUMMARY OF SAR AND AIRCRAFT PARAMETERS DURING SARSEX-7 (5 SEPTEMBER 1984).

CV-580 AIRCRAFT PARAMETERS

PASS	HEADING (TRUE)	VELOCITY (KNOTS)	ALTITUDE (FEET)	START TIME (EDT)	STOP TIME (EDT)	START LATITUDE	START LONGITUDE	STOP LATITUDE	STOP LONGITUDE
1	310	249	22000	13:18:31	13:23:22	40:45.9	72:40.1	40:58.7	73:00.4
2	131	266	22000	13:34:03	13:38:34	40:58.4	73:00.6	40:45.4	72:40.6
3	310	246	22000	13:51:27	13:57:30	40:42.5	72:35.6	40:58.6	73:00.6
4	161	244	22000	14:11:10	14:25:16	40:38.6	72:41.6	39:44.8	72:17.4
5	225	210	22000	14:40:15	14:45:59	39:54.7	72:11.5	39:40.6	72:29.9
6	225	210	22000	15:03:31	15:09:15	39:54.7	72:11.5	39:40.6	72:29.9
7	225	212	22000	15:38:37	15:44:19	39:57.0	72:14.5	39:42.6	72:32.7
8	135	262	22000	16:00:32	16:05:08	40:01.3	72:35.6	39:47.1	72:17.1
9	285	231	22000	16:17:31	16:22:48	39:52.5	72:15.4	39:57.7	72:41.1
10	225	211	22000	16:38:54	16:44:39	40:01.6	72:23.8	39:47.4	72:42.4
11	255	209	22000	17:03:47	17:09:34	39:57.7	72:17.9	39:52.5	72:43.3
12	285	235	22000	17:27:06	17:32:15	39:52.5	72:15.4	39:57.8	72:40.8

SAR PARAMETERS

PASS	WAVELENGTHS	SAR MODE	LOOK	ANTENNA DEPRESSION ANGLE	POLARIZATION TRANS	POLARIZATION REC	DIGITAL CHANNEL	RANGE DELAY (µSEC)	GAIN SETTINGS (dB ATTENUATION) X-B OPT.	L-B OPT.	X-B DIG.	L-B DIG.	TRANS POWER (WATTS) X-B	L-B
1	X,L	4-CHANNEL	R	28	H	HV	XHH,LHH	42	20	38	21	46	1675	5547
2	X,L	4-CHANNEL	L	28	H	HV	XHH,LHH	42	20	38	20	48	1698	6138
3	X,L	4-CHANNEL	R	28	H	HV	XHH,LHH	42	20	38	18	48	1706	5984
4	X,L	WIDE-SWATH	R	28	H	H	XHH,LHH	42	16	33	5	36	1744	6318
5	X,L	WIDE-SWATH	R	28	H	H	XHH,LHH	42	16	33	12	41	1741	6180
6	X,L	WIDE-SWATH	R	28	H	H	XHH,LHH	42	16	33	12	41	1686	6500
7	X,L	WIDE-SWATH	R	28	H	H	XHH,LHH	42	15	33	14	41	1706	6729
8	X,L	WIDE-SWATH	R	28	H	H	XHH,LHH	42	17	32	10	41	1721	6937
9	X,L	WIDE-SWATH	L	28	H	H	XHH,LHH	42	17	32	13	41	1735	6567
10	X,L	WIDE-SWATH	L	28	H	H	XHH,LHH	42	17	33	14	41	1715	6675
11	X,L	WIDE-SWATH	L	28	H	H	XHH,LHH	42	17	33	14	41	1726	6209
12	X,L	WIDE-SWATH	L	28	H	H	XHH,LHH	42	16	33	14	41	1697	6545
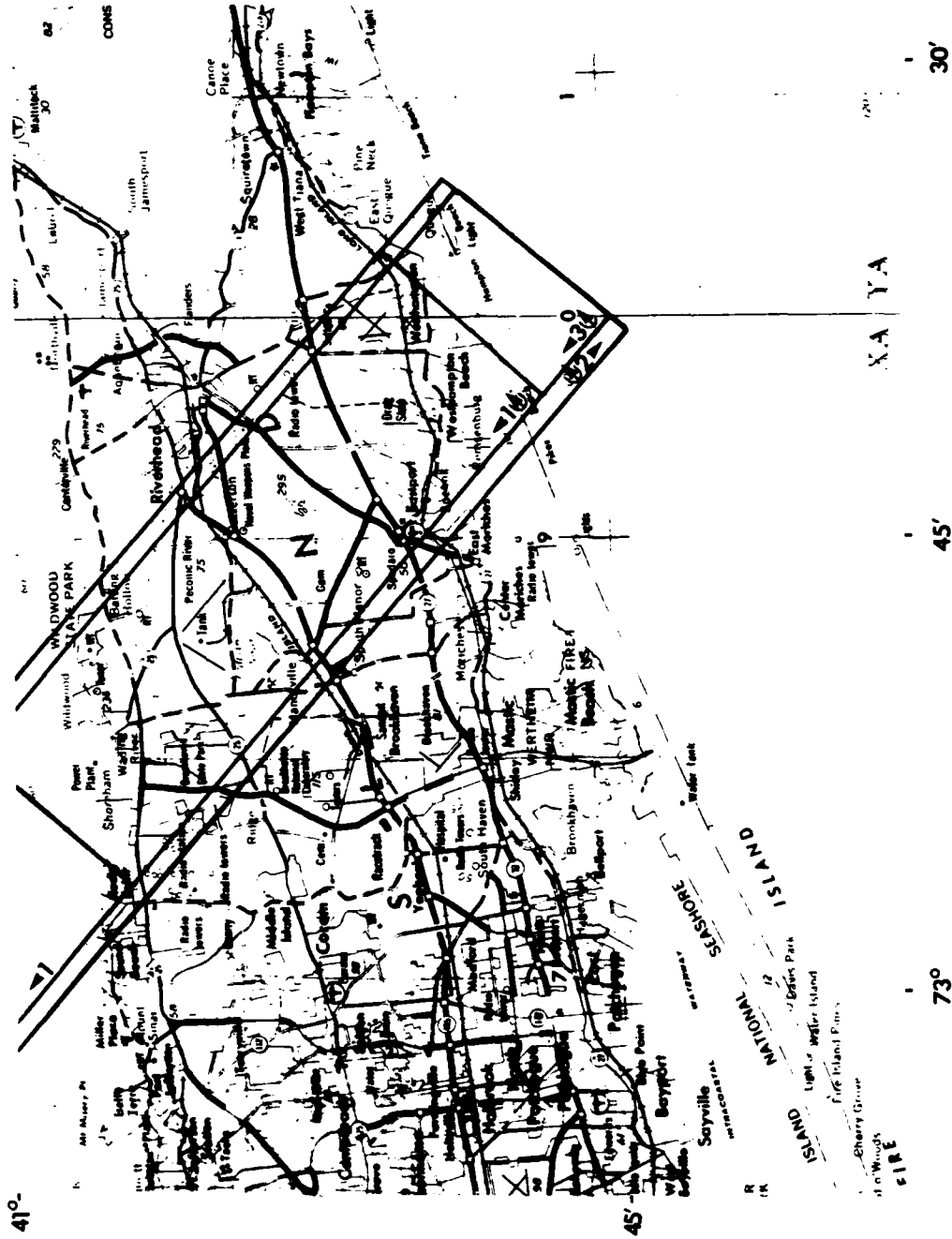
Figure 19.   Locations of SAR Ground Coverage During SARSEX-7, Passes 1-3
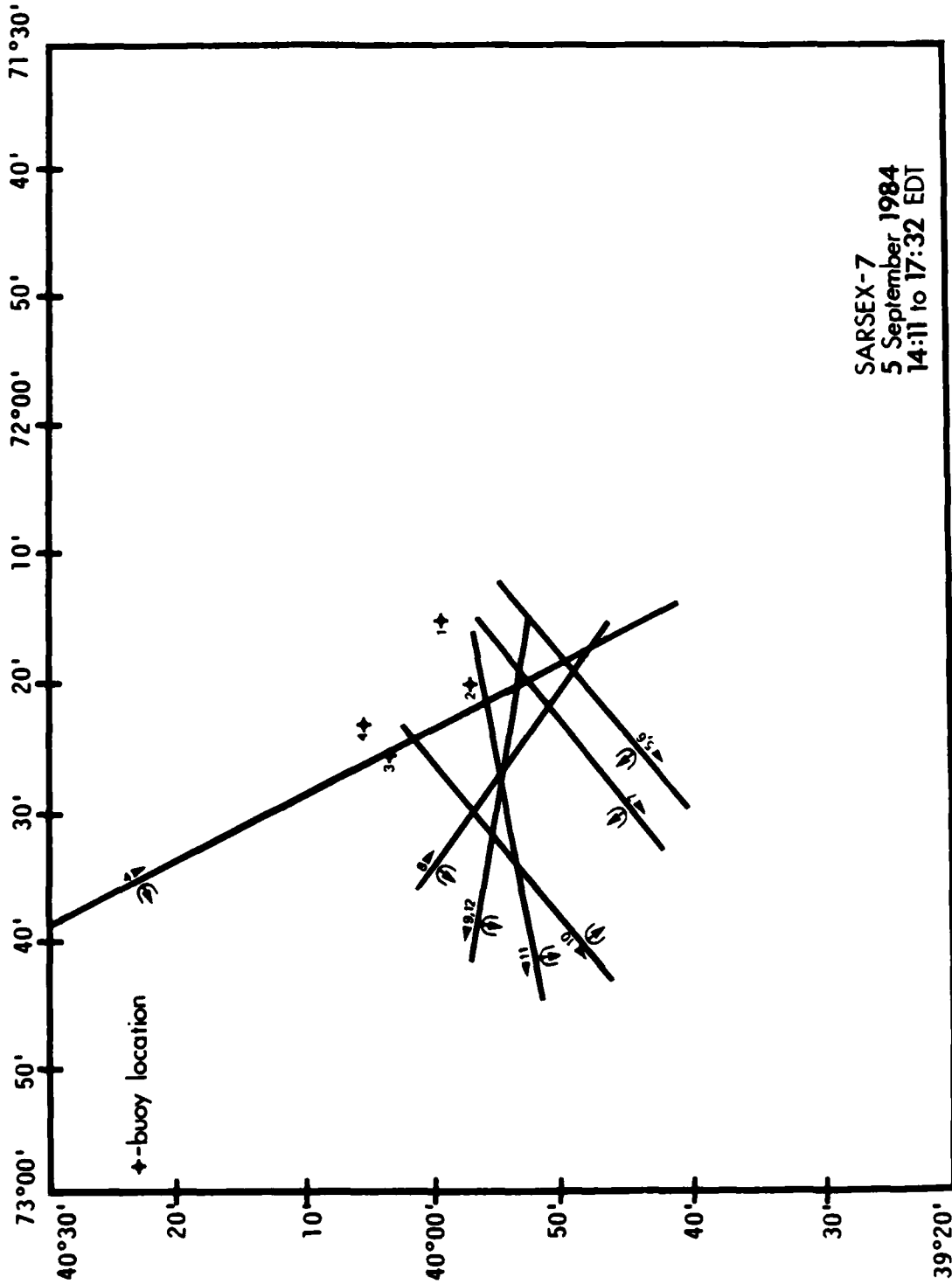
Figure 20. Locations of Aircraft Ground Tracks During SARSEX-7, Passes 4-12

SARSEX-7
5 September 1984
14:11 to 17:32 EDT

+-buoy location

ΣERIM

X-Band

L-Band

Figure 21. Optically-Processed X- and L-Band Imagery Collected During SARSEX-7, Pass 7

55

4.1.8 SARSEX-8 (6 September 1984 - 8:47 to 12:12 EDT)

The purpose of this mission was to collect multiple-azimuth angle and variable altitude SAR imagery of internal wave surface patterns present in the SARSEX test area. Two passes of SAR imagery were collected over the calibration array and eight passes over the SARSEX area.

The aircraft and SAR system parameters for the SARSEX-8 mission are summarized in Table 13. The flight lines are presented in Figures 22 and 23.

The quality of the optically-processed imagery collected from this mission was excellent for both X- and L-bands. Again, the optically-recorded X-band calibration signals were extremely saturated during this mission. Further analysis is required to determine if the digitally-recorded signals are suitable for calibration purposes. The L-band calibration signals appear to be suitable for calibration purposes.

Figure 24 presents optically-processed X-band imagery collected during Passes 4, 7, 8. Figure 25 presents X- and L-band digitally-processed imagery from Pass 8. The L-band image has been normalized to reduce the range fall-off due to the R^4 power loss and the antenna pattern.

TABLE 13. SUMMARY OF SAR AND AIRCRAFT PARAMETERS DURING SARSEX-8 (6 SEPTEMBER 1984).

CV-580 AIRCRAFT PARAMETERS

PASS	HEADING (TRUE)	VELOCITY (KNOTS)	ALTITUDE (FEET)	START TIME (EDT)	STOP TIME (EDT)	START LATITUDE	START LONGITUDE	STOP LATITUDE	STOP LONGITUDE
1	310	259	22000	8:47:18	8:51:56	40:45.6	72:40.4	40:58.6	73:00.7
2	130	272	22000	9:03:31	9:07:59	40:58.6	73:00.6	40:45.4	72:40.3
3	154	249	22000	9:34:59	9:38:43	39:59.3	72:17.1	39:45.4	72:08.3
4	240	218	22000	9:51:05	9:59:48	39:56.3	71:49.0	39:4C.6	72:24.5
5	15	322	22000	10:16:58	10:20:45	39:40.0	72:23.3	39:53.5	72:16.6
6	150	315	3000	10:43:21	10:48:17	39:59.8	72:18.1	39:42.3	72:04.9
7	240	209	5000	11:06:14	11:13:16	39:55.5	71:58.7	39:43.1	72:26.3
8	240	207	5000	11:30:26	11:36:15	39:53.3	72:03.7	39:43.1	72:26.1
9	15	195	5000	11:47:09	11:53:24	39:40.6	72:22.2	40:00.3	72:15.6
10	330	209	5000	12:04:18	12:11:32	39:41.9	72:07.5	40:03.9	72:23.8

SAR PARAMETERS

PASS	WAVELENGTHS	SAR MODE	LOOK	ANTENNA DEPRESSION ANGLE	POLARIZATION TRANS	REC	DIGITAL CHANNEL	RANGE DELAY (USEC)	GAIN SETTINGS (dB ATTENUATION) X-B OPT.	L-B OPT.	X-B DIG.	L-B DIG.	TRANS POWER (WATTS) X-B	L-B
1	X,L	4-CHANNEL	R	28	H	HV	XHH,LHH	43	21	38	24	54	1683	5611
2	X,L	4-CHANNEL	L	28	H	HV	XHH,LHH	43	26	35	21	51	1690	6382
3	X,L	WIDE-SWATH	R	28	H	H	XHH,LHH	43	21	30	11	42	1710	6486
4	X,L	WIDE-SWATH	R	28	H	H	XHH,LHH	43	21	30	12	41	1711	6596
5	X,L	WIDE-SWATH	R	28	H	H	XHH,LHH	43	21	30	12	41	1706	5768
6	X,L	WIDE-SWATH	R	28	H	H	XHH,LHH	43	23	30	12	41	1721	6108
7	X,L	WIDE-SWATH	R	5	H	H	XHH,LHH	6	23	23	20	32	1727	6446
8	X,L	WIDE-SWATH	R	5	H	H	XHH,LHH	10	22	27	12	40	1733	5942
9	X,L	WIDE-SWATH	R	5	H	H	XHH,LHH	8	22	27	8	40	1705	5925
10	X,L	WIDE-SWATH	L	5	H	H	XHH,LHH	8	22	27	8	40	1743	6462
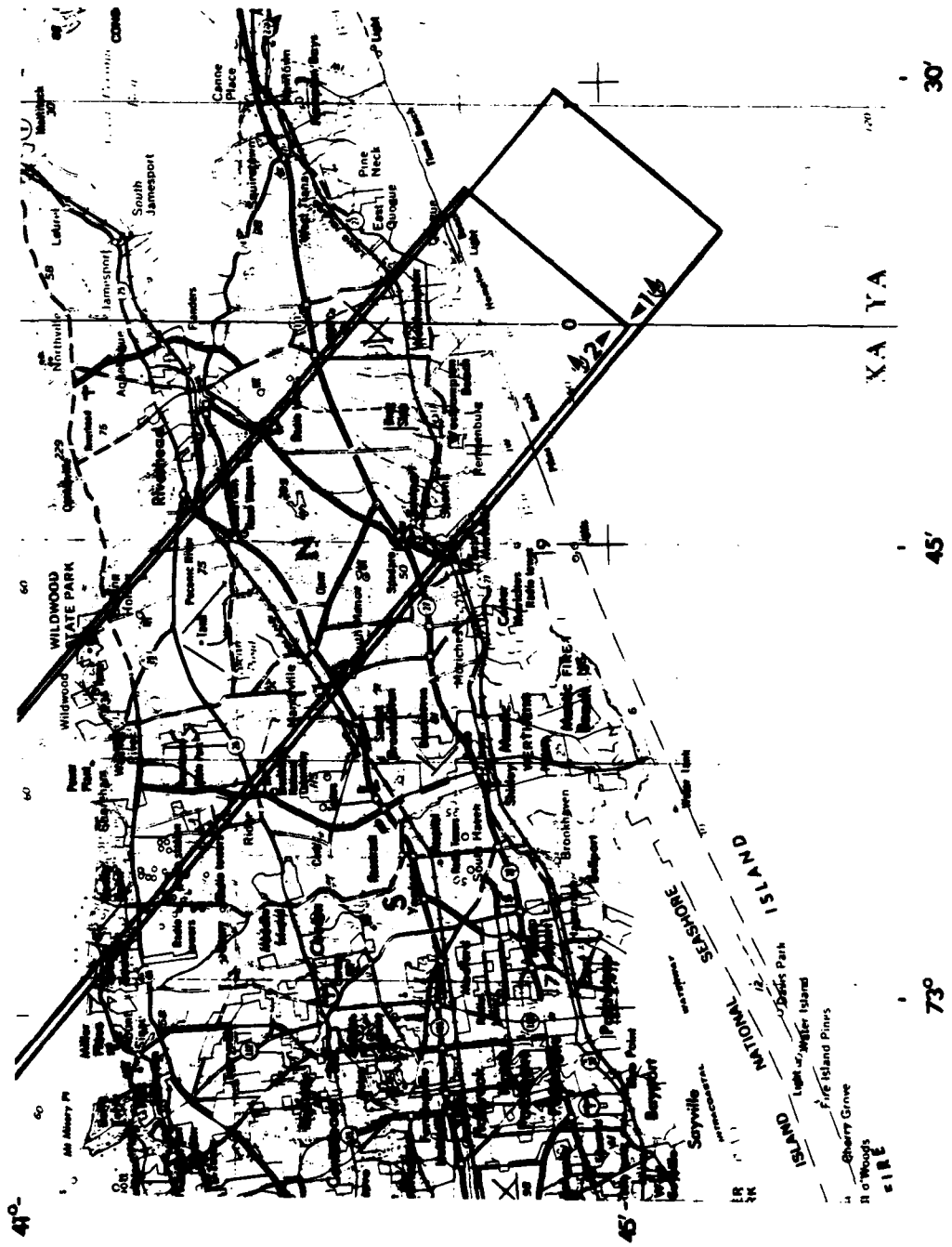
Figure 22. Locations of SAR Ground Coverage During SARSEX-8, Passes 1-2

SARSEX-8
6 September 1984
9:35 to 12:12 EDT

+ - buoy location
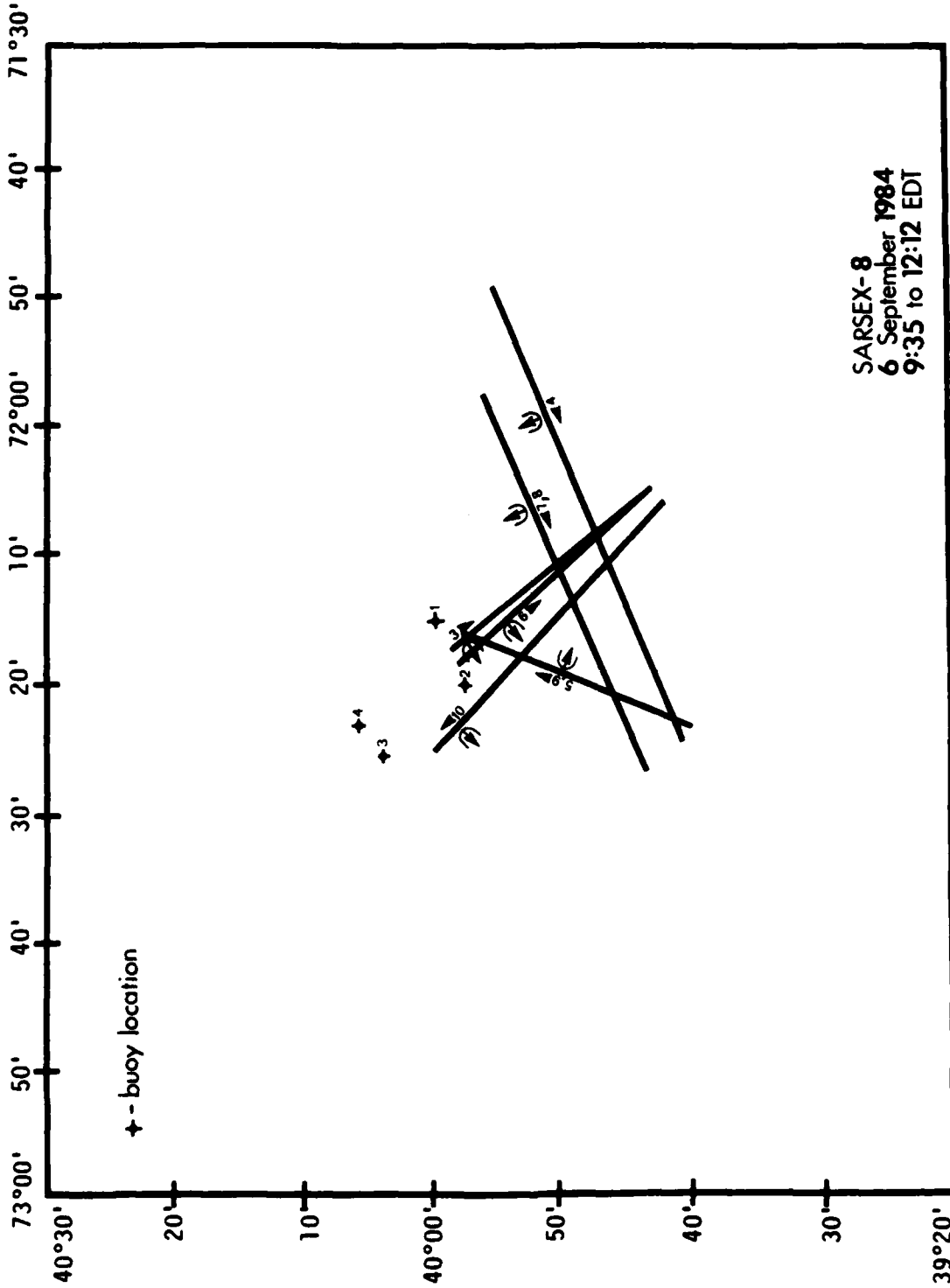
Figure 23. Locations of Aircraft Ground Tracks During SARSEX 8, Passes 3-10
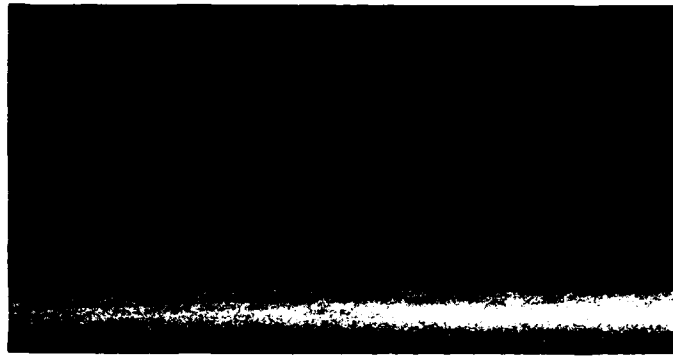
Pass 4, 22,000 ft
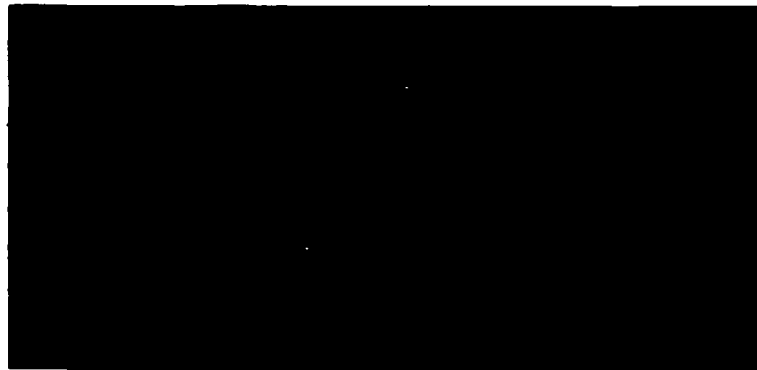
Pass 8, 5,000 ft

Pass 7, 3,000 ft

Figure 24. Optically-Processed L-band Imagery Collected During SARSEX-8, Passes 4, 7 and 8
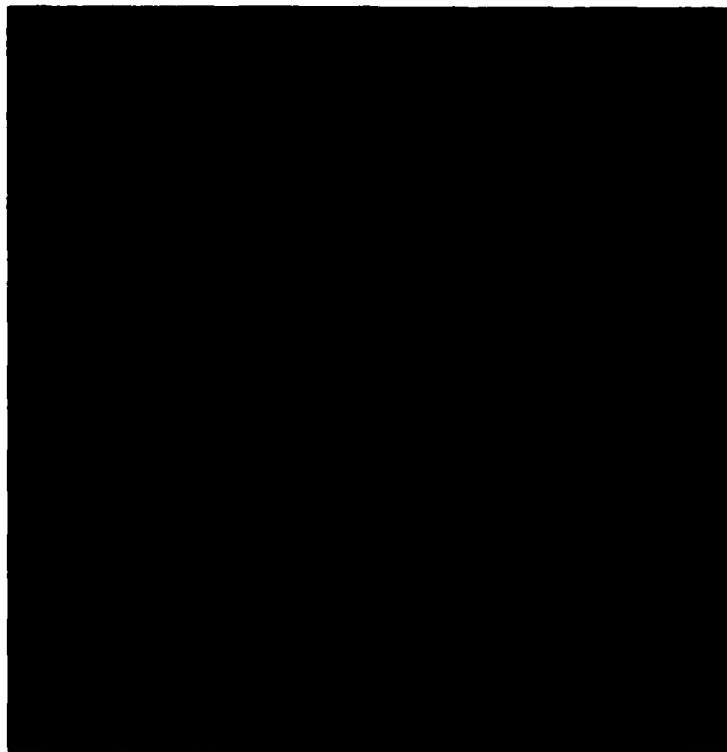
X-BAND

L-BAND

0 1000 m

Figure 25. Digitally-Processed X- and L-band SAR Imagery Collected During SARSEX-8, Pass 8, Illustrating Azimuthal Streaking

4.1.9 <u>SARSEX-9 (6 September 1984 - 14:35 to 16:42 EDT)</u>

The purpose of this mission was to collect multiple-incidence angle SAR data of internal wave surface patterns present in the SARSEX area. Six passes of imagery were collected over the SARSEX area.

The aircraft and SAR system parameters for the SARSEX-9 mission are presented in Table 14. The flight lines are presented in Figure 26.

The quality of the optically-processed imagery was excellent for both X- and L-bands. Again, the X-band calibration signals recorded optically during this mission were saturated. The L-band calibration signals appear to be suitable for calibration purposes.

Figure 27 presents X- and L-band imagery generated from digitally-processed SAR data collected during SARSEX-9, Pass 2.

TABLE 14. SUMMARY OF SAR AND AIRCRAFT PARAMETERS DURING SARSEX-9 (6 SEPTEMBER 1984).

CV-580 AIRCRAFT PARAMETERS

PASS	HEADING (TRUE)	VELOCITY (KNOTS)	ALTITUDE (FEET)	START TIME (EDT)	STOP TIME (EDT)	START LATITUDE	START LONGITUDE	STOP LATITUDE	STOP LONGITUDE
1	220	222	22000	14:35:33	14:40:59	40:02.1	72:05.3	39:46.7	72:22.2
2	40	295	22000	14:58:13	15:02:18	39:45.9	72:21.2	40:01.3	72:04.2
3	220	226	22000	15:22:24	15:27:44	40:01.4	72:04.6	39:46.1	72:21.2
4	40	313	22000	15:43:04	15:46:56	39:45.9	72:21.4	40:01.3	72:04.6
5	220	228	22000	16:19:11	16:24:28	40:07.8	72:16.1	39:52.5	72:33.0
6	40	298	22000	16:37:44	16:41:45	39:52.2	72:32.7	40:07.6	72:15.9

SAR PARAMETERS

PASS	WAVELENGTHS	SAR MODE	LOOK	ANTENNA DEPRESSION ANGLE	POLARIZATION TRANS	POLARIZATION REC	DIGITAL CHANNEL	RANGE DELAY (USEC)	GAIN SETTINGS (dB ATTENUATION) X-B OPT.	L-B OPT.	Y-B DIG.	L-B DIG.	TRANS POWER (WATTS) X-B	L-B
1	X.L	WIDE-SWATH	R	28	H	H	XHH,LHH	43	20	23	11	42	1683	5890
2	X.L	WIDE-SWATH	L	28	H	H	YHH,LHH	43	22	25	8	36	1686	5520
3	X.L	WIDE-SWATH	R	28	H	H	YHH,LHH	43	22	29	2	33	1722	6594
4	X.L	WIDE-SWATH	L	28	H	H	XHH,LHH	43	22	29	2	33	1690	5507
5	X.L	WIDE-SWATH	L	28	H	H	XHH,LHH	43	22	29	11	39	1711	6255
6	Y.L	WIDE-SWATH	R	28	H	H	XHH,LHH	43	21	28	11	39	1740	6119

63
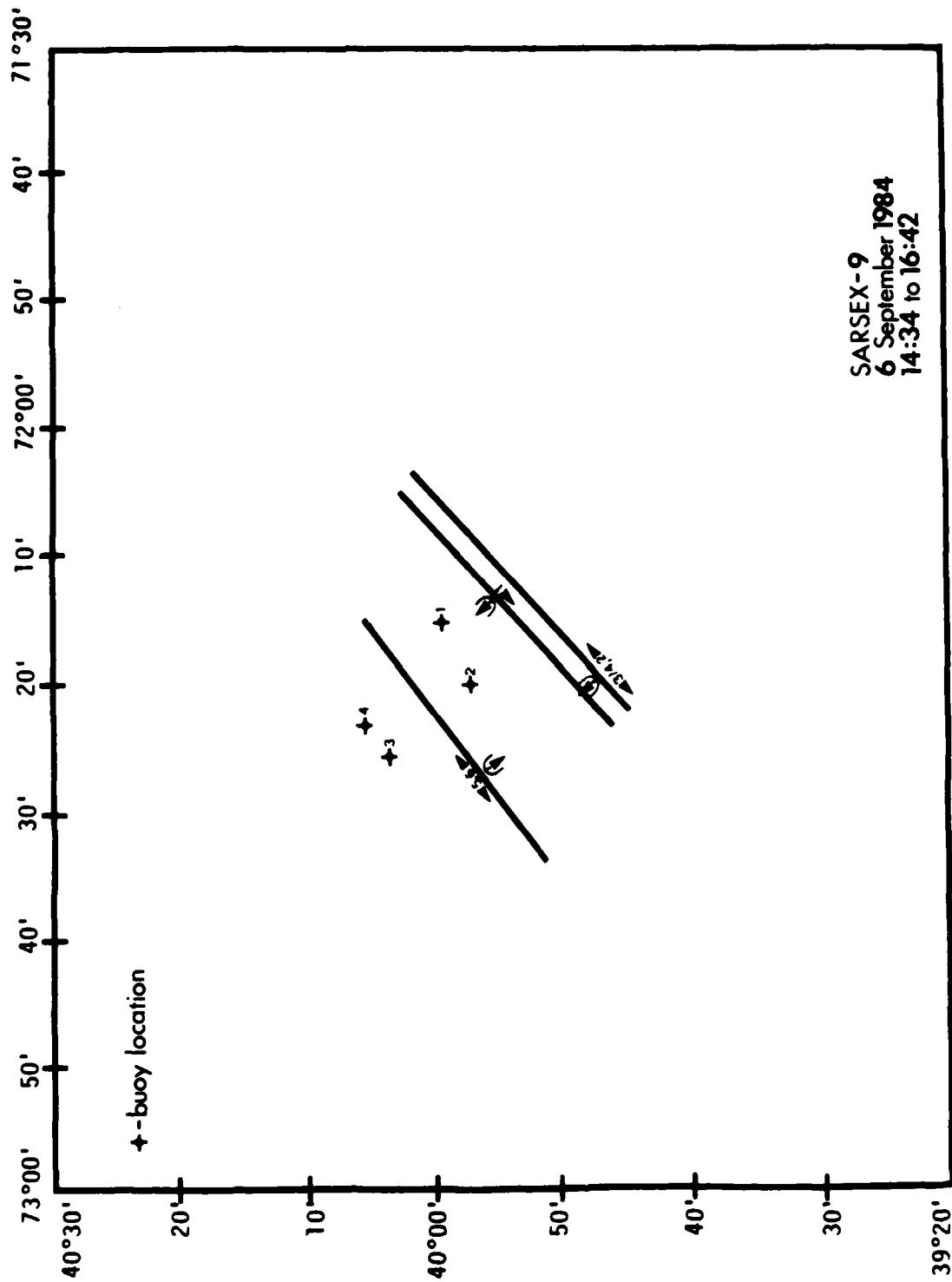
Figure 26.   Locations of Aircraft Ground Tracks During SARSEX-9,   Passes 1-6

SARSEX-9
6 September 1984
14:34 to 16:42

+-buoy location

ΣERIM
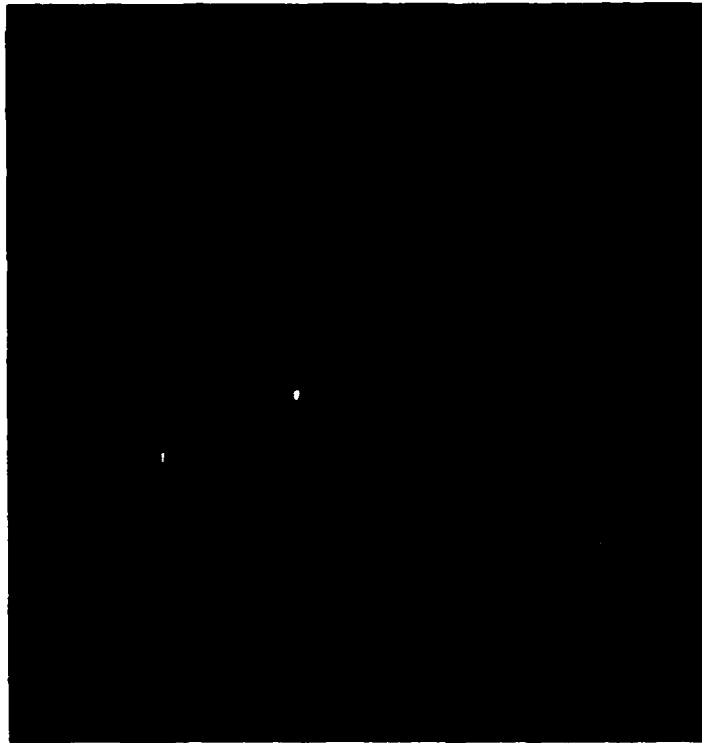
L-BAND

X-BAND

55°—
50°—
45°—
40°—
30°—
20°—
0°—

0   1000m
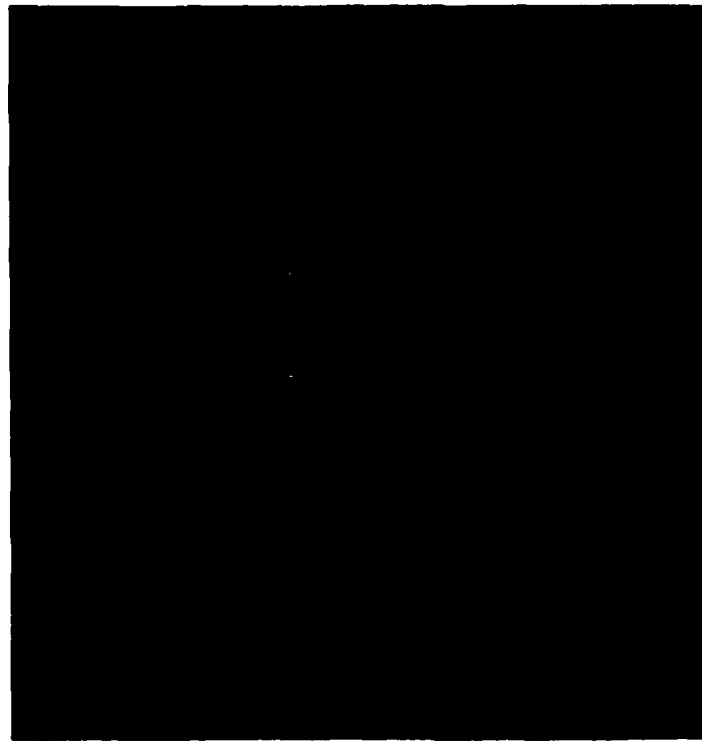
Figure 27. Digitally-Processed X- and L-band SAR Imagery Collected
During SARSEX-9, Pass 2

4.1.10   SARSEX-10 (7 September 1984 - 10:26 to 12:53 EDT)

The purpose of this mission was to collect calibration data and SAR imagery of surface internal wave patterns coincident with the DREP laser scatterometer. Four passes of imagery were collected over the calibration array and four passes over the SARSEX area.

The aircraft and SAR system parameters for the SARSEX-10 mission are summarized in Table 15. The flight lines are summarized in Figures 28 and 29.

The quality of the optically-processed imagery was excellent for both X- and L-bands. Again, the optically-recorded X-band calibration signals recorded optically during this mission were saturated. Further analyses is needed to determine the suitability of the X-band calibration signals for calibration of the SAR data. The L-band calibration signals appear to be suitable for calibration purposes.

TABLE 15. SUMMARY OF SAR AND AIRCRAFT PARAMETERS DURING SARSEX-10 (7 SEPTEMBER 1984).

CV-580 AIRCRAFT PARAMETERS

PASS	HEADING (TRUE)	VELOCITY (KNOTS)	ALTITUDE (FEET)	START TIME (EDT)	STOP TIME (EDT)	START LATITUDE	START LONGITUDE	STOP LATITUDE	STOP LONGITUDE
1	310	228	11000	10:26:18	10:32:01	40:44.3	72:37.6	40:58.1	72:59.8
2	130	257	11000	10:56:41	11:02:34	41:00.4	73:03.2	40:44.1	72:37.6
3	310	226	11000	11:18:35	11:25:14	40:45.1	72:36.5	41:01.0	73:01.7
4	130	257	11000	11:36:19	11:42:11	41:00.2	73:03.4	40:44.1	72:37.6
5	176	260	11000	11:50:39	11:54:00	40:09.5	72:28.6	39:55.0	72:27.2
6	237	251	11000	12:07:59	12:12:55	40:09.6	72:20.5	39:58.6	72:42.9
7	57	237	11000	12:24:43	12:32:28	39:59.1	72:42.8	40:15.7	72:09.3
8	327	227	11000	12:46:15	12:53:08	40:01.0	72:22.9	40:22.7	72:41.1

SAR PARAMETERS

PASS	WAVELENGTHS	SAR MODE	LOOK	ANTENNA DEPRESSION ANGLE	POLARIZATION TRANS	POLARIZATION REC	DIGITAL CHANNEL	RANGE DELAY (uSEC)	GAIN SETTINGS (dB ATTENUATION) X-B OPT	L-B OPT	X-B DIG	L-B DIG	TRANS POWER (WATTS) X-B	L-B
1	X,L	4-CHANNEL	R	15	H	HV	XHH,LHH	29	20	39	26	53	1690	6824
2	X,L	4-CHANNEL	L	15	H	HV	XHH,LHH	29	32	39	26	53	1675	6715
3	X,L	4-CHANNEL	R	15	V	VH	XVV,LVV	29	25	33	26	53	1706	7081
4	X,L	4-CHANNEL	L	15	V	VH	XVV,LVV	29	27	33	26	53	1713	6637
5	X,L	4-CHANNEL	R	15	V	VH	XVV,LVV	29	21	24	0	0	1709	6820
6	X,L	4-CHANNEL	R	15	V	VH	XVV,LVV	29	20	24	12	45	1726	6984
7	X,L	4-CHANNEL	L	15	V	VH	XVV,LVV	29	21	23	12	43	1715	6797
8	X,L	4-CHANNEL	L	15	V	VH	XVV,LVV	29	21	24	12	43	1715	7368
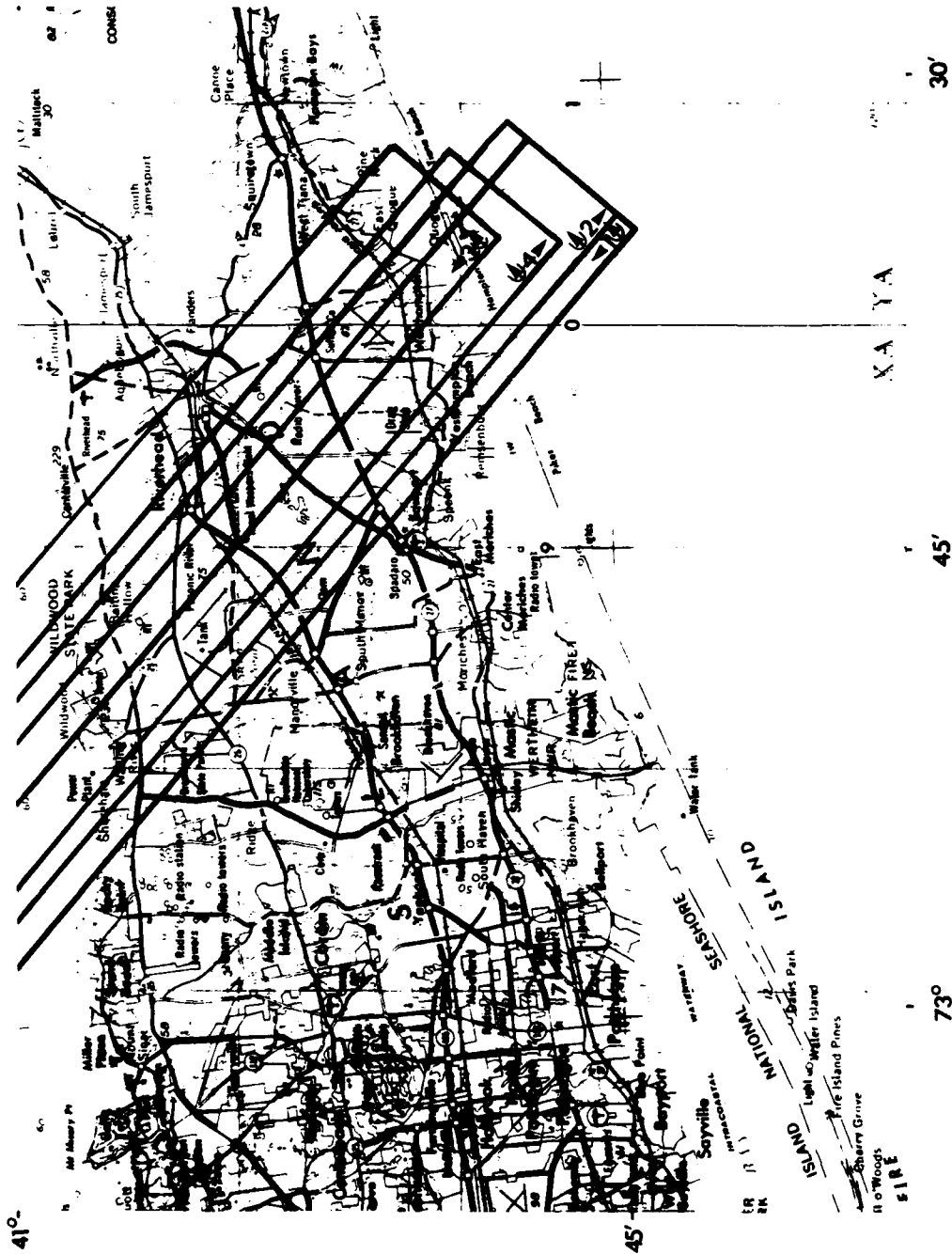
Figure 28.   Location of SAR Ground Coverage During SARSEX-10, Passes 1-4
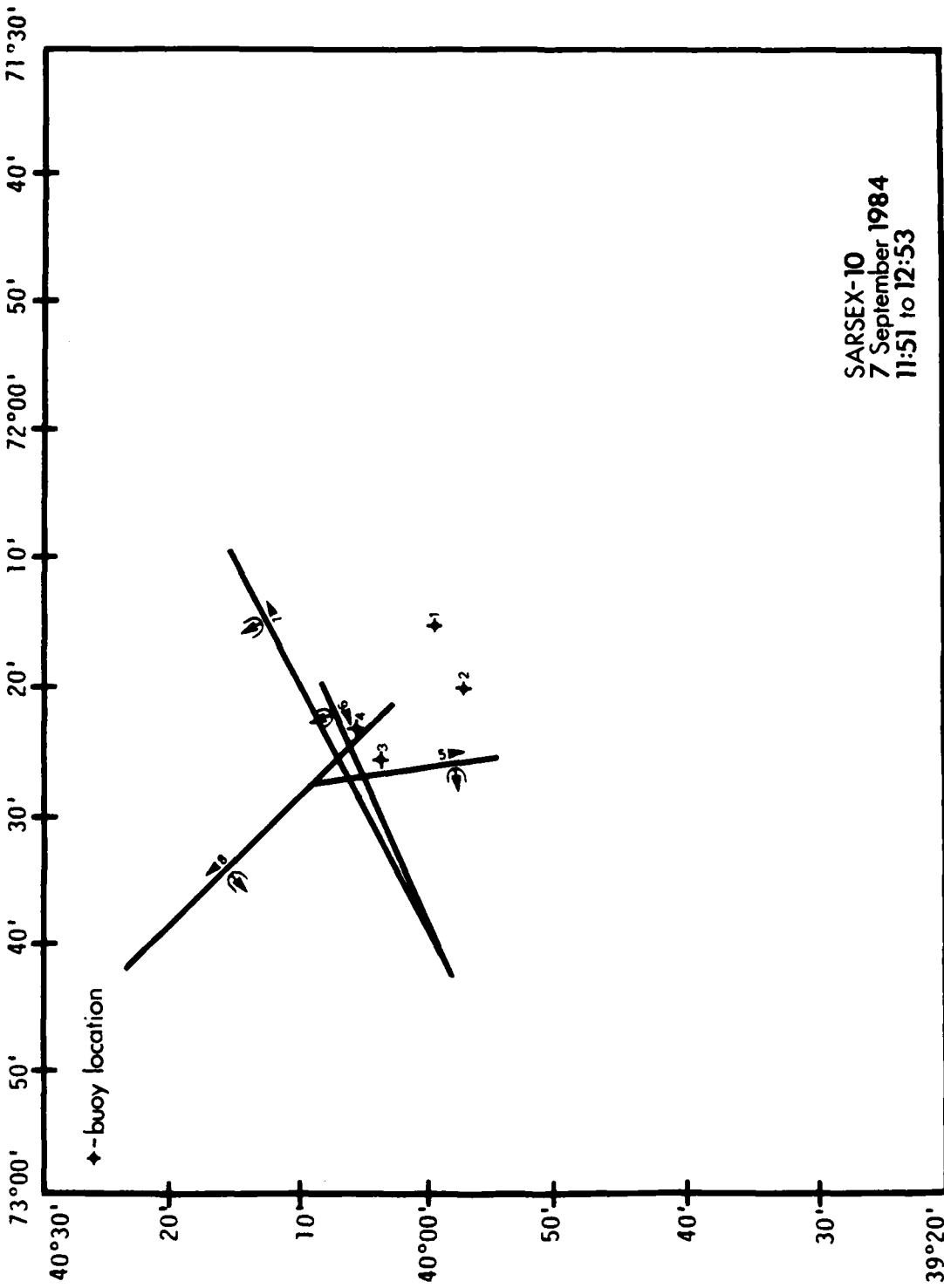
Figure 29.   Location of Aircraft Ground Tracks During SARSEX-10, Passes 5-8

SARSEX-10
7 September 1984
11:51 to 12:53

+ - buoy location

4.2 SAR CALIBRATION DATA

The data acquired during SARSEX to assist in the calibration of the SAR imagery are discussed in this section. These data include images of a calibrated corner reflector array and images of internally generated calibration signals.

The calibrated corner reflector array was located at the Grumman Peconic River Airport. This array was successfully imaged a total of 22 times during SARSEX in order to provide a calibrated reference for the SAR imagery. Table 16 lists the types and sizes of corner reflectors which were deployed in the array. The positions of these reflectors are presented in Figures 30 to 32.

Four different types of reflectors were used in the calibration array (see Figure 33):

a. Aluminum trihedral – square and triangular precision trihedral reflectors of known radar cross section.

b. Styrafoam trihedral – square trihedral reflectors constructed of aluminum coated styrofoam used for large L-band reflectors and for antenna pattern corrections.

c. Luneberg lens – a specialized spherical reflector used primarily to calibrate X-band SAR data (see Walker and Larson, 1981).

d. Active Radar Calibrator (ARC) – an active transponder used to calibrate airborne and spaceburne SAR data (see Brunfeldt and Ulaby, 1984).

Figure 34 presents X- and L-band imagery of the corner reflector array generated from digitally recorded data collected durirg SARSEX-10, Pass 1 (7 September 1984). The individual corner reflectors can clearly be seen on this imagery.

TABLE 16
SUMMARY OF CORNER REFLECTORS DEPLOYED AT PECONIC RIVER AIRPORT DURING AUGUST/SEPTEMBER 1984

Designation	Number of Reflectors	Reflector Type*	Reflector Size (cm)	Radar Cross Section X-Band (m^2)	L-Band (m^2)
A	1	AR1	—	—	1538
B	3	SQS	119	73828	1429
C	1	AR2	—	—	631
D	2	TRA	119	8200	159
E	3	TRA	116	7406	143
F	2	TRA	91	2805	54
G	1	TRA	88	2453	48
H	2	TRA	68	874	17
I	3	TRA	61	566	11
J	1	TRA	52	300	6
K	1	LLS	—	262	—
L	2	TRA	45	168	3
M	3	LLS	—	104	—
N	1	TRA	39	95	2
O	1	SQA	22	89	2
P	2	TRA	38	85	1.5
Q	2	LLS	—	32	—
R	3	TRA	29	30	—
S	1	SQA	17	30	—
T	1	TRA	23	11	—
U	2	TRA	22	10	—
V	20	SQS	61	5097	99

---

*AR1 – Single Polarization Active Radar Calibrator
AR2 – Dual Polarization Active Radar Calibrator
LLS – Luneberg Lens
SQA – Square Aluminum Precision Corner Reflector
SQS – Square Styrofoam Corner Reflector (Aluminum Coated)
TRA – Triangular Aluminum Precision Corner Reflector

Peconic River Airport
Calibration Array
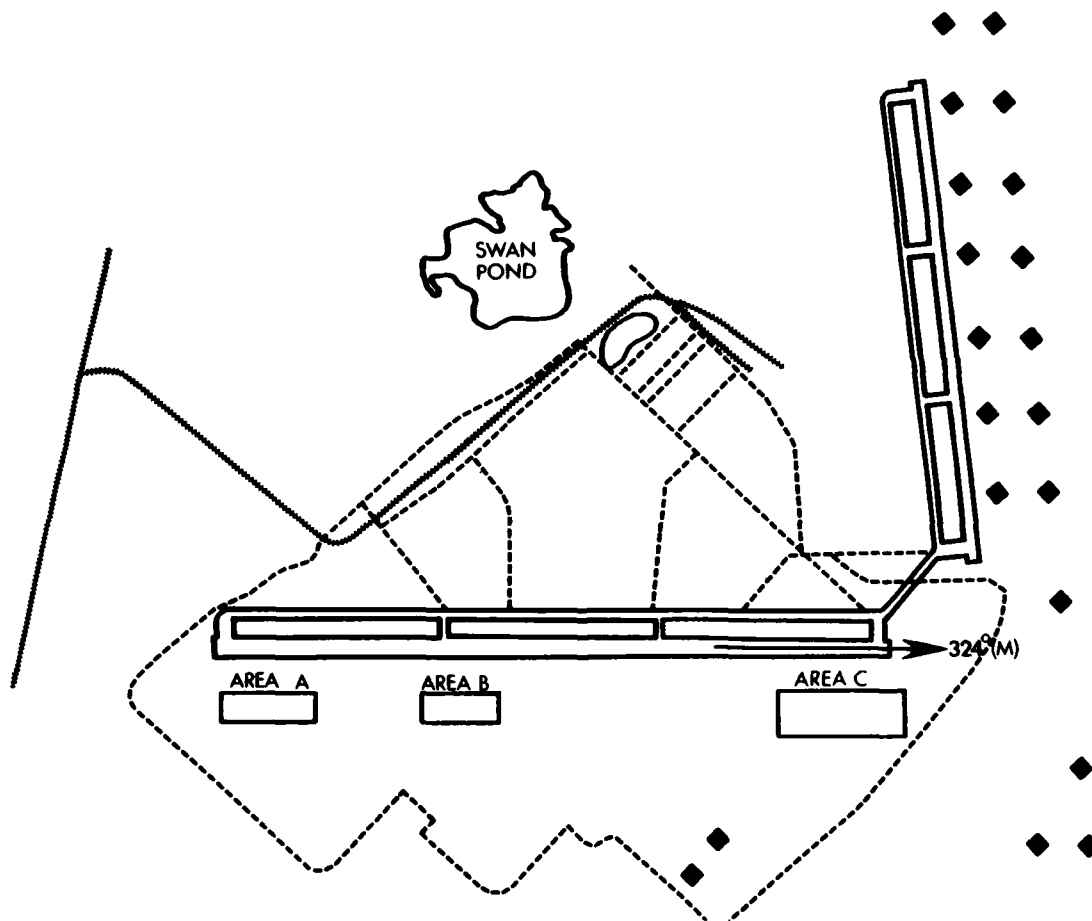
Figure 30.   Location of Calibrated Reflectors Sites at Peconic River
Airport

72

AREA A

234°(M)

◆ B(11")

◆ B(11")

◆ B(11")

◇ A

- -

AREA B

234° (M)

▽ E(11")

▽ D(9')

▽ E(10')   ▽ G(10.5')

▽ E(7.5')

▽ F(9.5')

KEY

▽ D(9.5')

◇ Active Radar Calibration

◇ Aluminum Precision Corner Reflector   ▽ F(10')

◆ Square Styrofoam Reflector

▽ Triangular Precision Corner Reflector
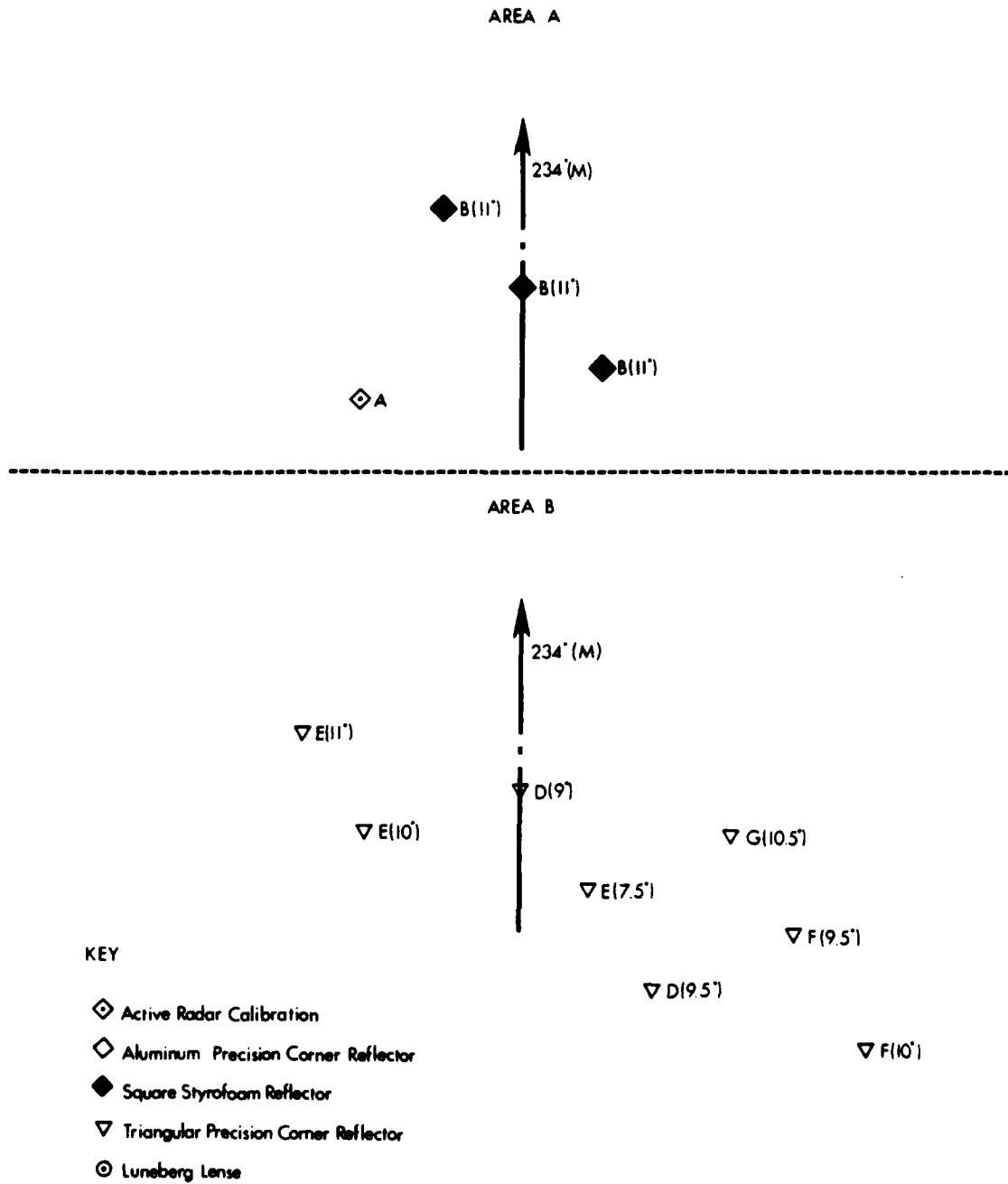
⊙ Luneberg Lense

Figure 31. Location of Calibrated Reflectors Located at Areas A and B

ΣERIM

AREA C

234'(M)

◇S

○

◇

▽U

▽R

▽T

▽R

▽P(8')

▽N(10')

▽R

▽P(9')

▽T

○Q ○M

○Q

○M

○K

○M

▽L(8')

▽J(10')

▽L(9')

▽I(12.5')

▽I(8')

▽H(10.5') ▽I(10')

▽H(11')

◇C

KEY

◇ Active Radar Calibration

◇ Aluminum Precision Corner Reflector

◆ Square Styrofoam Reflector

▽ Triangular Precision Corner Reflector

⊙ Luneberg Lense

Figure 32. Location of Calibrated Reflectors at Area C

74

STYROFOAM TRIHEDRAL

ACTIVE RADAR CALIBRATOR

ALUMINUM TRIHEDRAL

LUNEBERG LENSE

Figure 33. Typical Calibrated Reflectors Deployed at the Peconic River Airport

Figure 34. Digitally-Processed X- and L-band SAR Imagery of the
                Peconic River Airport Calibration Array

An engineering evaluation of the calibration data is presented in Chapter 5. In summary, the imagery collected over the calibration array appears to be of high quality. Most of the calibration signals are suitable for calibration purposes. The images of the calibration signals collected during SARSEX-5 appears to be unfocused, and may not be suitable for calibration purposes. The X-band calibration signals from SARSEX-7 through SARSEX-10 appear to be saturated. These signals may or may not be suitable for calibration purposes.

5
PRELIMINARY ENGINEERING ASSESSMENTS

The engineering assessments performed on the SAR data collected during SARSEX were divided into three parts: (1) assessment of the optically-processed data; (2) assessment of the digitally-processed data; and (3) assessment of the calibration data. An individual section of this chapter is devoted to each one of these topic areas.

5.1 OPTICALLY-PROCESSED DATA

Although the primary emphasis of the analysis of SARSEX data will be placed on the digitally-recorded and processed SAR data, the optically-recorded data still fulfills several important functions. First, the optically-processed imagery serves as an efficient means to review the SAR coverage during a specific mission and to obtain an idea of the types of internal wave surface patterns present during that mission. This imagery also provides a means to monitor the SAR system performance during a specific mission. By recognizing specific image characteristics, those passses which may have limitations for further processing and analysis (because of a system malfunction) can be identified.

Three distinct image characteristics were noted on the SAR imagery from SARSEX which to some extent reduced the image quality. These characteristics are: (1) modulation intensity variation, (2) low image signal-to-noise; and (3) unfocused imagery. In addition, on several occasions, the L-band optical recorder malfunctioned, resulting in no optical data being recorded for several passes. For examples of the above image characteristics, the reader is referred to Kasischke, et al. (1983).

Excessive aircraft motion caused by areas of high turbulence during data collection sometimes creates a range-oriented banded pattern within the imagery. These bands are referred to as modulation intensity variations. This type of image characteristic is most often found in X-band data.

The CV-580 X-band SAR employs a clutterlock system to insure that the Doppler spectrum of the returned phase histories remains centered during the data collection flight. The clutterlock system uses a spectrum analyzer to track the phase of the return signal. When weak signals are encountered, such as those from a water surface, the clutterlock system does not function well and the Doppler spectrum can wander, resulting in areas of unfocused imagery.

During SARSEX, higher than normal gain settings were utilized in order to obtain stronger returns from the water surface. In some cases, however, the gain settings were not high enough, creating imagery with low signal-to-noise over water.

Each pass of optically-processed X- and L-band imagery from the like-polarized channel (VV or HH) was evaluated. The degree to which the above mentioned image characteristics were present in the imagery was noted. The following rating criteria were used:

+   slight reduction in image quality,
*   moderate reduction in image quality, or
-   severe reduction in image quality.

In addition to noting the types and severity of the characteristics present in the imagery, the quality of each pass of imagery was rated using the following categories:

7   Excellent imagery

6

5   Good imagery

4

3   Fair Imagery

2

1   Poor Imagery

0   Data not recorded or of insufficient quality to be useful.

A rating of excellent implies that the data are of the highest quality and require *no additional precision processing.* A rating of good implies that there are slight or moderate image perturbations present, which usually can be removed through precision processing of the imagery. A rating of fair implies there is much usuble data present, and that the moderate to severe image perturbations may be removed through precision processing. A rating of poor implies that the severe image perturbations generally cannot be removed through precision processing.

It should be noted that the above ratings are based upon the subjective opinions of several people and are intended to serve as an indicator of the overall quality of the imagery collected during SARSEX. Table 17 summarizes the ratings of the SAR imagery. Note from Table 17 that it is possible to have a number of image pertur-bations and still have high quality imagery. Care was taken when reviewing each pass to base the rating on the quality of the imagery over the target site.

From the ratings in Table 17, the following generalizations can be made concerning the quality of the X-band optically-processed imagery: 89 percent of the imagery has a quality rating of good or better, and 98 percent of the imagery has a rating fair or better. Therefore, with special processing of the imagery, it should be pos-sible to use most of the X-band imagery for further analysis. The L-band optically-processed imagery is of very high quality. With the exception of two passes where no data were recorded, all the imagery is of good quality or better and 92 percent is of excellent quality. Therefore, little special processing of the L-band data will have to be performed.

TABLE 17
SUMMARY OF IMAGE CHARACTERISTICS AND IMAGE QUALITY RATINGS

Mission	Pass	Radar Frequency	Area	Image Quality	Image Characteristics MIV	LSN	UFI	NDR
SARSEX-1	1	X	IW	6	+			
		L		7				
	2	X	IW	5	+			
		L		7				
	3	X	IW	6	+			
		L		7				
	4	X	IW	5	+			
		L		7				
	5	X	IW	2		−		
		L		3		−		
	6	X	IW	2	+	−		
		L		3		−		
SARSEX-2	1	X	CA	5	+		+	
		L		0				−
	2	X	CA	6	+		+	
		L		7			+	
	3	X	CA	2	−		−	
		L		7	+			
SARSEX-3	1	X	CA	6	+			
		L		7				
	2	X	CA	7	+			
		L		7				
	3	X	IW	6	+			
		L		7				
	4	X	IW	6	+			
		L		6	+			
	5	X	IW	5	+			
		L		7				
	6	X	IW	6	+			
		L		7				
	7	X	IW	6	+			
		L		7				
	8	X	IW	6	+			
		L		7				
	9	X	IW	6	+			
		L		7				

Key

Image

    7 – Excellent
    6
    5 – Good
    4
    3 – Fair
    2
    1 – Poor

Image Characteristics

    MIV – Modulated Intensity Variation
    LSN – Low Image Signal-to-Noise
    UFI – Unfocused Imagery
    NDR – No Data Recorded

    + : Slight Reduction in Image Quality
    * : Moderate Reduction in Image Quality
    − : Severe Reduction in Image Quality

TABLE 17
SUMMARY OF IMAGE CHARACTERISTICS AND
IMAGE QUALITY RATINGS (CONTINUED)

Mission	Pass	Radar Frequency	Area	Image Quality	M I V	L S N	U F I	N D R
					Image Characteristics			
SARSEX-4	1	X	IW	4	+			
		L		7				
	2	X	IW	5	+			
		L		7				
	3	X	IW	4	+	+		
		L		7				
	4	X	IW	4	+	+		
		L		7				
	5	X	IW	4	+	+		
		L		7				
	6	X	IW	5	+			
		L		7				
	7	X	IW	4	+	+		
		L		7				
	8	X	IW	5	+			
		L		7				
	9	X	IW	5	+	+		
		L		7				
	10	X	CA	Aborted				
		L						
	11	X	CA	7	+			
		L		7				
	12	X	CA	5	+		+	
		L		7				
SARSEX-5	1	X	CA	5	+			
		L		7				
	2	X	CA	6	+			
		L		7				
	3	X	CA	4	*			
		L		7				
	4	X	IW	5	+			
		L		5		+		
	5	X	IW	5	+			
		L		7				
	6	X	IW	5	+			
		L		7				

Key

Image

    7 - Excellent
    6
    5 - Good
    4
    3 - Fair
    2
    1 - Poor

Image Characteristics

    MIV - Modulated Intensity Variation
    LSN - Low Image Signal-to-Noise
    UFI - Unfocused Imagery
    NDR - No Data Recorded

    + : Slight Reduction in Image Quality
    * : Moderate Reduction in Image Quality
    - : Severe Reduction in Image Quality

TABLE 17
SUMMARY OF IMAGE CHARACTERISTICS AND
IMAGE QUALITY RATINGS (CONTINUED)

					Image Characteristics			
Mission	Pass	Radar Frequency	Area	Image Quality	M I V	L S N	U F I	N D R
SARSEX-5	7	X	IW	6	+			
		L		7				
	8	X	IW	4	+	*		
		L		7				
	9	X	IW	4	+	*		
		L		7				
	10	X	IW	5	+	+		
		L		7				
	11	X	IW	5	+	+		
		L		7				
	12	X	IW	5	+	+		
		L		7				
SARSEX-6	1	X	CA	7	+			
		L		7	+			
	2	X	CA	7	+			
		L		7				
	3	X	CA	6	*			
		L		6				
	4	X	CA	6	*			
		L		7				
	5	X	IW	5	*			
		L		7	+			
	6	X	IW	5	*			
		L		7	+			
	7	X	IW	5	*			
		L		7				
	8	X	IW	5	*			
		L		7				
	9	X	IW	6	*			
		L		7				
	10	X	IW	6	+			
		L		7				
	11	X	IW	6	*			
		L		7				

Key

Image

     7 - Excellent
     6
     5 - Good
     4
     3 - Fair
     2
     1 - Poor

Image Characteristics

     MIV - Modulated Intensity Variation
     LSN - Low Image Signal-to-Noise
     UFI - Unfocused Imagery
     NDR - No Data Recorded

     + : Slight Reduction in Image Quality
     * : Moderate Reduction in Image Quality
     - : Severe Reduction in Image Quality

TABLE 17
SUMMARY OF IMAGE CHARACTERISTICS AND
IMAGE QUALITY RATINGS (CONTINUED)

Mission	Pass	Radar Frequency	Area	Image Quality	Image Characteristics MIV	LSN	UFI	NDR
SARSEX-7	1	X	CA	7	+			
		L		7				
	2	X	CA	7	+			
		L		7				
	3	X	CA	7	+			
		L		7				
	4	X	IW	5	+			
		L		7				
	5	X	IW	7	+			
		L		7				
	6	X	IW	7	+			
		L		7				
	7	X	IW	7	+			
		L		7				
	8	X	IW	7	+			
		L		7				
	9	X	IW	7	+			−
		L		0				−
	10	X	IW	7	+			
		L		7				
	11	X	IW	7	+			
		L		7				
	12	X	IW	7	+			
		L		7				
SARSEX-8	1	X	CA	7	+			
		L		7				
	2	X	CA	6	*			
		L		7				
	3	X	IW	7	+			
		L		7				
	4	X	IW	7	+			
		L		7				
	5	X	IW	7	+			
		L		7				
	6	X	IW	7	+			
		L		7				

Key

Image

　　7 – Excellent
　　6
　　5 – Good
　　4
　　3 – Fair
　　2
　　1 – Poor

Image Characteristics

　　MIV – Modulated Intensity Variation
　　LSN – Low Image Signal-to-Noise
　　UFI – Unfocused Imagery
　　NDR – No Data Recorded

　　　+ : Slight Reduction in Image Quality
　　　* : Moderate Reduction in Image Quality
　　　− : Severe Reduction in Image Quality

TABLE 17
SUMMARY OF IMAGE CHARACTERISTICS AND IMAGE QUALITY RATINGS (CONCLUDED)

Mission	Pass	Radar Frequency	Area	Image Quality	MIV	LSN	UFI	NDR
SARSEX-8	7	X	IW	7	*			
		L		7				
	8	X	IW	7	+			
		L		7				
	9	X	IW	7	+			
		L		7				
	10	X	IW	7	+			
		L		7				
SARSEX-9	1	X	IW	7	+			
		L		7				
	2	X	IW	7	+			
		L		7				
	3	X	IW	7	+			
		L		7				
	4	X	IW	7	+			
		L		7				
	5	X	IW	7	+			
		L		7				
	6	X	IW	7	+			
		L		7				
SARSEX-10	1	X	CA	6	*			
		L		7				
	2	X	CA	7	+			
		L		7				
	3	X	CA	5	*	+		
		L		7				
	4	X	CA	6	*			
		L		7				
	5	X	IW	7	+			
		L		7				
	6	X	IW	7	+			
		L		7				
	7	X	IW	7	+			
		L		7				
	9	X	IW	7	+			
		L		7				

Key

Image

    7 - Excellent
    6
    5 - Good
    4
    3 - Fair
    2
    1 - Poor

Image Characteristics

    MIV - Modulated Intensity Variation
    LSN - Low Image Signal-to-Noise
    UFI - Unfocused Imagery
    NDR - No Data Recorded

    + : Slight Reduction in Image Quality
    * : Moderate Reduction in Image Quality
    - : Severe Reduction in Image Quality

END

FILMED

DTIC

MICROCOPY RESOLUTION TEST CHART

NATIONAL BUREAU OF STANDARDS – 1963 – A

5.2 DIGITALLY-PROCESSED DATA

During SARSEX, two channels of SAR data were recorded digitally. These data consisted of the first 6.1 km in slant range of the X_{HH} or X_{VV} and L_{HH} or L_{VV} channels from the CV-580 SAR system. Only one major problem was encountered which affects the digitally-recorded data: during SARSEX-7, an operator error apparently resulted in no digital data being recorded during Passes 4 through 6.

In order to assess the quality of the digitally-recorded SAR data set from SARSEX, a set of measurements were made on two digitally processed SAR scenes collected over the calibrated corner reflector array. These measurements include (for both X- and L-band) impulse response resolution and sidelobe level, system background noise, signal-to-noise ratio, clutter-to-noise ratio, and image contrast. The scenes selected for analysis were from SARSEX-4, Pass 12 and SARSEX-10, Pass 1.

In the remaining portions of this section, we will first define the image quality measurements, then present the actual measurements, and finally discuss their significance.

5.2.1 SYSTEM IMPULSE RESPONSE (IPR)

SAR system impulse response (IPR) is defined as the output signal, including sidelobes, arising from a unit impulse input. A point reflector, such as a corner reflector, approximates a unit impulse in a SAR system. An intensity scan of the image of a corner reflector thus provides system impulse response. Typically, IPR scans are made in both the range and azimuth dimensions. These scans can be used to measure system resolution and sidelobe levels. The IPR value corresponding to resolution is the width of the mainlobe taken at a level 3 dB below the mainlobe peak. This width defines the Rayleigh resolution of the system. IPR measurements are given in terms of mainlobe width and level of the first sidelobe.

A total of 20 IPR scans were made on the X-band digitally proc-essed imagery and 19 IPR scans on the L-band digitally processed imagery. Figure 35 presents typical IPR scans from an X-band corner reflector imagery and Figure 36 presents typical L-band IPR scans. Marked on these scans are the -3 dB resolution and the level of the first sidelobe. Table 18 summarizes the measurements made on the 39 IPR scans.

The IPR scan measurements are comparable to or better than sim-ilar measurements made on data collected during the Georgia Strait Experiment (see Kasischke, et al., 1983). Comparison of the X-band measurements reveals a relative consistency between the two different days. However, the L-band measurements appear better on 7 September than they did on 31 August.

5.2.2 SYSTEM BACKGROUND NOISE

System background noise is measured as the average image inten-sity of an area where no radar return is received. Such areas include shadows, regions of specular reflection such as airport run-ways and undisturbed water, and the region around calibration sig-nals. The measured system noises for the two data sets are presented in Table 19. The system background noise levels are comparable to previous measurements.

5.2.3 SIGNAL-TO-NOISE RATIO

Signal-to-noise ratio (SNR) is defined as the ratio of the max-imum level found on the image to the background noise, expressed in dB. The SNR values listed in Table 19 are consistent with those obtained from SAR data collected during the Georgia Strait Experiment.
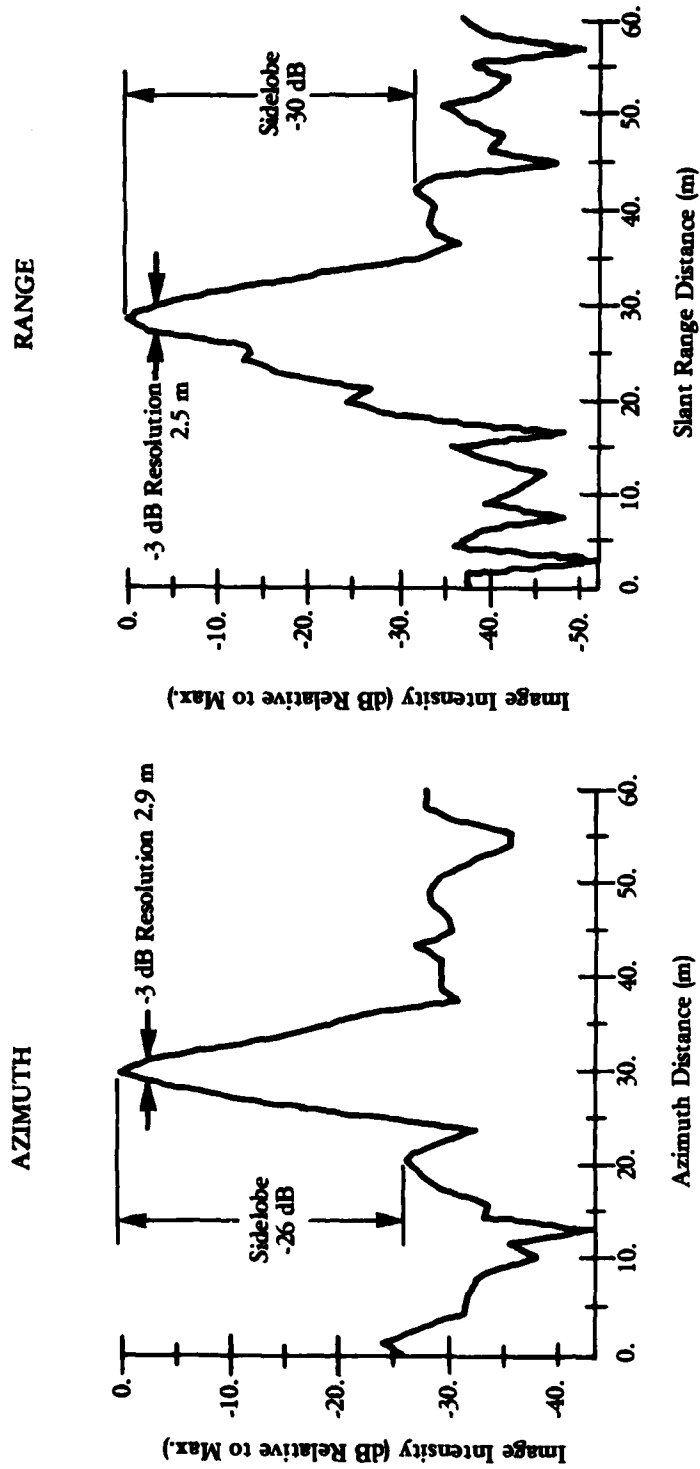
Figure 35. Impulse Response Scans From X-band Digitally-Processed SAR Data
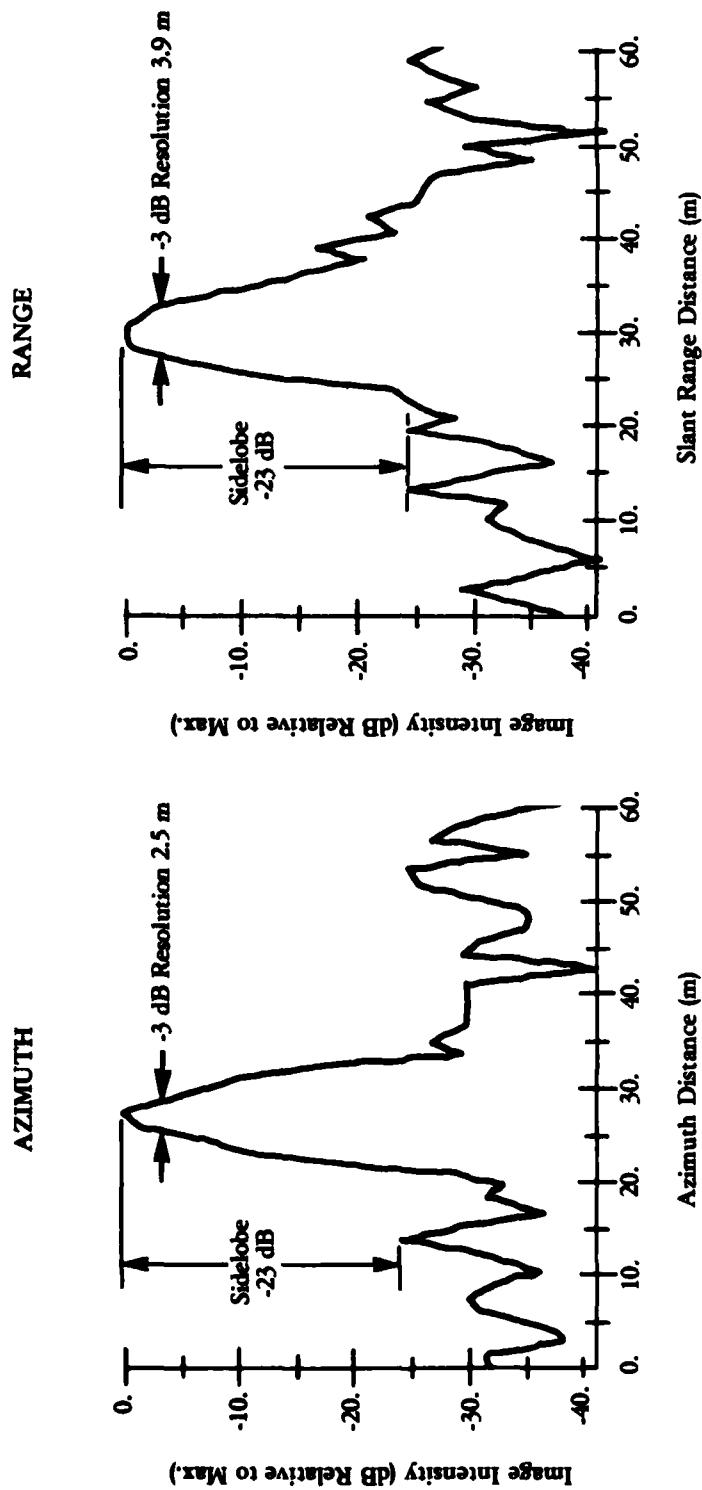
Figure 36. Impulse Response Scans From L-band Digitally-Processed SAR Data

TABLE 18
SUMMARY OF IMPULSE RESPONSE SCAN MEASUREMENTS

	-3 dB Width (m)				First Sidelobe Levels (dB)			
	SARSEX-4, Pass 12 (31 August 1984)		SARSEX-10, Pass 1 (7 September 1984)		SARSEX-4, Pass 12 (31 August 1984)		SARSEX-10, Pass 1 (7 September 1984)	
	Azimuth	Range	Azimuth	Range	Azimuth	Range	Azimuth	Range
X-band								
Number	10	10	10	10	10	10	10	10
Average	2.6	3.6	2.6	2.9	-19.8	-22.3	-21.6	-25.5
Minimum	2.5	2.7	2.5	2.8	-27.9	-27.9	-25.3	-35.8
Maximum	3.8	3.8	2.7	3.1	-4.0	-14.7	-13.5	-13.0
L-Band								
Number	9	9	10	10	9	9	10	10
Average	4.1	5.6	2.6	3.9	-5.7	-12.8	-15.7	-13.9
Minimum	2.6	3.7	2.1	3.2	-14.0	-17.9	-26.4	-20.3
Maximum	6.6	7.2	4.7	4.7	-1.3	-3.0	-6.1	-5.7

TABLE 19
SUMMARY OF IMAGE QUALITY MEASUREMENTS MADE
ON SARSEX SAR DATA

	SARSEX-4, Pass 12 (31 August 1984)		SARSEX-10, Pass 1 (7 September 1984)	
	X-Band	L-Band	X-Band	L-Band
System Background Noise Intensity	4142	691	6918	1516
Signal-to-Noise Ratio	46.6 dB	38.4 dB	46.8 dB	45.0 dB
Clutter-to-Noise Ratio	12.6 dB	7.7 dB	11.6 dB	9.7 dB
Image Contrast	20.4 dB	10.9 dB	18.8 dB	12.8 dB

5.2.4 CLUTTER-TO-NOISE RATIO

Clutter is defined as the average background return over a spec-
ified distributed target area. A clutter-to-noise ratio (CNR) is
obtained by measuring the image intensity over low and high intensity
distributed targets such as agricultural fields, averaging them, and
dividing by the system noise value. Again, the CNR values obtained
during SARSEX and listed in Table 19 are consistent with those ob-
tained from SAR data collected during the Georgia Strait Experiment.

5.2.5 IMAGE CONTRAST

Image contrast is defined as the spatial change expressed in dB
corresponding to a step-function change in a scene from bright return
to no return. For example, the change from a highly reflecting lake
edge to the still, non-reflecting water can be used as an indication
of contrast. (Note: this definition is for purposes of these engi-
neering evaluations. Other definitions are also valid.) Samples of
the image contrast scans are presented in Figure 37. The values are
listed in Table 19. The values between the two dates are consistent.

5.2.6 DISCUSSION

The image quality measurements made on the SAR data from
SARSEX-4, Pass 12 and SARSEX-10, Pass 1 indicate the SAR was per-
forming well during the SARSEX data collection. Comparison of these
measurements to those made on APL-processed imagery, along with com-
parison of the calibration procedures, should provide a valid means
to combine the imagery from both systems in the SARSEX analyses dis-
cussed in the next chapter.

5.3 CALIBRATION DATA

The optically-recorded and processed images of the calibrated
corner reflector array and the internal calibration signals (see
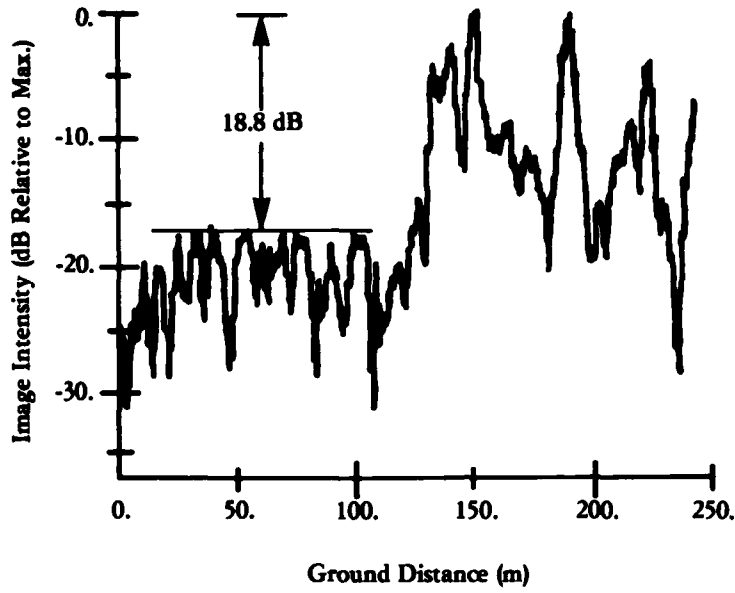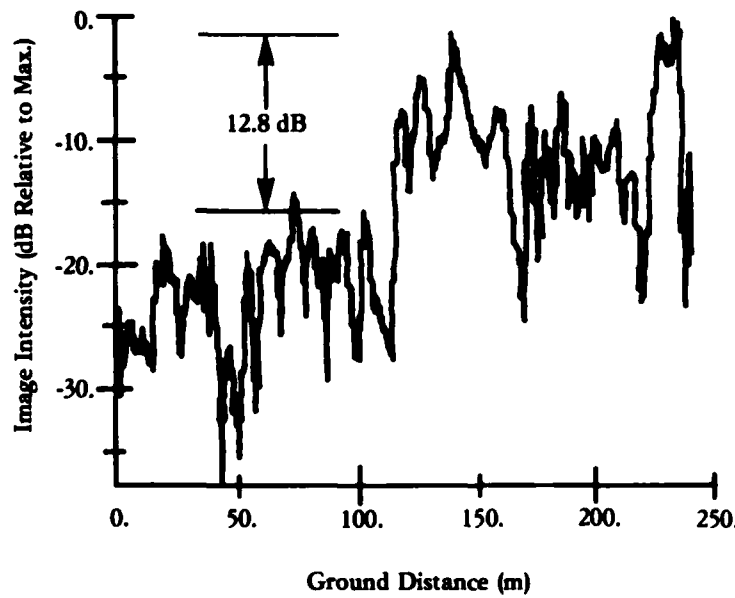
Figure 37. Image Contrast Scans Generated From Digitally-Processed X-
and L-band SAR Data

94

Section 3.2) were reviewed and assessed for utility to calibrate the SAR imagery. Table 20 presents information on this assessment. Listed in Table 20 are the SARSEX mission number, the pass, the incidence angle of the corner reflector array, the quality of the calibration array imagery (see Section 4.1 for a discussion of these ratings, and the quality of the calibration signal images), and the quality of the calibration signal images.

The key to the calibration signal images rating is as follows: a two-star (**) rating indicates the images are suitable for calibration purposes; a one-star (*) rating indicates there is some question as to the suitability of these data, and further assessment is needed; and a no-star rating indicates the images are not suitable for calibration purposes.

Several problems with the optically-recorded calibration signal images were noted: (1) no images were optically recorded after several passes; (2) both the X- and L-band calibration signal images were unfocused during SARSEX-5, and (3) the X-band calibration signal images appear to be saturated for SARSEX-6 through SARSEX-10.

It was not clear whether these latter two problems preclude the use of the signals for calibration purposes. To address this question, further analyses are being performed on the calibration signals recorded digitally. Data sets selected for analysis include the calibration signals after SARSEX-4, Pass 12; SARSEX-5, Pass 2 and SARSEX-8; Pass 4.

$\sum$ERIM

TABLE 20
SUMMARY OF CALIBRATION DATA QUALITY

Mission	Pass	Incidence Angle	Calibration Array Image Quality[+]		Calibration Signal Quality[++]	
			X	L	X	L
SARSEX-1	1				**	**
	2				**	**
	3					
	4				**	**
	5				*	*
	6					
SARSEX-2	1	38°	5	0		
	2	42°	6	7	**	**
	3	28°	2	7		
SAkSEX-3	1	39°	6	7	**	**
	2	39°	7	7		**
	3				**	**
	4				**	**
	5				**	**
	6				**	**
	7				**	**
	8				**	**
	9				**	**
SARSEX-4	1				**	**
	2				**	**
	3				**	**
	4				**	**
	5				**	**
	6				**	**
	7				**	**
	8				**	**
	9				**	**
	10				Aborted	
	11	38°	7	7	**	**
	12	56	5	7	**	**

[+]See Section 5.1.

[++]Key

**Data suitable for calibration purposes.

*Data may be suitable for calibration purposes, more analysis required.

No Star - Data not suitable for calibration purposes.

96

TABLE 20
SUMMARY OF CALIBRATION DATA QUALITY
(Continued)

Mission	Pass	Incidence Angle	Calibration Array Image Quality[+]		Calibration Signal Quality[++]	
			X	L	X	L
SARSEX-5	1	43°	5	7	*	*
	2	41°	6	7	*	*
	3	40°	4	7	*	*
	4				*	*
	5				*	*
	6				*	*
	7				*	*
	8				*	*
	9				*	*
	10				*	*
	11				*	*
	12				*	*
SARSEX-6	1	42°	7	7	**	**
	2	41°	7	7	**	**
	3	37°	6	6		
	4	48°	6	7	**	**
	5		6	7	**	**
	6		6	7	**	**
	7		6	7	**	**
	8		6	7	**	**
	9		6	7	**	**
	10		6	7	**	**
	11		6	7	**	**
SARSEX-7	1	40°	7	7	**	**
	2	44°	7	7		
	3	42°	7	7	**	**
	4				**	

[+]See Section 5.1.

[++]Key

**Data suitable for calibration purposes.

*Data may be suitable for calibration purposes, more analysis required.

No Star – Data not suiable for calibration purposes.

TABLE 20
SUMMARY OF CALIBRATION DATA QUALITY
(Continued)

Mission	Pass	Incidence Angle	Calibration Array Image Quality[+]		Calibration Signal Quality[++]	
			X	L	X	L
SARSEX-7	5				**	**
	6				*	**
	7				*	**
	8				*	**
	9				*	**
	10				*	**
	11				*	**
	12				*	**
SARSEX-8	1	47°	7	7	*	**
	2	45°	6	7	*	**
	3				*	**
	4				*	**
	5				*	**
	6				*	**
	7				*	**
	8				*	**
	9				*	**
	10				*	**
SARSEX-9	1				*	**
	2				*	**
	3				*	**
	4				*	**
	5				*	
	6				*	**

[+]See Section 5.1.

[++]Key

**Data suitable for calibration purposes.

*Data may be suitable for calibration purposes, more analysis required.

No Star - Data not suiable for calibration purposes.

TABLE 20
SUMMARY OF CALIBRATION DATA QUALITY
(Concluded)

Mission	Pass	Incidence Angle	Calibration Array Image Quality[+]		Calibration Signal Quality[++]	
			X	L	X	L
SARSEX-10	1	63°	6	7		
	2	59°	7	7	*	**
	3				*	**
	4	54°	6	7	*	**
	5				*	**
	6				*	**
	7				*	**
	8				*	**

[+]See Section 5.1.

[++]Key

    **Data suitable for calibration purposes.

    *Data may be suitable for calibration purposes, more analysis required.

    No Star – Data not suiable for calibration purposes.

6
PROPOSED DATA PROCESSING AND ANALYSIS ACTIVITIES

The overall analysis plan for SARSEX is presented in Apel, et al. (1985). The purpose of this chapter is to present in more detail those activities which will be carried out by scientists and engineers at ERIM. It is anticipated that these activities will be conducted over a two-year period.

There are four major processing and analysis activities:

1. Engineering Evaluation - Overall, the SAR data collected during SARSEX represents a high quality set of SAR imagery. There were few system malfunctions, but the impact of these have to be assessed and evaluated prior to proceeding with in-depth analyses of the impacted SAR data. Prior to final selection of the passes to use to meet the program objectives, an engineering analysis of the candidate data sets will be performed.

   In addition, under this activity, a comparison of image quality parameters made on ERIM-processed data (see Section 5.2) will be made with those made on APL-processed imagery. These measurements are necessary to insure that the imagery from each processor can be validly compared.

2. Data Processing - Two separate tasks will be pursued under this activity: (a) transcription of raw SAR signal histories from high density digial tapes to computer compatible tapes, and (b) processing of the raw signal histories into SAR images using ERIM's digital strip map processor (Jackson, et al., 1984).

3. Extraction of Radar Backscatter Measurements - Under this activity, radar backscatter signatures of surface internal wave patterns and from the ocean surface "background noise"

101

will be extracted from the digital SAR image scenes. These backscatter measurements will be calibrated in an absolute or relative sense, depending upon the application. These calibration procedures are discussed in greater detail below.

4. <u>Generation of Simulated SAR Images</u> - A major objective of SARSEX is to further evaluate and validate hydrodynamic/ electromagnetic models which predict how a SAR will image the ocean surface. The tasks included in this activity are further development of theoretical SAR imaging models and comparison of simulated SAR imagery from these models to actual SAR imagery collected during SARSEX. The tasks associated with this activity will be discussed in greater detail below.

Table 21 (after Apel, et al., 1985) summarizes the analysis activities which are to be carried out on the SARSEX data set. Table 22 presents a summary of the analysis tasks which will be pursued using the SARSEX data set and which imagery will be used to address each task. In the following sections, we will discuss in more detail those activities which will be pursued at ERIM during the analysis of the SARSEX data set.

6.1 EXTRACTION OF SAR INTERNAL WAVE SURFACE SIGNATURES

Once the digitally recorded SAR signal histories have been transcribed to CCTs and processed into image format, a careful set of steps will be performed in order to geometrically correct the imagery as well as calibrate the data in an absolute or relative sense.

6.1.1 GEOMETRIC CORRECTION OF SAR DATA

Because of their sidelooking geometry, SARs produce imagery in the slant range plane. The across-track position of an object in a SAR image is determined by its slant range, the straight line distance of the object from the SAR platform. Ground range, the

TABLE 21
ANALYSIS PLAN SUMMARY-PHASE I MEASUREMENTS
(AFTER GASPAROVIC, ET AL; 1985)

OBJECTIVE	ANALYSIS PRODUCTS	PRIORITY DATA SETS
Test validity of SAR internal wave signature prediction model.	Surface currents vs. position in IW packet. (APL)	31 Aug-PM (SARSEX-4)
	IW phase speeds. (APL)	3 Sept-PM (SARSEX-5)
	Measured surface wave spectrum in IW packet. (APL)	6 Sept-PM (SARSEX-9)
	Radar backscatter modulation at multiple incidence angles. (NRL)	
	SAR image intensity modulation. (ERIM/APL)	
	Comparison of measurements and model predictions for wave perturbations, backscatter modulations, and SAR intensity modulations. (APL/ERIM)	
Test validity of surface wave-internal wave hydrodynamic interaction model.	Same as above minus SAR image intensity modulations. (APL/NRL)	28 Aug-AM
Radar backscatter modulation vs. incidence angle.	Normalized backscatter modulation vs. incidence angle as a function of surface current and sea state. (NRL)	28 Aug-AM
		31 Aug-PM
		3 Sept-PM
		6 Sept-PM

TABLE 21
ANALYSIS PLAN SUMMARY-PHASE I MEASUREMENTS
(AFTER GASPAROVIC, ET AL; 1985) (CONCLUDED)

OBJECTIVE	ANALYSIS PRODUCTS	PRIORITY DATA SETS
SAR intensity modulation vs. incidence angle.	Normalized SAR image intensity modulation vs. incidence angle for range-travelling internal waves. (ERIM/APL)	31 Aug-PM (SARSEX-4) 5 Sept-PM (SARSEX-7) 6 Sept-PM (SARSEX-9)
	Comparison of SAR and radar backscatter results (ERIM/NRL)	
	Comparison with model predictions for incidence angle dependence. (ERIM/APL)	
SAR intensity modulation vs. azimuth angle.	Normalized SAR image intensity modulation vs. azimuth angle relative to IW propagation direction. (ERIM)	30 Aug-PM (SARSEX-3) 5 Sept-PM (SARSEX-7)
	Comparison with model predictions for azimuth angle dependence. (ERIM/APL)	
SAR intensity modulation vs. v/h ratio.	Normalized SAR image intensity modulation vs. v/h ratio at several incidence angles. (ERIM)	6 Sept-AM (SARSEX-8)
SAR Ocean background statistics vs. sea state.	Mean, variance, and wavenumber spectrum of SAR ocean background image intensity as a function of wind and sea state. (ERIM/APL)	TBD
	Comparison of measurements with SAR simulation model predictions. (ERIM)	

TABLE 22
SUMMARY OF DIGITAL SAR DATA PROCESSING
FOR SARSEX

▲ — High Priority   ■ — Medium Priority   ● — Low Priority

Analysis Requirement:
- Model Validation
- Calibration
- Engineering Evaluation
- SAR Backscatter vs. Incidence Angle
- SAR Backscatter vs. Azimuth Angle
- SAR Backscatter vs. Surface Strain
- SAR Backscatter vs. Ambient Surface Conditions
- SAR Backscatter vs. Radar Frequency
- H/V Analysis
- Background Noise Analysis
- SAR vs. CW Radar Comparison
- SAR vs. Laser Scatterometer Comparison
- SAR vs. Video Camera Comparisons

105

distance of the object from the ground track of the vehicle, is the representation desired by most image interpreters and analysts.

Figure 38 illustrates the relationship between slant range and ground range. In actuality, the earth's surface is curved, but from aircraft altitudes, the curvature is small enough to be ignored. However, from spacecraft altitudes, the earth's curvature must be accounted for.

In this section, we will discuss the relationship between slant and ground range on a flat, horizontal earth. The relationship between slant and ground range is non-linear, but simple. The trigonometric relationship for flat earth is

$$R_g = R_s \sin \theta , \qquad (1)$$

where θ is the incidence angle, R_s refers to slant range, and R_g refers to ground range. The slant range distance between two points is always smaller than the ground range distance and is highly dependent upon the angle at which the terrain is viewed. The relationship between the change in slant range to the change in ground range is

$$\Delta R_g = \Delta R_s / \sin \theta . \qquad (2)$$

The relationship between ΔR_g and ΔR_s determines the scale of the image. Because this relationship differs at near range compared to far range, the range scale of the slant range image is not constant. This type of distortion is at its maximum when looking at the nadir of the vehicle, where the incidence angle is $0°$. Near the nadir, a comparatively small change in slant range will produce a large change in ground range. As the incidence angle is increased, a smaller and smaller change will occur in ground range for every change in slant range. At the limit when the incidence angle is $90°$ (the radar beam is grazing the ground and parallel to the ground), there is no distortion, because the change in slant range is
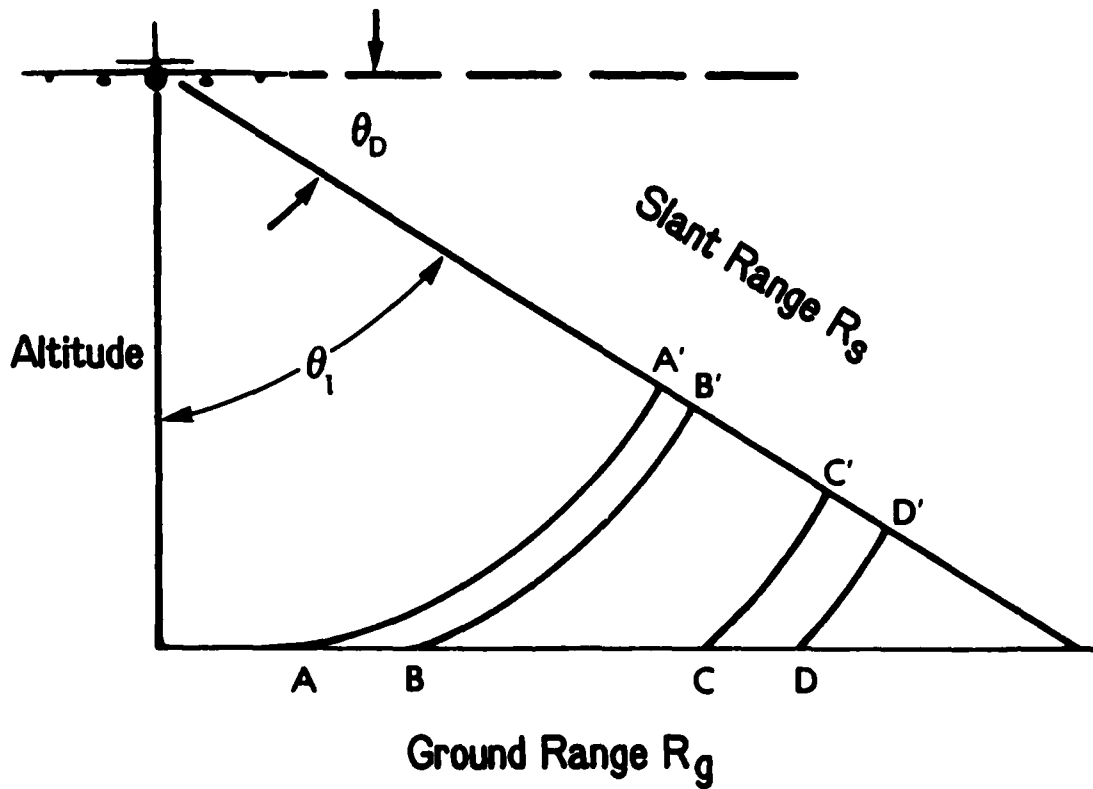
Figure 38. Slant Range Versus Ground Range Perspective in an Imaging
             Radar System

identical to the change in ground range. Because of this continuous change in range scale across the image, only one range exists where the slant range scale equals the along-track scale. At nearer range, the map scale will be smaller, and at a farther range the map scale will be larger in the slant range presentation of the image.

The slant-to-ground range distortion can be removed by digitally resampling the data in the range direction. To do this, the slant-ground range relationship can be rewritten as

$$R_g = \sqrt{R_s^2 - h^2} \, , \qquad (3)$$

for the flat earth or low-altitude case, where h is the platform altitude.

Because the range and azimuth scales are not the same after the slant-to-ground range conversion has been applied, the range dimension is usually resampled to match the azimuth line spacing. Two types of resampling techniques are commonly used, depending upon the type of scene, the required accuracy, and the acceptable cost for the correction. The simplest and least expensive resampling technique is the nearest-neighbor method. In this method, a grid is set up having equal intervals of ground range, ΔR_g, beginning at the nearest range sample, R_{go}. That is, the ground range at grid point n is

$$R_{gn} = R_{go} + n\Delta R_g. \qquad (4)$$

The ground range spacing ΔR_g is usually chosen to equal the distance between samples in the along-track direction, so that the image will have unity aspect ratio when displayed on a device which has pixel elements of equal size in both dimensions.

The resampling is then carried out by considering each value of R_{gn} in turn, and computing the corresponding ground range from Eq. (4). The input range sample nearest to this computed ground

range is then copied into the output data set. The maximum error in
the location of any pixel using this method is one half of the ground
range distance between pixels. Usually, this is an acceptable error,
particularly if the scene reflectivity distribution is relatively
smooth.

Another method of resampling interpolates between samples to find
the data value at the required location. The same steps as described
above are carried out except that instead of choosing the input range
sample nearest to the computed slant range for the output pixel under
consideration, an interpolation formula is used which involves the
data values at several locations surrounding this pixel. Several
different interpolation formulas have been used, most of them varia-
tions or approximations of a sinc (i.e., [sin x]/x) function
(Shuchman, et al., 1977). This procedure results in a theoretically
more exact reconstruction of the image but is more difficult to
implement and requires more computer time for its operation.

Slant-to-ground correction of digital SAR imagery using Eq. (3)
requires determination the slant range (R_s) to each pixel in a
scene as well as the altitude (h) of the aircraft when the SAR data
were collected. However, there are several subtle factors involved
in determining R_s and h. Two factors which affect the calculation
of R_s are the range location of each point in the imaged scene
(P_i) and the range delay in microseconds (R_d) to the beginning
of the scene. Using these two factors, R_s can be calculated as

$$R_s = 150 R_d + 1.5 P_i \tag{5}$$

where 150 is the one-way distance (in meters) a beam of light travels
in one microsecond and 1.5 is the width (in meters) of the pixel.

P_i is given within the SAR scene and R_d is usually obtained
from the log sheet from a specific mission. However, this nominal
R_d may require several modifications, depending upon the SAR
wavelength.

Based upon discussions with SAR system engineers from both ERIM and CCRS, it appears the actual range delay is 0.2 μsec less than the recorded value. The 0.2 μsec value is based upon actual measurements made on the SAR system.

Another factor which affects the X-band range delay has to do with the way in which the X- and L-band pulses are transmitted. The transmitter on the ERIM/CCRS SAR System operates such that the L-band pulse ends approximately 0.2 μsec prior to the center of the X-band pulse (see Figure 39). Since the image of the target which reflected the pulse is formed at the center of the pulse, a given point on an X-band image will theoretically appear 1.1 μsec, or 165 m, later than the same point appears on the L-band image. This theoretical difference was calculated using a pulse width of 2.7 μsec at X-band and 1.8 μsec at L-band. The actual difference may vary, depending upon how the SARs were adjusted on any given day.

To investigate the difference between X- and L-band, the SAR phase histories and processed images of a calibrated reflector were examined. This analysis showed that the range positions coincide when the phase histories of the SAR images were compared, but that the locations of the corner reflectors in X-band were 0.94 μsec later in the image than the positions at L-band. Therefore, when no point targets or nadir and visible in the SAR image, it is recommended that the range delay used for X-band imagery be 1.0 μsec longer than the range delay used for L-band. If nadir or a point target is visible in the SAR images, then the distance, and hence range delay, between the X- and L-band images can readily be calculated by comparing the range positions of a target on the two images.

The recorded altitude (h) of the CV-580 aircraft was determined by reading an altimeter which calculates altitude by measuring the difference in barometric pressure between the aircraft and a point on the ground, usually the airport where the airplane takes off and

110
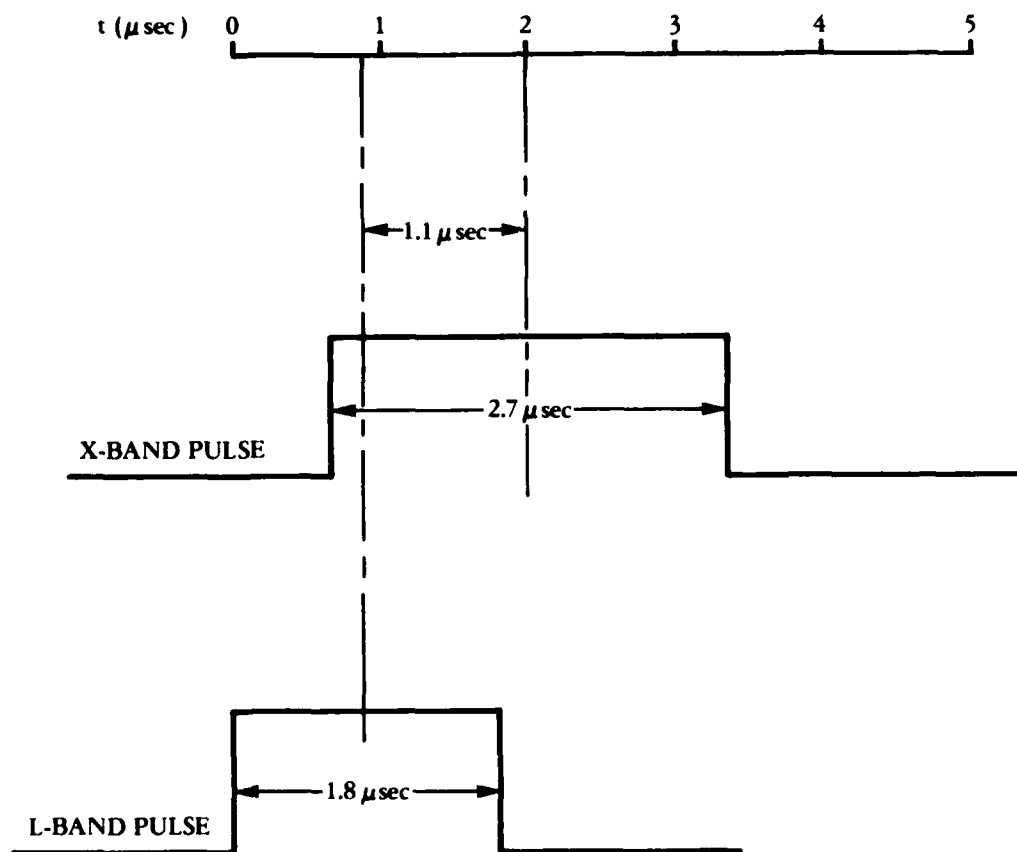
Figure 39. Relative Positions and Lengths of X- and L-band
Transmitted Pulses

111

lands. Naturally occuring variations in atmospheric pressure can result in variations in the actual altitude of the aircraft. Studies have shown that these altitude variations are often as high as 50 m (Lyden, 1983; Kasischke, et al., 1983), which can lead to errors in ground range when calculated using Eq. (3).

To avoid this altitude ambiguity, during the SARSEX experiment the range delay was adjusted so that the nadir return (i.e., the specular reflection from the earth's surface directly below the SAR) was visible on the SAR images. Figure 40 illustrates this nadir return for an L-band image (SARSEX-4, Pass 5), which was collected using a range delay (R_d) of 45 μsec at a recorded altitude (h) of 6706 m.

The theoretical range delay to this nadir (R_{dn}) is

$$R_{dn} = \frac{h}{150} + 0.9 \ \mu sec \tag{6}$$

or 45.61 μsec, since the image of the nadir is formed 0.9 μsec (one-half a pulse width) after it is detected. From the SAR image, we can calculate the actual range delay $(R_{dn'})$ to the nadir as

$$R_{dn'} = 44.8 + \frac{R_{sn}}{150} \tag{7}$$

where 44.8 is the actual range delay to the near edge of the image (45 - 0.2 μsec) and R_{sn} is the slant range width of the null region (111 m). For the SAR image in Figure 40,

$$R_{dn} = 45.61 \ \mu sec, \ and$$

$$R_{dn'} = 45.54 \ \mu sec.$$

Therefore, during this pass, the SAR was actually the range equivalent of 0.07 μsec (10 m) lower than the recorded altitude. The correct altitude to use when calculating ground ranges or calibrating the data from SARSEX-4, Pass 5 is 6696 m.

Nadir ──────▶ 　　　　　　　　　　　　　　　　　　　　　 } Null Region (R_{sn})
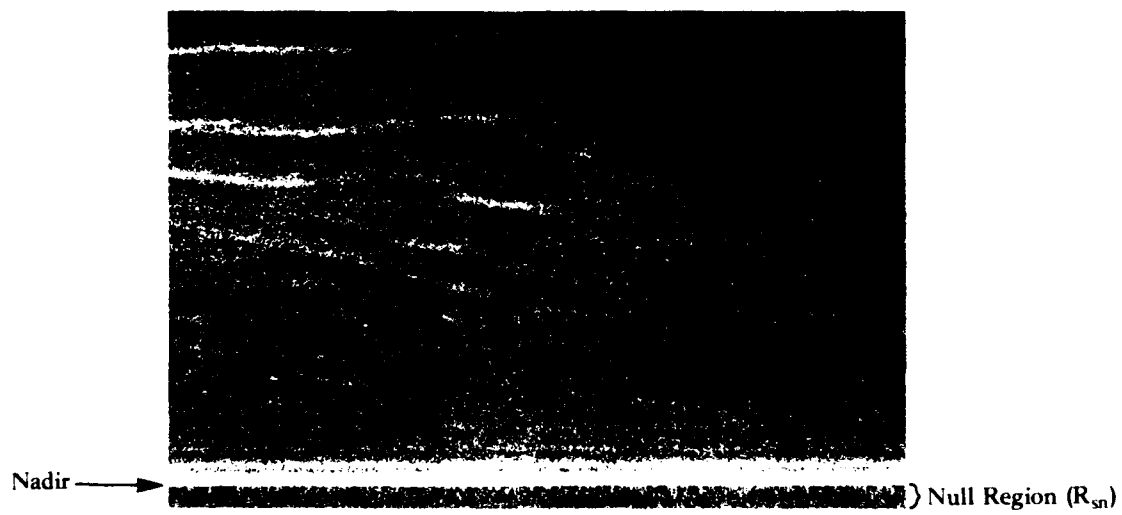
Figure 40.　Digitally-Processed X-band Image Illustrating Image Null
(R_{sn}) and Image Nadir

6.1.2 CALIBRATION OF SAR DATA

Calibration of SAR data is a relatively straight-forward concept to understand in a theoretical sense, although the implementation of a total calibration algorithm requires a careful, routinized procedure in order to keep track of all the factors which can affect each step in the algorithm. In this section, we will discuss the fundamentals of SAR image calibration. For a more in-depth discussion of calibration, the reader is referred to Walker and Larson (1981), Larson, et al. (1982, 1985) and Larson and Maffett (1985). In our discussion, we will use data from SARSEX 4, Pass 5 to illustrate the basic concepts behind SAR image calibration.

The goal of the calibration algorithm is to relate the measured intensity, P_I, from a processed SAR image to radar cross-section (σ). Assuming the SAR is operating within its linear region, this relationship can be expressed as

$$P_I = \frac{P_T G^2(\theta) \lambda^2 H_s \sigma}{(4\pi)^3 R^4} + P_n \qquad (8)$$

where P_T is the transmitted power,

   $G(\theta)$ is the antenna gain as a function of the incidence angle, θ,

   λ is the radar wavelength,

   H_s is the radar system transfer function or radar system gain,

   R is the slant-range distance to the target, and

   P_n is the system noise.

Using SAR imagery of calibrated reflectors of known radar cross-section (σ) and internal calibration signals, the basic calibration approach used at ERIM is as follows:

1. Inspect the candidate SAR imagery for artifacts and satura-
    tion to determine its potential for calibration,

2. Digitally process the SAR data set,

3. Calculate H_s and P_n for the scene to be calibrated using
    the calibration signals for that scene and the calibration
    reflector scene, and

4. Calculate σ for the image scene using P_I from that scene
    and the specific parameters for that scene (e.g., a new
    P_T, $G(\theta)$ and R).

Figure 41 outlines the overall procedure used to calibrate SAR
imagery. The first two steps (inspection and processing of the SAR
data) appear to be straightforward, but in fact are crucial steps in
the analysis and calibration process. The importance of this step
cannot be overemphasized.

In selection of a SAR data set to address a specific analysis
topic (see Table 22), it is necessary to determine if the SAR sig-
natures are within the linear response region of the SAR system as
well as determine whether or not the calibration signals are adequate
for use in determining the SAR system gain. Once these two questions
have been addressed, the SAR data can be processed into imagery and
the calibration procedure begun.

Figure 42 presents image intensity scans through the internal
wave surface patterns present in Figure 13. The scan was made in
the range direction, with the ship present in the image being the
center location for the scan. The scan was started 48 elements
(72 m) beyond the ship locaation. The scan was generated by averag-
ing 100 lines in azimuth and performing a running average of every
19 elements in range. It is these intensity values which will be
used to illustrate the calibration process.
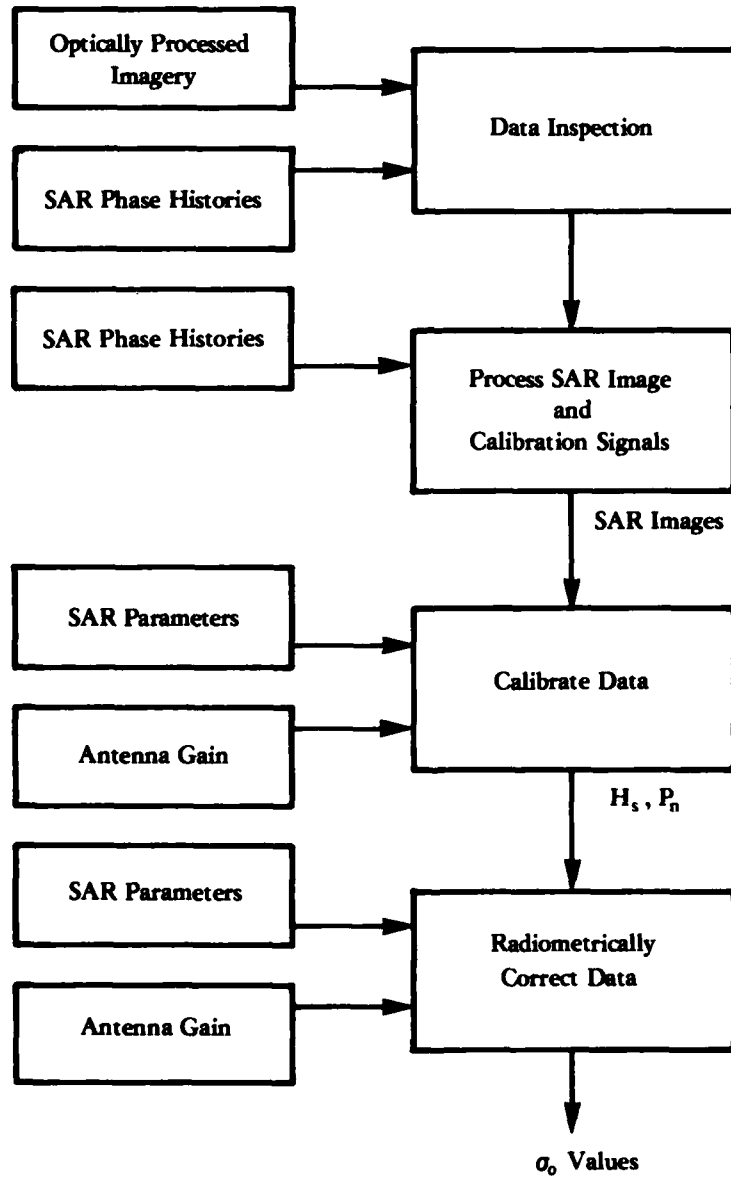
Figure 41. Outline of Major Steps in the SAR Image Calibration Procedure

116
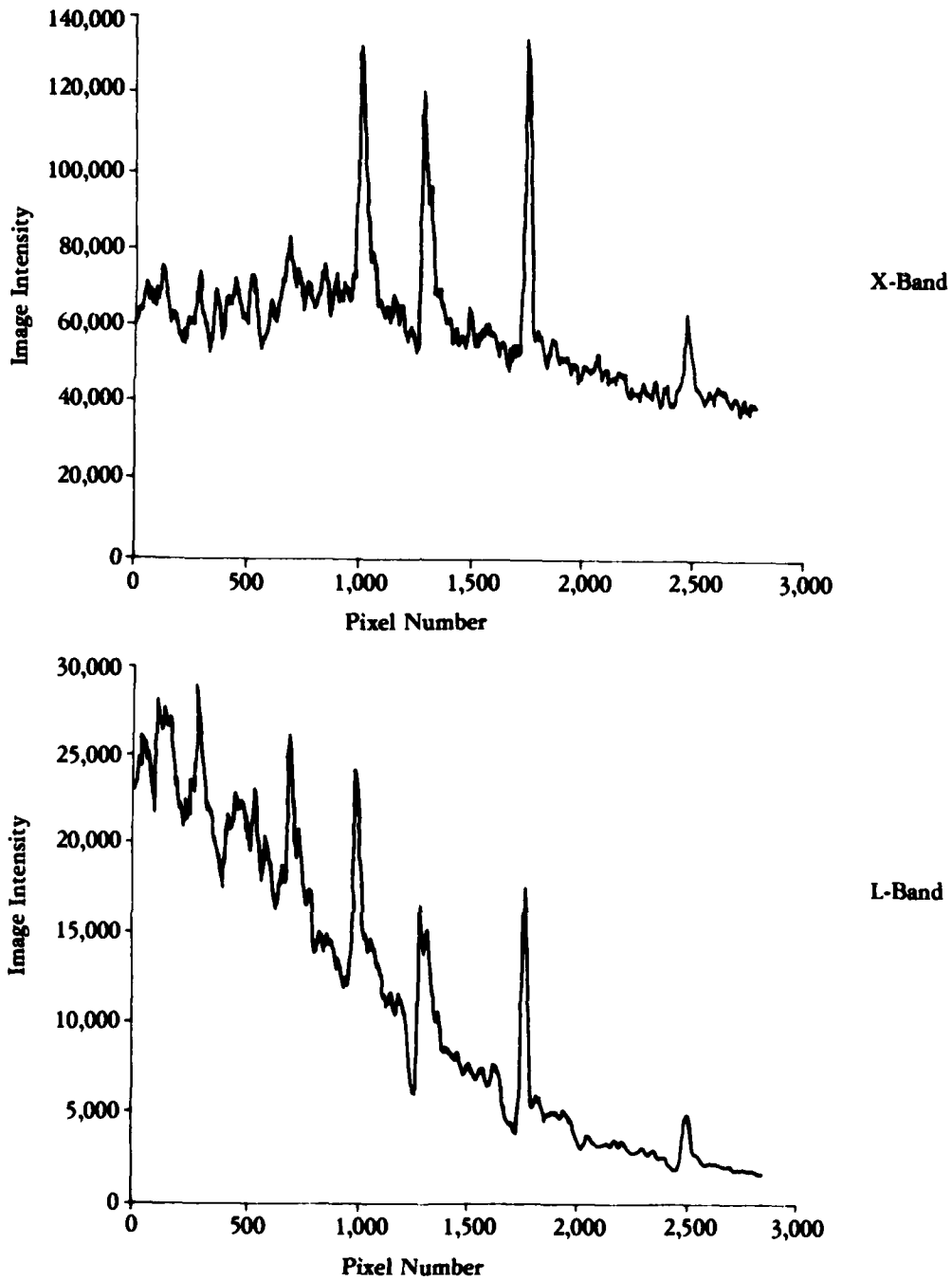
Figure 42.　Uncalibrated SAR Image Intensity Scans Through Surface
Internal Wave Patterns From SARSEX-4, Pass 5 (Scans
Are in Range Direction and Begin 48 Pixels Beyond
USNS Bartlett)

An examination of the intensities of the SAR signal histories
will indicate whether the SAR system is operating in the linear
region in the area of interest, i.e., whether the signals are satu-
rated or not. To do so requires comparing the signals from an area
of interest to a curve of the intensities from the calibration sig-
nals, some of which are saturated. The intensities of the SAR signal
histories are illustrated in Figure 43, which presents a curve gen-
erated from the internal calibration signals along with the location
of the intensities of the ship, background level and brightest in-
ternal wave value. For the SARSEX-4, Pass 5 data, it can be seen
that the data of interest are not saturated.

The second step in the calibration procedure is to calculate each
of the factors in Eq. (8). This step includes using the SAR imagery
of the set of calibrated reflectors discussed in Section 4.2. Once
the SAR images of the reflectors are processed, an intensity, P_I,
is extracted for each corner reflector in the scene. This intensity
is calculated as

$$P_I = \sum_{i=1}^{n} \sum_{j=1}^{m} (x_{ij})^2 \qquad (9)$$

where x_{ij} is the amplitude of a pixel,

      i is the line number, and

      j is the element number.

It should be noted that the same number of elements (i) and lines
(j) should be used to calculate P_I for each reflector. Figure 44
presents the P_I vs. σ curves generated for the calibration array
imaged during SARSEX-4, Pass 12.

From the data presented in Figure 44, we can calculate a regres-
sion line,

$$P_I = a\sigma + b \qquad (10)$$

118
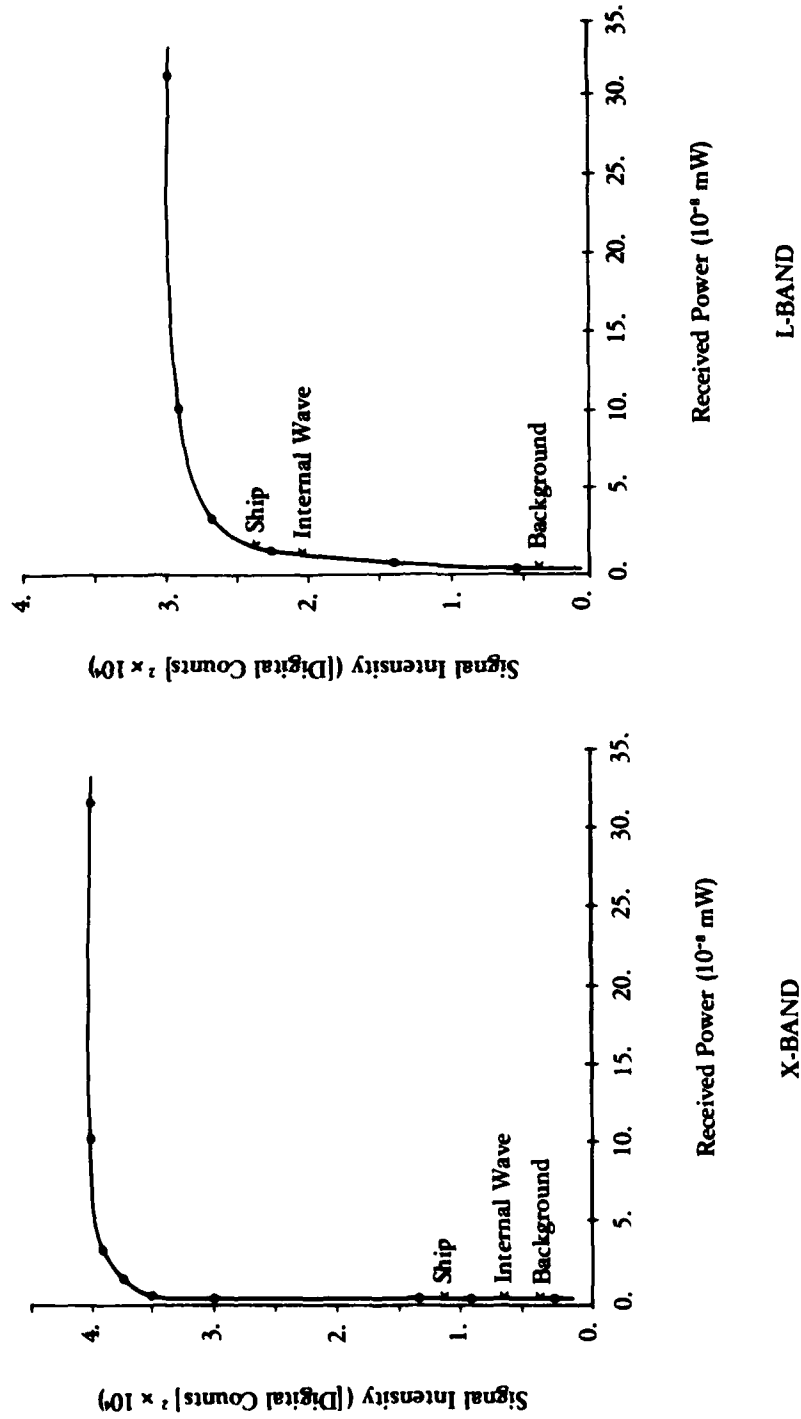
Figure 43. X- and L-band System Response Curves for SARSEX-4, Pass 5
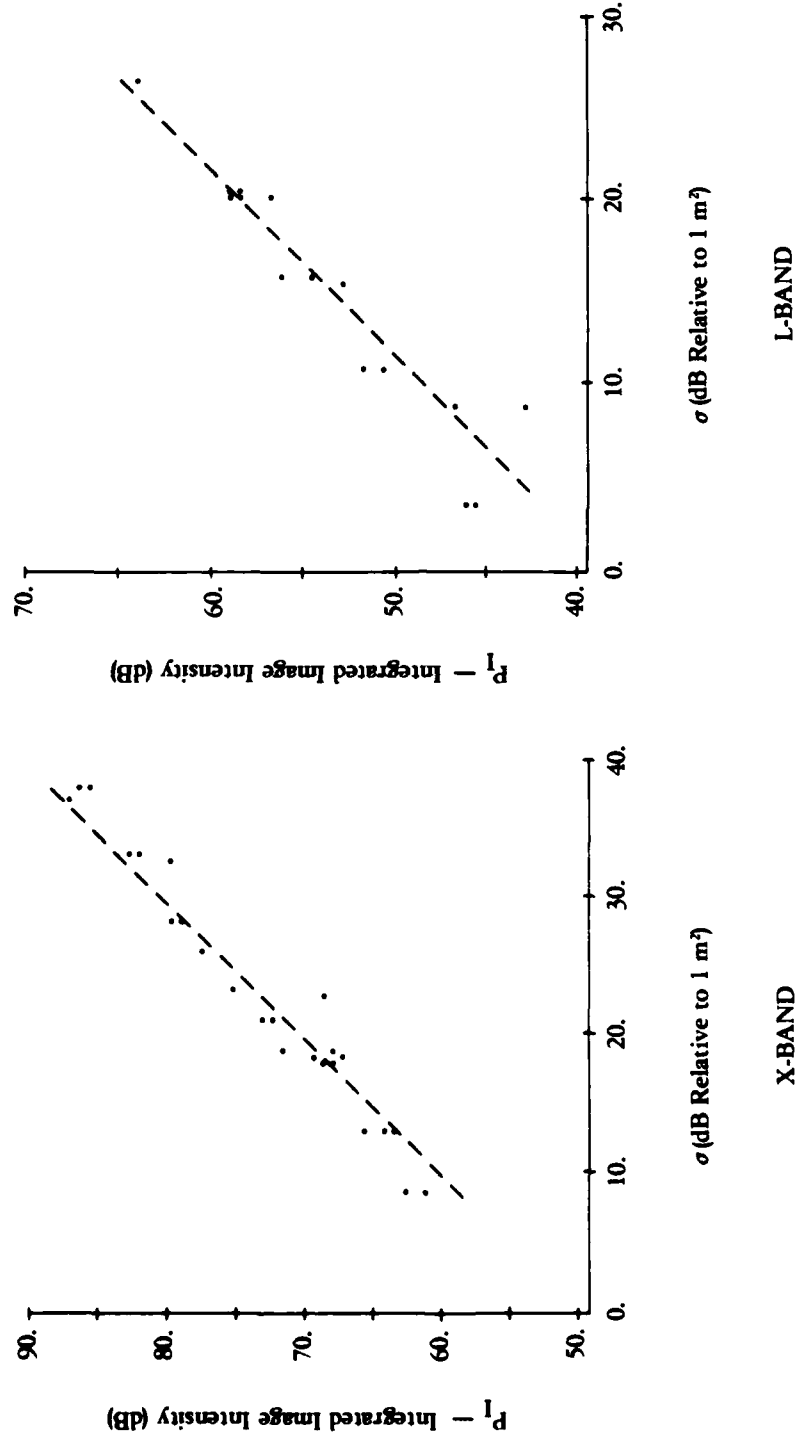
Figure 44. Image Intensity Versus Radar Cross Section of Calibrated Reflectors From SARSEX-4, Pass 5 and X- and L-band Data

If we assume that the y-intercept, b, is equivalent to the system noise P_n, then

$$a = \frac{P_I - P_n}{\sigma} \qquad (11)$$

We can now arrange Eq. (8) to calculate H_s for the calibrated reflector array. Specifically

$$H_s = \frac{P_I - P_n}{\sigma} \frac{(4\pi)^3 R^4}{P_T G^2(\Theta)\lambda^2} \qquad (11)$$

Note that the system gain term, H_s, now encompasses the linear relationship between P_I and σ for the calibration scene. Table 23 lists the various factors to calculate H_s for the SARSEX-4, Pass 12 calibration array.

The next step in the calibration algorithm is to calculate the system gain, H_s, for the imaged scene. This is accomplished through measurement of the calibration signals generated before or after each pass of SAR imagery. These signals are measured in much the same manner as the reflector images using Eq. (10). However, instead of measuring a clutter factor, a system noise factor is calculated and subtracted from the power value (see Lyzenga and Shuchman, 1984). These power values are then plotted against the input power used to generate the signal. A curve is generated using both sets of calibration signals (for the calibration array and the SAR image to be calibrated). The difference between the linear portions of these curves (k) is the system gain difference between the two passes. The calibration signal curves at X-band for the SARSEX-4, Passes 5 and 12 are presented in Figure 45. The system gain for the image scene, H_s calculated from Eq. (12), is thus calculated by adding or subtracting k from H_s. For our example, k equals 18.0 dB at L-band and 18.5 dB at X-band. These compare quite favorably to the digital gain setting differences listed between Passes 5 and 12 in Table 9 (19 dB at L-band at 18 dB at X-band).

TABLE 23
SAR SYSTEM PARAMETERS USED TO CALIBRATE
SAR IMAGERY

a.) Parameters for Calculation of H_S for Calibration Reflectors
from SARSEX 4, Pass 12

Parameter	X-Band	L-Band
$\dfrac{P_I - P_n}{\sigma}$	76,504	5,248
λ	0.032 m	0.24 m
R	9,666 m	9,516 m
$G^2(\theta)$	48.6 dB	28.2 dB
P_T	1,741 W	5,650 W
H_S	1.0301×10^{19} W^{-1}	3.9974×10^{17} W^{-1}

b.) Parameters for calculation of σ values for SARSEX-4, Pass 5

P_n	11,442	204
λ	0.032 m	0.24 m
R	7,675 to 11,785 m	7,675 to 11,785 m
θ_I	29° to 55°	29° to 55°
θ_I(Peak)	62°	62°
$G^2(\theta)$	Variable Dependent on θ_I and θ_I(Peak)	
P_T	1,700 W	5,452 W
H_S	7.2923×10^{20} W^{-1}	2.5222×10^{19} W^{-1}
h	6696	6696

122
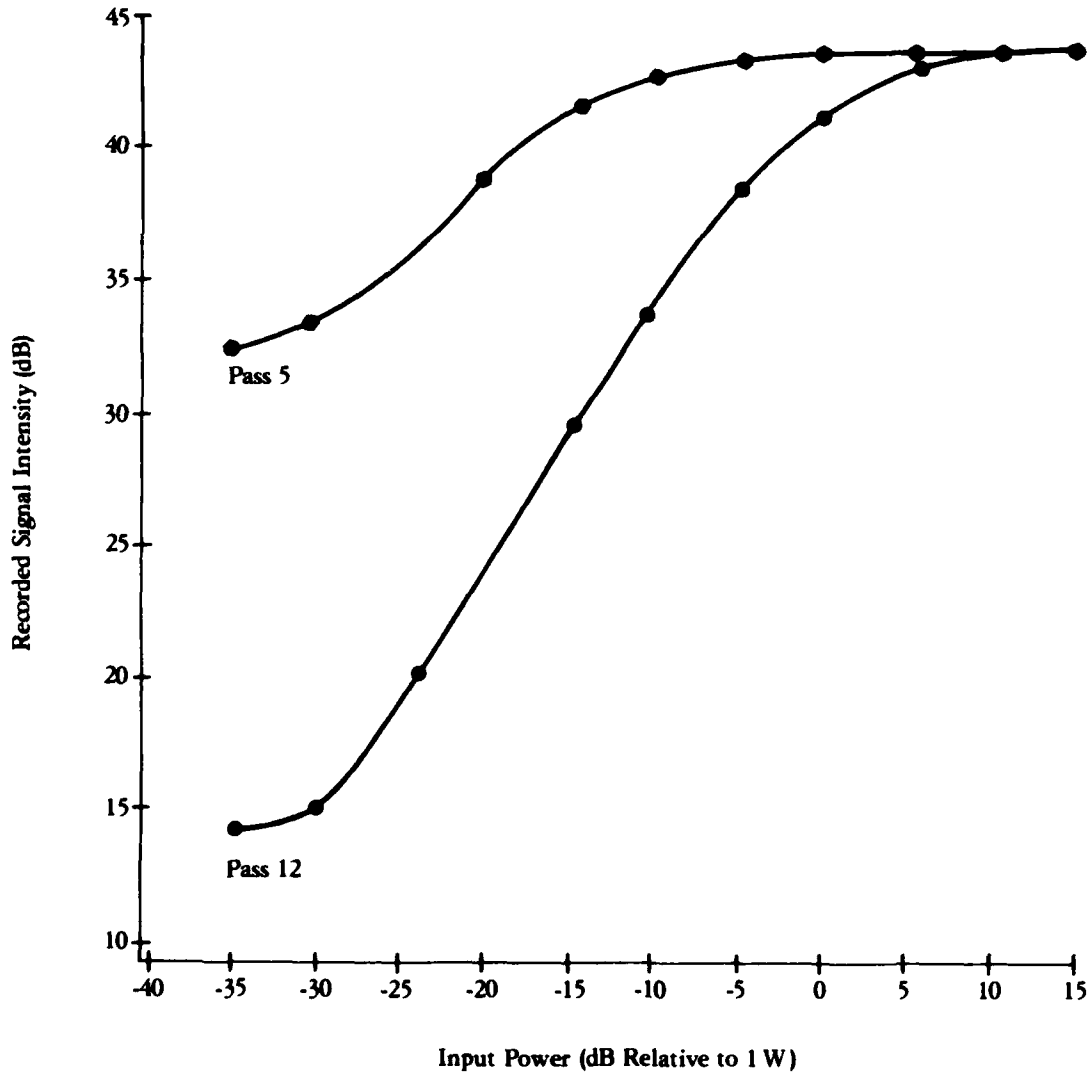
Figure 45. X- and L-band System Response Curves Generated From
            Calibration Signals for SARSEX-4, Passes 5 and 12

123

Finally, a radar cross section for any pixel in the image scene can be calculated

$$\sigma = \frac{(P_I - P_n)(4\pi)^3 R^4}{P_T G^2(\theta)\lambda^2 H_s}$$ (13)

where P_T if the transmitted power and P_n is the system noise for that scene, and R and $G(\theta)$ are calculated specifically for that pixel.

The two factors in Eqs. (8) and (13) which effect the intensity (P_I), and hence radar cross-section, of a given pixel are the range to the target and the gain of the antenna [$G(\theta)$]. For a given scene, all other variables are constant. For example, if the same target is imaged at two different ranges, where $R_1 < R_2$, the intensity of the target in the near range, P_{I1}, will be greater than the intensity, P_{I2}, at the far range because from Eq. (8)

$$\frac{P_{I2}}{P_{I1}} \sim \frac{R_1^4}{R_2^4} < 1 \ .$$ (14)

Figure 46 plots the values of P_{I2}/P_{I1} for increasing slant range assuming a uniform scene.

The X- and L-band antennas of the CV-580 SAR System each have a unique pattern, with the peak gain [θ_I (peak) in Table 23] or intensity occuring at the center of the antenna beam. The gain falls off as a function of the angular distance away from the center of the beam, and hence, a target's intensity will be lower if it is located outside the beam's center.

During SARSEX-4, Pass 5, the antennas' beams were centered at an incidence angle of 62°. Figure 46 also illustrates the expected ratio of P_{I2}/P_{I1}, where P_{I1} is the intensity of a target located at the beam center. Note that the L-band antenna fall-off is gradual, whereas the X-band fall-off is rapid.

124

Incidence Angle (θ_I)
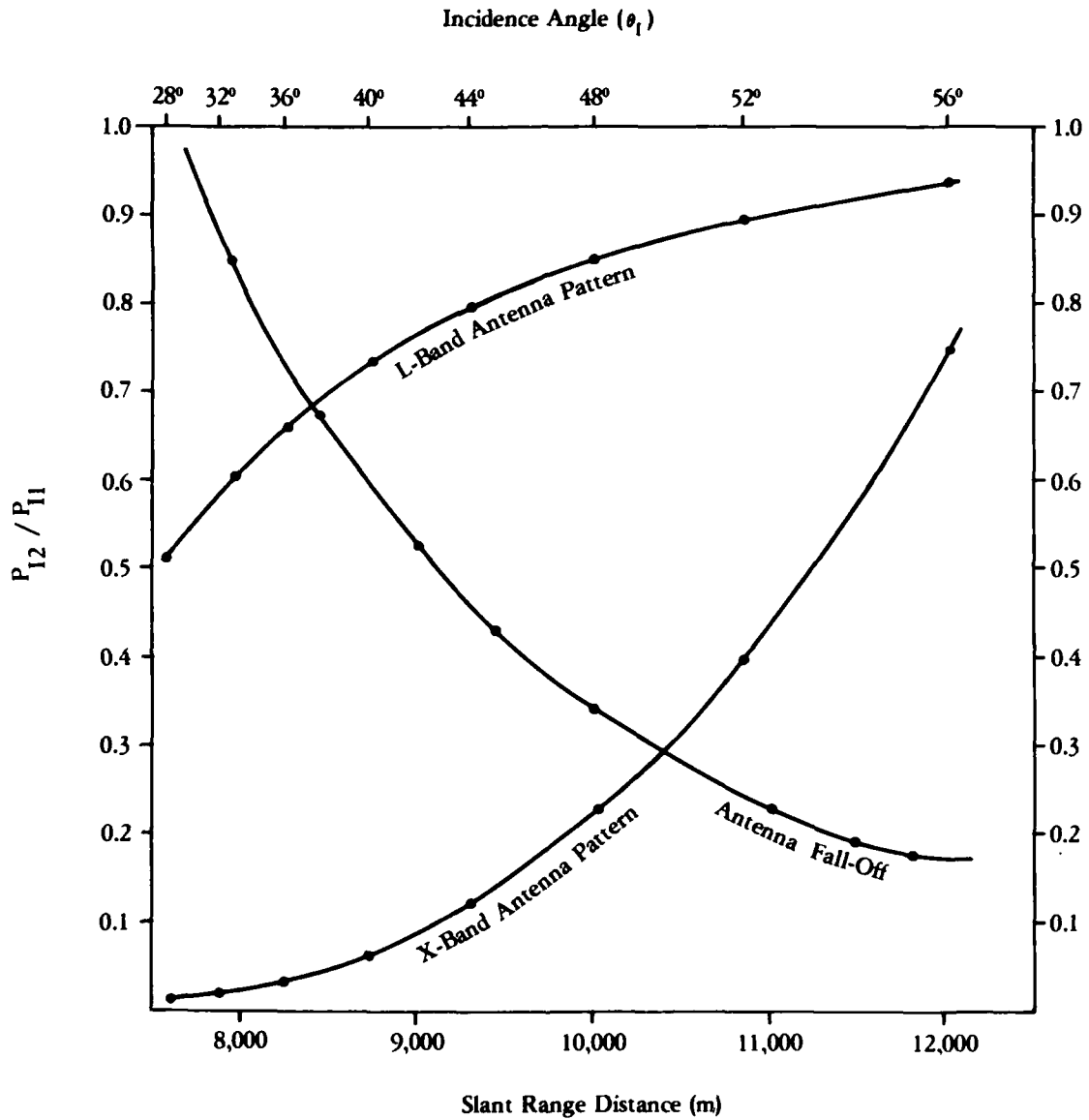
Figure 46.   The Effects of the X- and L-Band Antenna Pattern and Range
             Fall-Off on SAR Image Intensity

Using Eq. (13), a radar cross-section can be calculated for any pixel or area of the imaged scene. Figure 47 presents the calibrated radar cross-section curves for the SARSEX-4, Pass 5 SAR imagery.

6.1.3 INITIAL RESULTS

From Figure 47, the following observations can be made: the L-band signatures appear to have a distinct, separate bright and dark region, whereas the X-band signatures only have a bright region. The magnitude of the L-band signatures appears to be slightly stronger than those of the X-band signatures. Finally, there is a dramatic range fall-off of approximately 20 dB fopr the X-band scan. This fall-off may not be related to the scattering characteristic of the ocean scattering characteristic of the ocean surface, but to an incorrectly measured X-band antenna pattern. This pattern will be more accurately measured using the calibrated corner reflector data collected over the Peconic River Airport (see Section 4).

Additional scans were made on the Pass 5 imagery along the track of the R/V Cape, which was traveling parallel to and in the same direction as the USNS Bartlett at the time of the SAR overpass. The Cape's track was displaced approximately 1000 m to the northeast of the Bartlett's. Figure 48 presents the calibrated scans made through the Cape's track. From these scans, we can see that the magnitude of the L-band signature are much greater than the X-band signatures. For Wave 3, the peak of the X-band signature appears to occur slightly before the peak of the L-band signature. This is more clearly illustrated in Figure 49, which plots the positions of the X- and L-band scans for the Cape and Bartlett tracks. For the Bartlett track, there is no apparent displacement. For the Cape track, the X-band peak occurs approximately 25 m prior to the L-band peak.

Figure 47. Calibrated X- and L-band Radar Cross Sections Obtained
            From SARSEX-4, Pass 5 Data (Same Location as in Figure 42)

127

ΣERIM
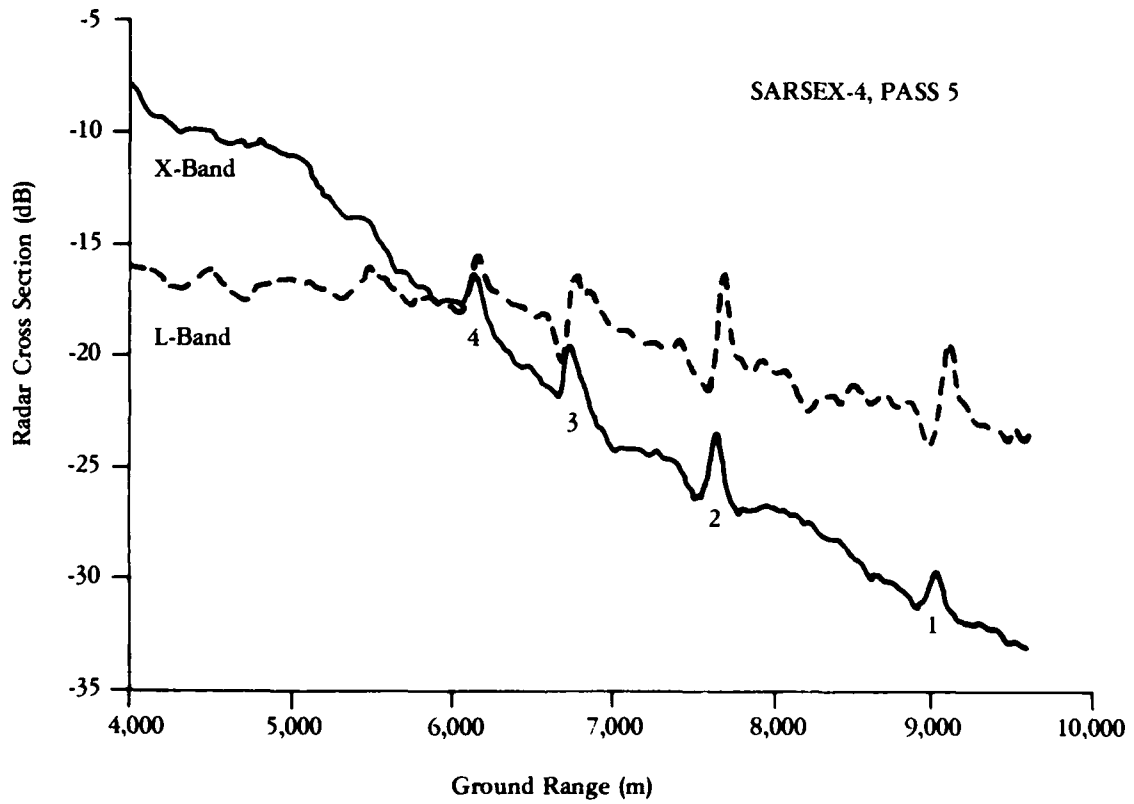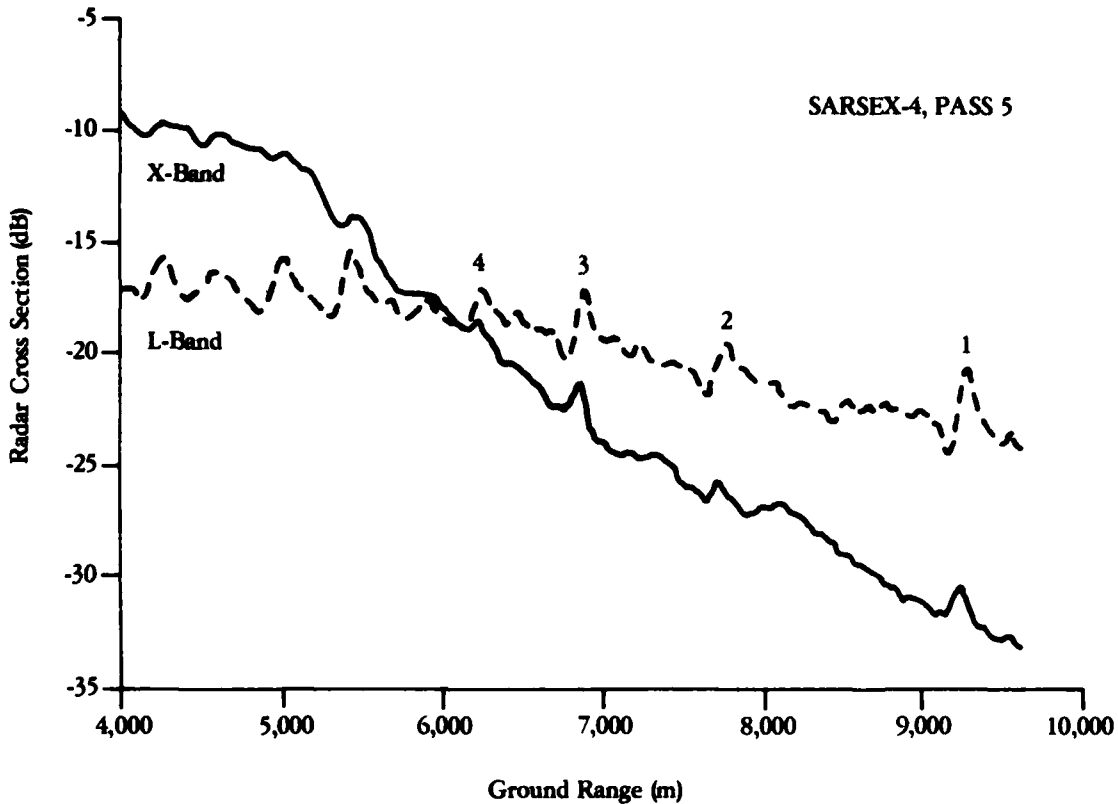
SARSEX-4, PASS 5

Peak-to-Trough Signal Intensity

Wave	X-Band	L-Band
1	1.4 dB	4.0 dB
2	1.0 dB	2.6 dB
3	1.0 dB	3.2 dB
4	0.7 dB	1.9 dB

Figure 48. Calibrated X- and L-Band Radar Cross Sections Obtained
from SARSEX-4, Pass 5 Data (Along the Track of the R/U
Cape

128
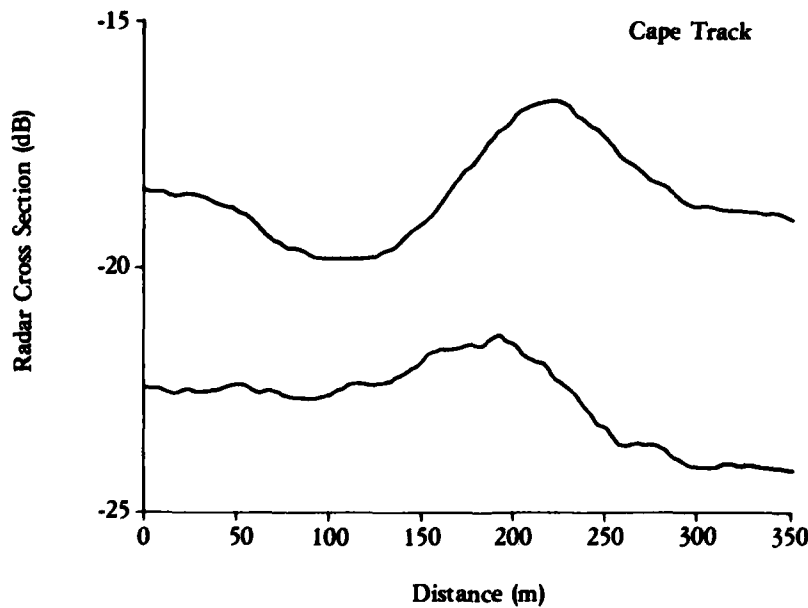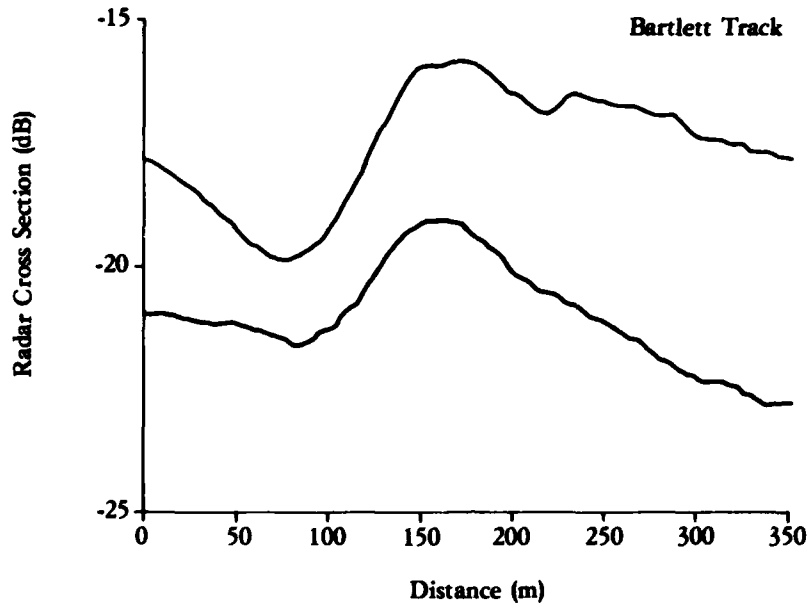
Figure 49. Comparison of Calibrated X- and L-Band Cross Sections for
Wave 3, SARSEX-4, Pass 5 for Cape and Bartlett Tracks

Figure 50 compares the L-band scan for the two different tracks. From these scans, we can see that the intensities for the Bartlett track are greater than those for the Cape track. This figure shows that there is a spatial, or an along-crest variation in the internal wave signature. This illustrates the need to make a scan as close as possible to the position of the surface and subsurface measurements to which the SAR data are being compared.

Finally, Figure 51 presents a comparison of the L-band cross-sections obtained during Pass 5 to those obtained during Pass 8. Both cross-section scans were made through the Bartlett, with the Pass 8 scan occuring at an incidence angle of 51°. These scans show that the L-band signature is greater for the range-travelling wave than it is for the azimuth-travelling wave. The signature for the azimuth scan appears to be broader or more spread out, which may indicate some smearing to scatter motion.

These empirical observations demonstrate the types of analyses which can be made using the SARSEX data set.

6.2 MODELING OF SAR OBSERVED OCEAN SURFACE PATTERNS

A primary analysis activity using the SARSEX data is to further develop and test SAR imaging models which predict radar backscatter as a function of SAR system and environmental parameters. This modeling effort can be thought of as two distinct, but inter-related activities. The first of these activities is the further development of the imaging models. New and more advanced theories on SAR imaging of the ocean surface are constantly being developed. The SARSEX data set can be used to further evaluate and quantify these theories. Once these new theories have been validated, they can be inputted into the SAR imaging model.

The second modeling activity will consist of making empirical comparisons between simulated SAR images generated from the models
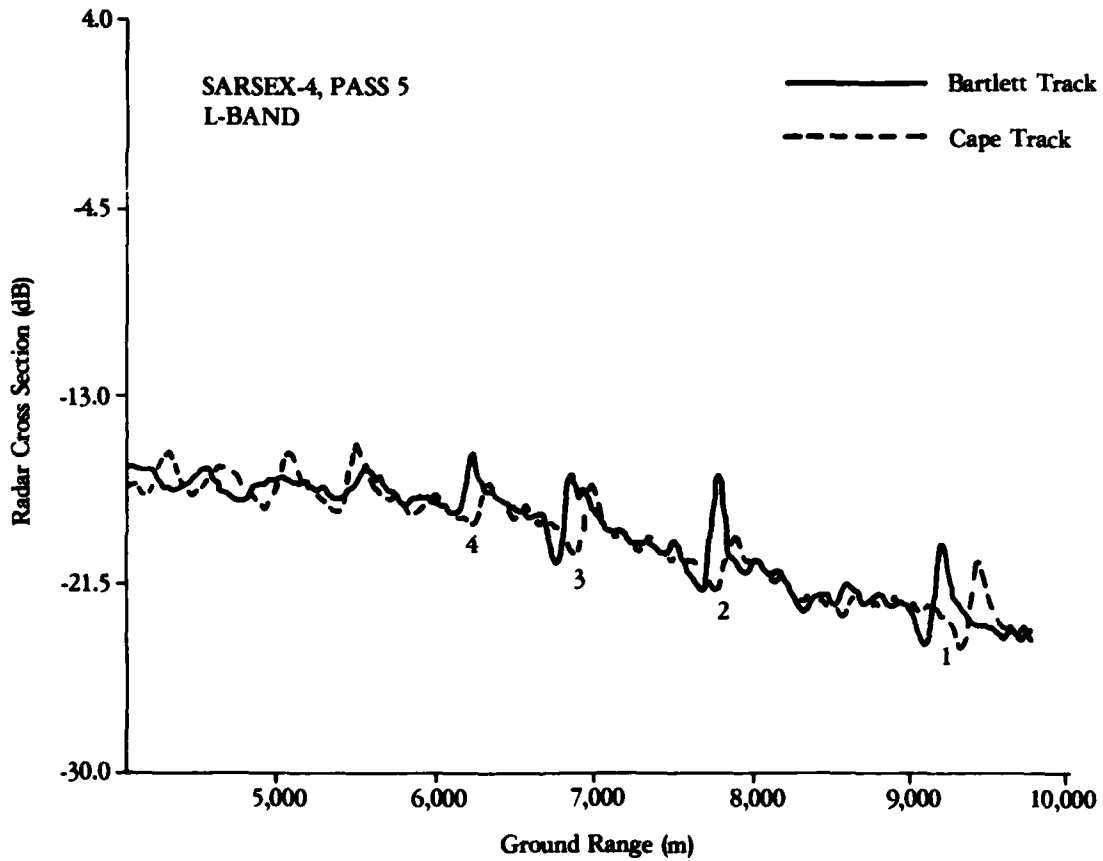
Figure 50. Comparison of Calibrated L-Band Cross Sections for Cape and Bartlett Tracks for SARSEX-4, Pass 5

131
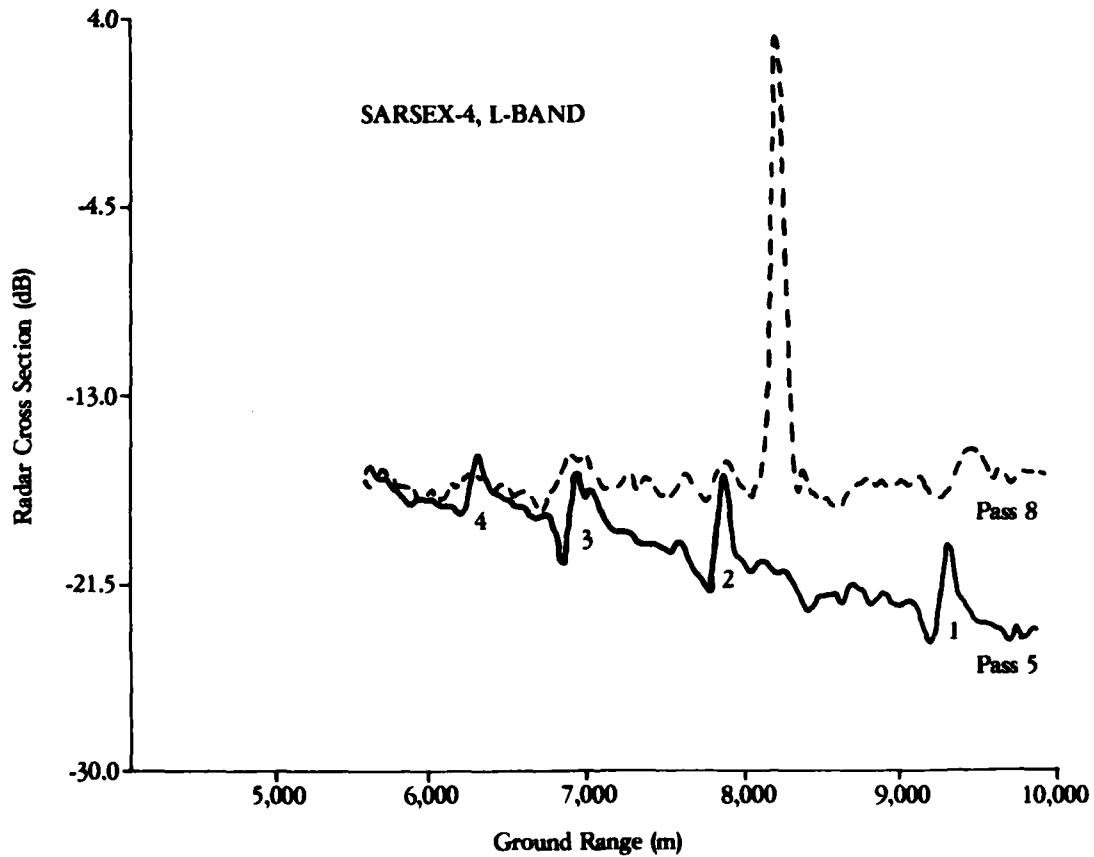
SARSEX-4, L-BAND

Peak-to-Trough Signal Intensity

Wave	Pass 5	Pass 8
1	4.5 dB	2.3 dB
2	5.3 dB	1.9 dB
3	4.0 dB	2.7 dB
4	2.9 dB	1.3 dB

Figure 51.   Comparison of Calibrated L-Band Cross-Sections for
SARSEX-4, Passes 5 and 8 (Bartlett Track)

to actual SAR imagery. These comparisons will allow an overall evaluation of the SAR imaging models, rather than focus on a specific portion of the model as the first activity does.

In this section, we will first briefly present the SAR imaging model which will be used. This will be followed by a discussion of the further theoretical development of this model which is planned using the SARSEX data. Finally, we will discuss some initial results from the model comparisons.

6.2.1 DESCRIPTION OF MODELS

The hydrodynamic and electromagnetic models which are currently in use for predicting the SAR response to internal waves are based almost exclusively on Bragg scattering. That is, the radar cross section of the surface is assumed to be proportional to the surface wave spectral density at the Bragg wavenumber

$$k_b = 2k_o \sin \theta \tag{15}$$

where k_o is the radar wavenumber and θ is the incidence angle (Valenzuela, 1978). Thus, the hydrodynamic problem is to compute the spectral perturbations (i.e., the local changes in the spectral density) at the Bragg wavenumber. These perturbations are considered to be the result of interactions between the surface waves and internal wave-induced surface currents, and are modeled using conservation of wave action principles, as described for example by Hughes (1978).

The hydrodynamic and electromagnetic models mentioned in the previous paragraph may be used to calculate the spatial variations in the radar cross section of the surface due to a given (measured or modeled) surface current field associated with a set of internal waves. Under a restricted set of conditions (to be defined below), the SAR image intensity may be assumed to be proportional to the

surface radar cross section. The hydrodynamic model output can then be interpreted directly as a SAR prediction, and compared with actual SAR image intensities.

Aside from SAR system considerations such as the effects of system noise, linearity, antenna gain patterns, geometric factors, and motion compensation or phase errors, there are at least two factors which must be taken into account in comparing the predictions of the first-order model described above with actual SAR images. These are the effects of coherent speckle and the effects of surface motions on the SAR imaging process.

The numerical SAR simulation model developed and implemented at ERIM (Lyzenga, et al., 1984) accounts for both speckle and surface motion effects. These motion effects include radial velocity, azimuth smearing and variations due to surface gravity waves.

6.2.2 ADDITIONAL MODEL DEVELOPMENT

The hydrodynamic, electromagnetic, and SAR imaging models discussed in the previous section contain numerous approximations and neglect effects which may be important in many cases. The degree to which these models approximate reality will be determined by comparisons with the data collected during SARSEX. In anticipation of some measure of disagreement, the following paragraphs summarize some of the areas in which model improvements should be made.

6.2.2.1 Quasi-Specular Scattering

A growing body of evidence, including both laboratory measurements (Kwoh and Lake, 1984) as well as field data (Lyzenga and Shuchman, 1984), points toward the inadequacy of a pure Bragg scattering model to describe the microwave scattering properties of the ocean surface. Preliminary examination of SARSEX images, including especially the data collected at low altitudes, suggests that this data will furnish additional evidence for the importance of non-Bragg

scattering mechanisms. Principally, this evidence is in the form of observations of highly localized, large-amplitude returns which appear as bright streaks in the low-altitude SAR imagery. These features appear to be associated with wave breaking (Lyzenga and Shuchman, 1983) and also seem to be inconsistent with a purely Bragg scattering mechanism.

The existence of non-Bragg scattering processes unfortunately greatly complicates the hydrodynamic as well as electromagnetic modeling effects. A demonstration of the importance of such processes would imply, at minimum, the necessity of including all surface wavelengths in the hydrodynamic calculations. At worst, it may require a complete reformulation of the hydrodynamic models to include nonlinear and finite wave amplitude effects.

In the electromagnetic modeling area, Bragg scattering models may need to be supplemented if not replaced by models incorporating specular scattering or wedge scattering mechanisms. Ultimately, the surface descriptions required to calculate the electromagnetic scattering properties will determine the course and complexity of the hydrodynamic modeling effects.

The inclusion of non-Bragg scattering in the SAR model will entail chiefly a reformulation of the surface motion calculations. Instead of incorporating only the orbital motions of the surface waves, the higher velocities associated with specular facets or wedge scattering elements may have to be accounted for. Methods of including these effects will be investigated as part of the SARSEX analysis activities.

Several investigations can be pursued with respect to non-Bragg or quasi-specular scattering from the ocean surface using the SARSEX data set. These investigations will be carried out using data collected during SARSEX-8, which exhibits a significant degree of azimuthal streaking (see Figures 24 and 25).

Lyzenga and Shuchman (1983) have hypothesized that the cause of the streaking is due to breaking waves. The degree of streaking on the SAR image can be measured by an autocorrelation of the SAR image spectrum. The following areas can be investigated using the SARSEX-8 imagery:

1. Determine where the highest degree of streaking occurs relative to the internal wave field.

2. Through a comparison with the video images of the ocean surface, determine the correlation between the density of breaking waves and the density of the streaking on the imagery.

3. Determine the variation in the amount of streaking as a function of incidence angle, azimuth angle and altitude.

4. Compare X- and L-band imagery to determine the degree of streaking in each, and whether or not the streaks in each band occur at the same place.

5. Compare CW radar data to SAR data and correlate specular spikes on the CW radar backscatter scans to the density of the streaking on SAR images.

Through the above analyses, we will be able to better predict the degree of non-Bragg or quasi-specular scattering which occurs and make adjustments to the imaging model.

6.2.2.2 Background Noise

The detection of surface patterns on SAR imagery is dependent on the oceanic phenomena itself and the ambient background noise. Factors which affect the background noise include surface tension (which is a function of air/sea temperature and surface films), wind and surface gravity waves. Although research has been done on the effects of wind on SAR imagery (Lyden, et al., 1983) and surface gravity wave imaging models exist (Shuchman and Lyzenga, 1985), these models have not yet been completely tested and validated.

In the background noise investigation, the effects of wind will be further quantified using low and high wind cases from the SARSEX data set. Wave buoy data from days where surface gravity waves were present on SAR imagery will be obtained. This information will be used as inputs into the SAR gravity wave model and the results compared to the SAR imagery. The wind and wave portions of the SAR imaging model will thus be further tested and validated.

6.2.3 INITIAL RESULTS

The hydrodynamic/electromagnetic interaction model was exercised using the environmental conditions present during SARSEX-4, Pass 5. The third wave of the observed internal wave packet (the first wave being the one the furthest out in the range dimension) was modeled.

The environmental conditions were provided by the Applied Physics Laboratory. During this pass, a westerly wind [towards $90°$ (T)] with a velocity of 6 m/s was present. Figure 52 (after Apel, et al., 1985) shows the predicted surface current and strain rates for Wave 3.

Using these inputs, the hydrodynamic/electromagnetic interaction model was exercised. Figure 53 shows the observed and predicted internal wave signatures at both X- and L-bands. Note at L-band, the model accurately predicts the observed trough and peak in the internal wave signature, although the magnitude of the peak is somewhat underestimated. As with past data sets, the X-band model does not predict the observed signature at all.

The underpredictions at both X- and L-bands probably lie in the fact that some other mechanisms are responsible for modulating the Bragg scatterers or causing backscatter to the SAR. One possible mechanism which has been suggested is a combined non-linear current/ long wave/Bragg wave interaction. Figure 54 illustrates the predicted magnitude of the spectral perturbation to a wave with a length
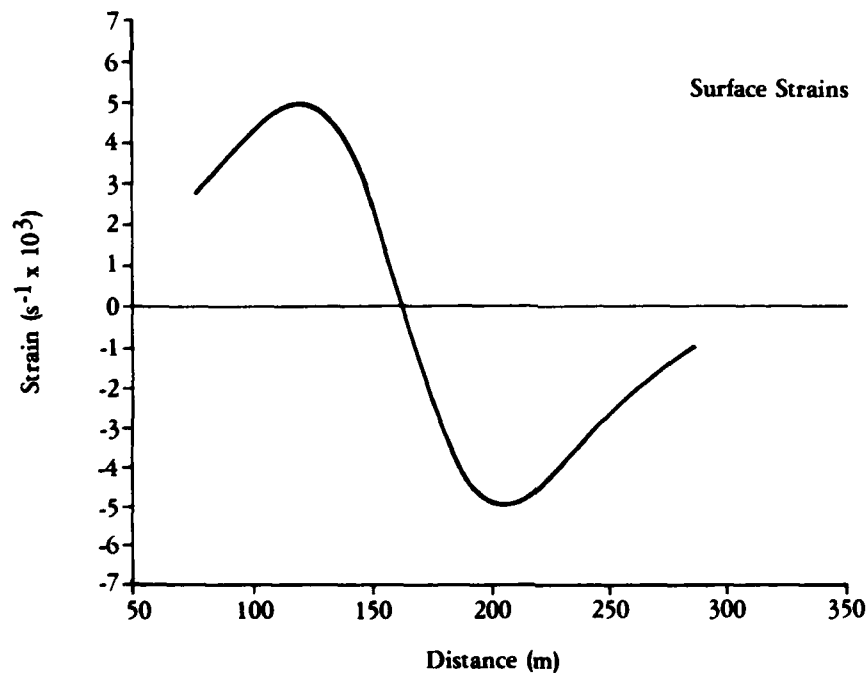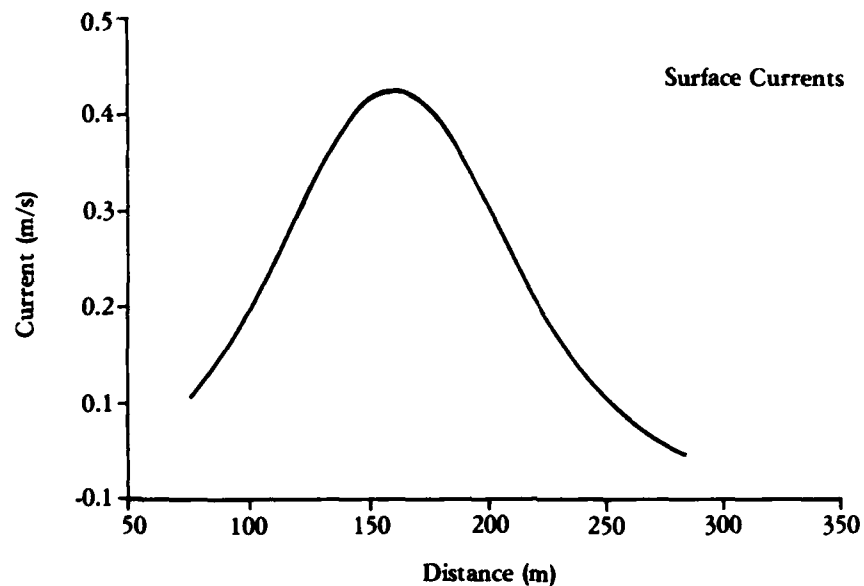
Figure 52. Surface Currents and Strain Rates for Wave 3, SARSEX-4
(After Apel, et. al., 1985)

138
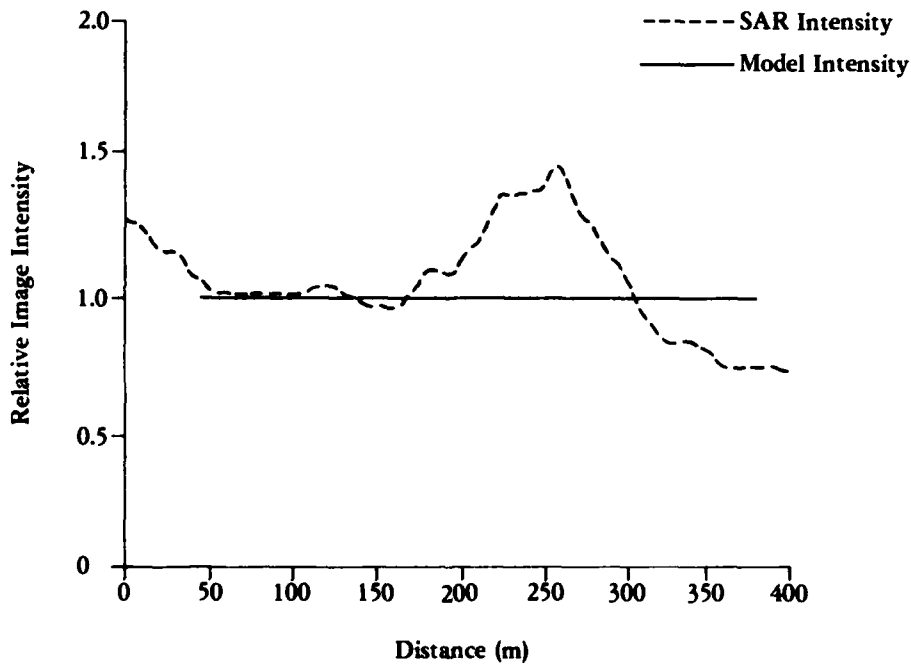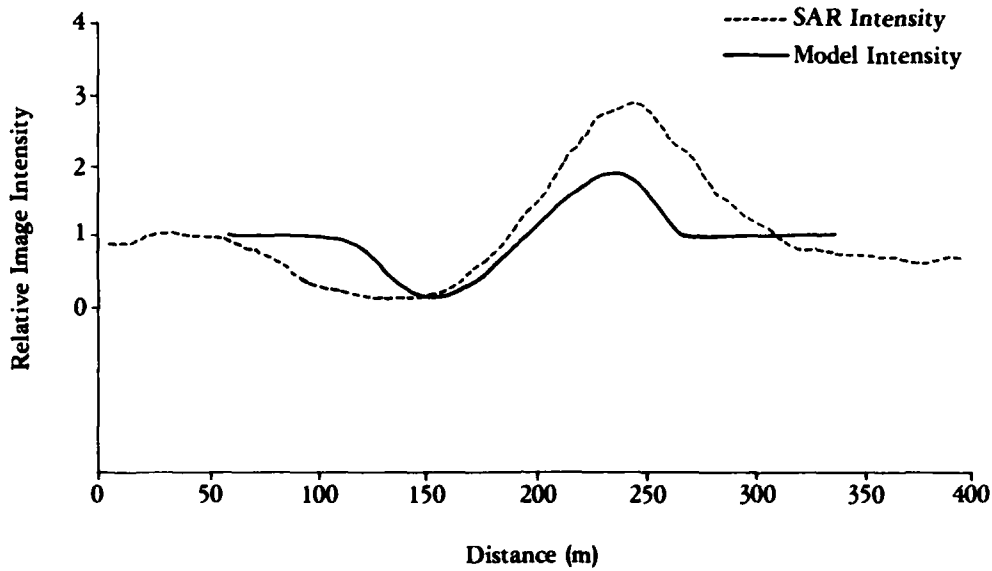
Figure 53. Modeled Versus Ovserved SAR Intensity for Wave 3,
   SARSEX-4, Pass 5

139
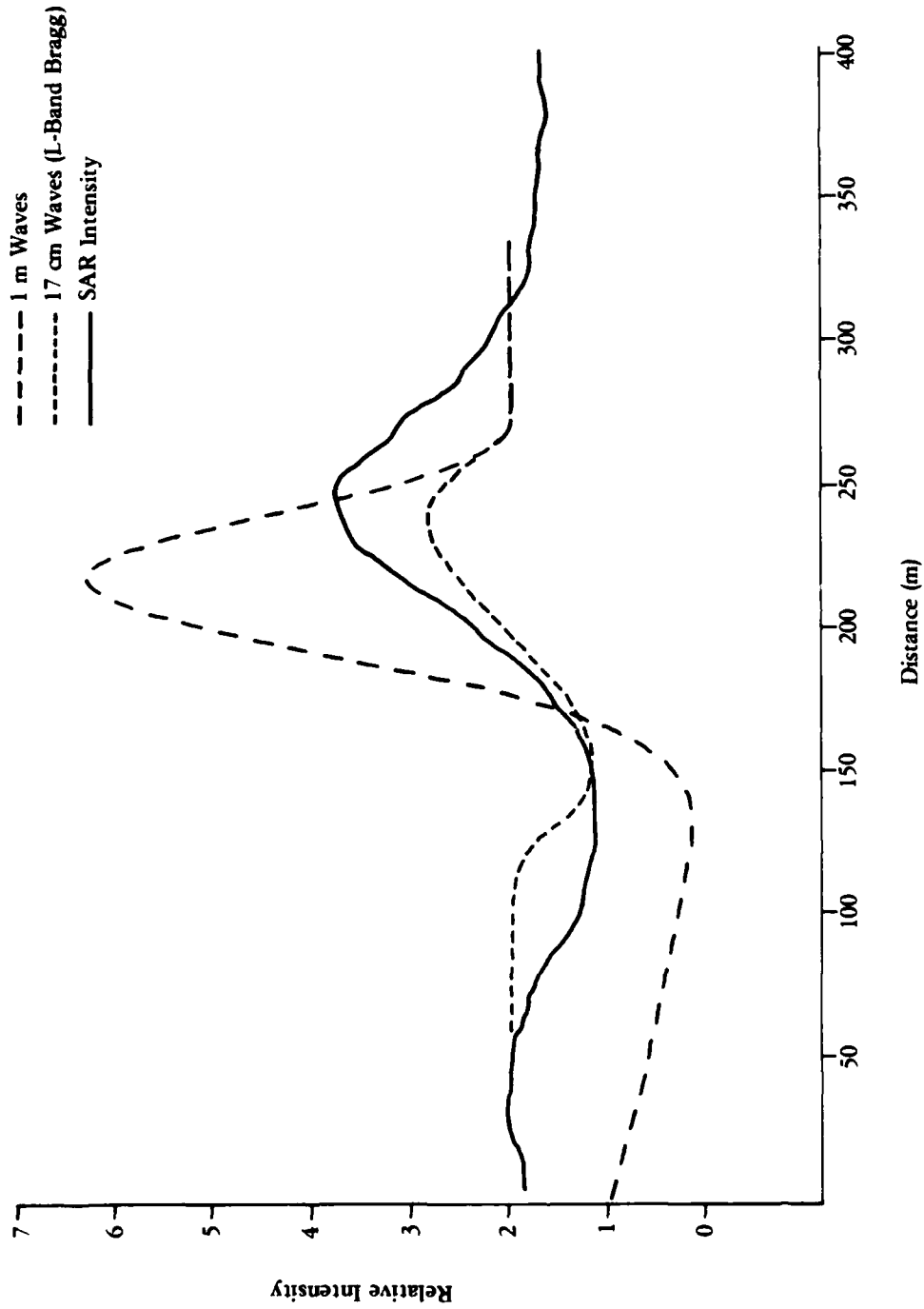
Figure 54. Modeled Versus Observed L-Band Intensity, Including
Perturbation to a 1 m Wave

140

of one meter due to interactions with the internal wave current. It is possible that the longer wave is interacting with the shorter Bragg waves in some non-linear manner, resulting in a stronger signature.

Figure 55 illustrates the modeled L-band internal wave signature intensity as a function of azimuth angle (where ±90° is equivalent to an azimuth travelling wave, and 0° is equivalent to a range travelling wave). Theory predicts that range-travelling waves have stronger signatures than azimuth-travelling waves, which agrees with the observations.

Finally, a combined Bragg/wedge scattering model proposed by Lyzenga, et al. (1983) predicts that the intensity of the sea surface backscatter will decrease with increasing incidence angles. For the incidence angles represented in the SARSEX-4, Pass 5 imagery (30° to 56°), the model predicted range fall-off is approximately 13 dB at both X- and L-bands. The observed fall-off was 23 dB at X-band and 6 dB at L-band. This indicates one of three things: (1) the models overpredict the range fall-off at L-band and underpredict at X-band, (2) the antenna patterns have not been correctly measured, or (3) the system noise inputted into the calibration algorithm was incorrect. We believe the reason to be a combination of the two.

6.3 DATA ANALYSIS AND MODEL COMPARISONS

Analysis of the SARSEX data falls into two categories. The first activity includes a purely empirical characterization of the observed SAR internal wave signatures as a function of the SAR viewing geometry (incidence angle and look direction), the SAR wavelength (X-band versus L-band), and the surface conditions (strain rate, wind speed, etc.). The second activity includes a comparison of the observed SAR intensity modulations with model predictions based upon the surface measurements.

**MODELED PEAK-TO-TROUGH L-BAND INTENSITY
AS A FUNCTION OF LOOK DIRECTION**
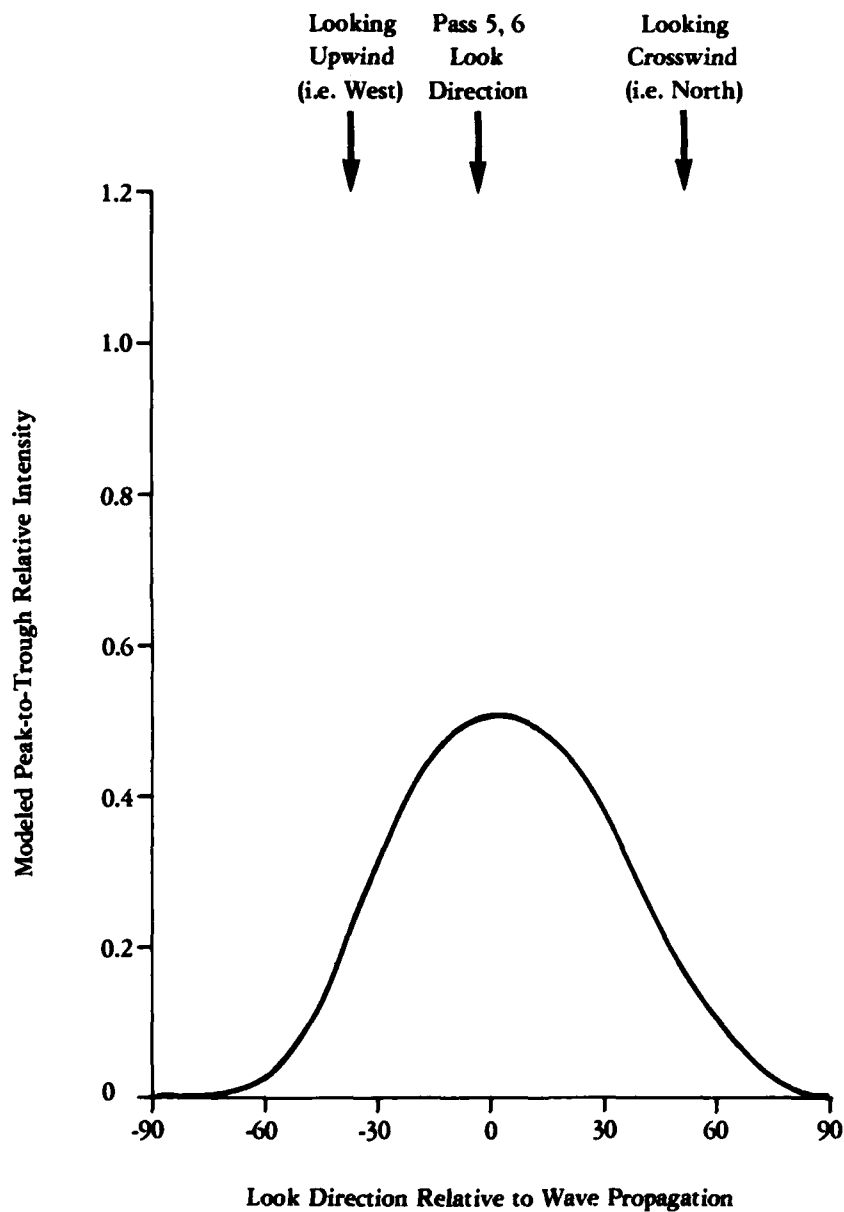
Figure 55.   Model L-Band Intensity as a Function of Azimuth Angle

142

SAR data were collected simultaneously at X-band and L-band using a series of multi-sided flight patterns, as described elsewhere in this report. The internal waves, for the most part, persisted long enough to be observed with a variety of incidence angles and look directions. Differences in the observed internal wave signatures can therefore be related directly to the changes in the viewing geometry, and the functional relationship between these can be directly investigated. Comparisons with surface currents measured by shipboard instrumentation can similarly be done, to establish a minimum detectable strain rate for the conditions under which the measurements were made.

Comparisons of measurements with model predictions can potentially be made on these levels. First, measurements of internal wave-induced surface currents can be used as inputs into hydrodynamic (wave/current interaction) models, and the resulting spectral perturbation predictions compared with measurements of the surface wave spectra. Second, predicted or measured surface wave spectra can be used as inputs into electromagnetic scattering models and the results compared with shipboard radar backscatter measurements. Third, predicted or measured radar cross sections can be used as inputs into the SAR model and the results compared with actual SAR images. First priority will be given to the data sets for which all three levels of comparison can be carried out.

In cases where some of the intermediate-level measurements are not available, end-to-end predictions of the confined hydrodynamic/ electromagnetic/SAR imaging models can still be carried out. Second priority will be given to such data sets, except possibly in some cases of particular interest, which will be given first priority.

Required inputs to the SAR model include measurements of the ambient wave spectra as well as the hydrodynamic/electromagnetic predictions for the internal waves. Outputs of the SAR model will

include simulated images, which will be quantitatively compared with actual SAR images. In some cases, the ambient wave field is directly observed in the images (outstanding examples include SARSEX-1 and SARSEX-6). In these cases, the properties of the observed wave images will be compared in detail with the simulated images to verify the part of the model. In other cases, the primary emphasis will be on the internal wave signatures and the background signal statistics.

A special set of analysis will be carried out on the low-altitude SAR passes (SARSEX-8) to investigate the bright streaks appearing on these images. It is anticipated that present models will not adequately predict these features, and that these observations will provide impetus and guidance for further model development. Included in the analysis of this data will be a determination of the total signal contributed by these features, the degree to which this signal is modulated by the internal waves, and the motion or Doppler characteristics of these signals to the SAR ocean imaging model.

REFERENCES

Apel, J.R., A Brandt, R.F. Gasparovic, B.L. Gotwols, R.E. Sterner, D.R. Thompson, J.S. Tochko, P. Van Dyke, B.A. Hughes, S.J. Hughes, E.S. Kasischke, R.A. Shuchman, D.R. Lyzenga, D.A. Burns, and D.L. Schuler, SARSEX Interim Report, APL Report No. STD-R-1200, The Johns Hopkins University, Laurel, MD (in press), 1985.

Brunfeldt, D.R. and F.T. Ulaby, Active Reflector for Radar Calibration, IEEE Trans. Geosci. Remote Sens., GE-22, pp. 165-169, 1984.

CCRS, CCRS CV-580, Ottowa, Ontario, in preparation, 1983.

Gasparovic, R.F., R.D. Whiting, and J.S. Tochko, SARSEX Experiment Plan, APL Report No. STD-R-1061, The Johns Hopkins University, Applied Physics Lab, Laurel, MD 50 pp., 1984.

Hughes, B.A., The Effect of Internal Waves on Surface Wind Waves: Part 2, Theoretical Analysis, J. Geophys. Res., 83, pp. 455-465, 1978.

Jackson, P.L., R.W. Larson, A.R. Dias, and D.B. Franczak, Digital Processing and Absolute Radar Calibration of a Stripmap Synthetic Aperture Radar (SAR), 1984 International Geosciene and Remote Sensing Symposium (IGARSS'84) Digest, Strasbourg, France, pp. 611-614, 1984.

Kasischke, E.S., R.A. Shuchman, D.R. Lyzenga, R.W. Larson, and S.R. Stewart, SAR Data Collection and Processing Summary - 1983 Georgia Strait Experiment, ERIM Topic Report No. 168400-1-T, Ann Arbor, MI, 200 pp., 1983.

Kwoh, D.S. and B.M. Lake, Microwave Backscattering from Short Gravity Waves: A Deterministic, Coherent and Dual-Polarized Laboratory Study, IEEE J. Oceanic Eng., OE-9, pp. 291-308, 1984.

Larson, R.W., R.E. Hamilton, F.L. Smith, and Capt. J.C. Haynes, Calibration of Synthetic Aperture Radar, 1981 International Geoscience and Remote Sensing Symposium Digest, Washington, D.C., pp. 938-943, 1981.

Larson, R.W., D.T. Politis, and J.L. Walker, Calibration Procedures and Test Plan for Synthetic Aperture Radar, ERIM Final Report No. 157400-10-F, Ann Arbor, MI, 191 pp., 1982.

Larson, R.W., D.T. Politis, and J.L. Walker, SAR Calibration: A Technology Review, IEEE Trans. Geoscience and Remote Sensing, (in press), 1985.

Lyden, J.D., D.R. Lyzenga, R.A. Shuchman, and W.L. Jones, Measurement of Ocean Surface Winds by Seasat Synthetic Aperture Radar, ERIM Topic Report No. 155900-15-T, Ann Arbor, MI, 96 pp., 1983.

REFERENCES (Continued)

Lyden, J.D., Altitude Inaccuracies During the 1978 Vancouver Island Experiment, ERIM Internal Memorandum RR-83-102, 1983.

Lyzenga, D.R. and R.A. Shuchman, Analysis of Scatterer Motion Effects in MARSEN X-Band SAR Imagery, J. Geophys. Res., 88, pp. 9769-9775, 1983.

Lyzenga, D.R., A.L. Maffett, and R.A. Shuchman, The Contribution of Wedge Scattering to the Radar Cross Section of the Ocean Surface, IEEE Trans. Geosci. Rem. Sens., GE-21, pp. 502-505, 1983.

Lyzenga, D.R., C.C. Wackerman and R.A. Shuchman, Synthetic Aperture Radar Image Simulations, Oceans 84 Conference Record, Marine Technology Society, Washington, D.C., 1984.

∨ Lygenga, D.R. and R.A. Shuchman (eds.), The DARPA SAR Program: Interim Report on the Georgia Strait Experiment, SAR Technology and Processing Investigations, ERIM Topic Report No. 168400-5-T, Ann Arbor, MI, CONFIDENTIAL (1984).

Rawson, R.F., R.E. Hamilton, C.L. Liskow, A.R. Dias, and P.L. Jackson, SP Mountain Data Analysis, ERIM Final Report No. 148000-1-F, Ann Arbor, MI, 72 pp., 1981.

Shuchman, R.A., P.L. Jackson, and G.B. Feldkamp, Problems of Imaging Ocean Waves with Synthetic Aperture Radar, ERIM Interim Technical Report No. 124300-1-T, Ann Arbor, MI, 111 pp., 1977.

Shuchman, R.A., E.S. Kasischke, A.D. Nichols, and R.F. Rawson, Multi-frequency and Multipolarization P-3 SAR Facility, ERIM Topic Report No. 176900-1-T, Ann Arbor, MI (in press), 1984.

R.A. Shuchman and D.R. Lyzenga, Oceanographic Measurements with Conventional and Non-Conventional Synthetic Aperture Radar Systems, IEEE J. Oceanic Eng. (in review), 1985.

Valenzuela, G.R., Theories for the Interaction of Electromagnetic and Oceanic Waves — A Review, Boundary Layer Meteorology, 13, pp. 61-85, 1978.

Walker, J.L. and R.W. Larson, SAR Calibration Technology Review, ERIM Final Report No. 150400-7-F, 151 pp., 1981.

END

FILMED

11-85

DTIC